ISSN 2583 - 2565

ST. TERESA'S COLLEGE
(AUTONOMOUS)
ESTD 1925

Teresian International Journal of Chemical Sciences

October-December 2022
Volume III, Issue IV

Double-blind
Peer Reviewed-Quarterly

ST. TERESA'S COLLEGE (AUTONOMOUS), INDIA

Contents

Editorial Board

Dr. Alphonsa Vijaya Joseph
Principal
St.Teresa's College (Autonomous), Ernakulam
Cochin-11, Kerala, India

Principal's Message

St. Teresa's College is on the threshold of its Centenary celebrations and we are pleased to publish the Volume 3, Issue 4 of the ***'Teresian International Journal of Chemical Sciences,'*** which is a unique venture of the Department of Chemistry and Centre for Research. The Centennial plan in the area of research envisages 'Institutionalisation of Research Culture' and this journal promises an exciting development towards this initiative providing a platform for researchers to disseminate and validate the findings of their research. This indeed is a platform to encourage researchers for publishing their research output in the form of journal articles that brings scholarly recognition to the College. This journal also contributes to the career development of faculty and researchers through their participation in the creation and sharing of innovations, research and development. The journal, in fact, is an academic voice and a venue for discourse that will move us forward to steady growth, both educationally and intellectually. I strongly believe that this research culture will continue to capture, investigate and interrogate emerging research fields in chemical sciences and scale up to a diversity of expertise matched by a shared culture of excellence and multidisciplinary collaboration.

I'm happy that the Department of Chemistry is contributing significantly to an innovative research culture and I wish the faculty and researchers the very best in all future endeavours.

Editorial

Dr. Saritha Chandran A.

Think aloud on the value of what we own

The editorial for the current issue throws light to some of the suggestions made by our students in class room interactions. As faculty members, we lend our ears to them. The editor submits to the scientific community, the essence of such an interaction as a submission.

First, it once had been made at the University of Chicago in 1944 on large scale energy production in India on the strength of the highest quantity of thorium present in Indian rare earth. It was a three-stage concept. Eight decades have elapsed. Many nations have developed similar projects. A couple of years back a neigh-bouring country has eclipsed many others in the world in large scale energy production using thorium. In this context, one question raised in the student interaction is very interesting. In the globe, our state of Kerala, especially its southern coastal land is the richest in thorium ore in the world. In Kerala, governments have been contesting each other in exporting rare earth sand for damn cheap price, to countries where science transforms sand to energy and other precious materials. Our students ask why these things happen. Besides, the popular governments boast, they get huge profits from export, students lament hearing these words. The subject is generation of energy. It reminds us of the huge resources of easily accessible thorium for large scale energy production, a major goal in its nuclear power programme.

contd.... to next Page

The editorial submits to the scientific community the following for their kind consideration. The elected members in the assembly require your advice. The governments heed to your words. Please create a scientific awareness on the precious rare earths we have been losing all these years. There shall be an awakening through deliberations like discussions, conferences, and debates. For several decades the rare earth sand is leaving Indian land, it is helping other countries. Academicians and researchers may kindly read this submission.

DNA Binding and α-amylase Enzyme Activity Studies of Cu(II) Complexes Derived from Heterocyclic Schiff bases

Dr. Shanty A. A.
Assistant Professor, Department of Chemistry
St. Teresa's College (Autonomos), Ernakulam
Park Avenue Road, Cochin-11, Ernakulam, Kerala, India
Email: shanty.sheen@gmail.com, shantyaa@teresas.ac.in.

Abstract

Novel copper(II) complexes of heterocyclic Schiff base ligands were synthesized and characterized. Copper complexes exhibited square pyramidal and square planar geometry. Their interaction with Herring sperm DNA (HS-DNA)was investigated through UV–Visible absorption, Circular Dichroism and Voltammetric studies.DNA-binding studies with HS-DNA indicate that copper complexes bind to DNA by intercalation modes**.** Upon electronic absorption spectral titrations, all the synthesized copper complexes showed hypochromism. Observed intrinsic binding constant (ranging from 10^3 - 10^5 M^{-1}) is comparable to other intecalaters. α-Amylase inhibition studies of Cu(II) complexes has been explored by DNS method. The inhibition mechanism was analyzed with Lineweaver-Burk plot. $[Cu(TMA)_2]\cdot H_2O$ complex is found to be an effective noncompetitive inhibitor of α-amylase.

Keywords: *Schiff base, Copper complexes, DNA binding, and α-Amylase inhibition.*

The pharmacology of heterocyclic Schiff bases and their metal complexes is the focus of research for bioinorganic chemists (A. A. Wasfi, et al. 386-89). The sulphur and nitrogen containing organic compounds and their metal complexes display a wide range of biological activities: antifungal, antitumor, antibacterial, and antiviral properties (B.S. Creaven, et al. 4048-58), (T. Aboul-Fadl, et al. 4578-86), and (T. Alessio, et al. 11220-226). Metal complexes that can bind to DNA are gaining considerable attention due to their diverse applications as new generation metallo-pharmaceuticals. Recent years have seen an increased interest in the study of molecules able to bind the deoxyribonucleic acid (DNA) in efforts to find agents that regulate gene expression and cell processes or to create new drugs with improved biological activity against cancer cells (C. Mala, et al. 3072-82). DNA plays a main role in the life process because it carries heritage information and instructs the biological synthesis of proteins and enzymes through the process of replication and transcription of genetic information (L. Xiaoquan, et al. 444-50). As DNA is an important target for studies with small molecules such as steroids, carcinogens and several classes of drugs, investigation of small molecule–DNA interaction is very important (G.W. Zhang, et al. 2638-47).

Metal-based pharmaceuticals emerging from the interface of inorganic chemistry and biology have witnessed spectacular successes (S. Shinde, et al. 60-67). Metal-imine complexes have been widely investigated due to antitumor and herbicidal utilization. They can work as models for biologically important species. The chelating ability and biological implementations of metal complexes have attracted remarkable attention (A.M. Ahmed and M. A. M. Ibrahim (119-33) and L. H. Abdel Rahman, et al. 79-95). The biological behaviour of Cu(II) complexes has been subjected to intense investigation for DNA binding and cleavage activities (K. Rishu, et al. 1-15). Copper accumulates in tumors due to the selective permeability of cancer cell membranes to copper compounds. Thus, a number of copper complexes have been screened for anticancer activity, and some of them were found to be active both *in vitro* and *in vivo* (S. Kannan, et al. 3380-91). Copper complexes being more biocom-patible, eliminates the risk for toxicity which is a major drawback for other metal complexes with medicinal importance. Recently, biologically synthesized metal complexes exhibiting diverse therapeutic potential are gaining more importance (X. B. Yang, et al. 55-59).

Diabetes Mellitus (DM) is a pathological condition, characterized by hyperglycemia due to relative or absolute deficiency of insulin, and associated with severe physiological imbalances (G. Kumar, et al. 1630-35). Therefore, a therapeutic approach to treat diabetes is to decrease postprandial hyperglycemia. This can be achieved by the inhibition of carbohydrate hydrolyzing enzymes like α-amylase. Amylase inhibition has gastrointestinal and metabolic effects that may aid not only in the treatment of diabetes but also to obesity (A.D.A. 94-102).

In our effort towards the development of metal based therapeutic agents, we present the synthesis, characterization, DNA binding and α-Amylase inhibition studies of Cu(II) complexes of heterocyclic Schiff bases.

Materials and Methods

All chemicals were purchased from Aldrich. Solvents employed were either of 99% purity or purified by known laboratory procedures (Vogel's 1989). 2-Aminophenol, 2-amino-4-nitrophenol,2-amino-4-methylphenol, thiophene-2-carbo-xaldehyde, pyrrole-2-carboxaldehyde and copper acetate monohydrate

were purchased from Aldrich. Herring sperm DNA (HS-DNA) and Tris (Hydroxymethyl) Aminomethane and Dinitro-salicylic acid (DNS) were purchased from Sigma Aldrich. α-amylase were obtained from Hi-media chemicals.

Electronic spectra of the compounds were recorded in DMF on a Thermo electron Nicolet evolution 300 UV-vis spectrophotometer. FT-IR spectra of the Schiff bases were recorded as KBr pellets with a JASCO-8000 FT-IR spectrophotometer. Elemental analyses of all the synthesized compounds were done using an Elementar Vario EL III CHN analyzer at SAIF. ^{1}H NMR spectra were recorded on a Burker Advance DRX 300 FT-NMR. TG-DTA-DTG analysis of the complexes were carried out under air and nitrogen at a heating rate of 20°C min^{-1} using a Perkin Elmer Pyres Diamond TG/DTA analyser in the 50-800°C range at the Sophisticated Test and Instrumentation Centre (SAIF), Cochin University of Science and Technology, Kochi, India. Molar conductivities of the complexes in DMSO solutions (10^{-3}M) at room temperature were measured using a Systronic model 303 Direct reading Conductivity Meter. The magnetic susceptibility measurements were done at room temperature on a Magway MSB Mk 1 Magnetic Susceptibility Balance. EPR spectra of the complexes were recorded in the solid state at RT, solid state at LNT and in DMF at LNT using Varian E-112 X-band spectrometer using TCNE (g=2.00277) as standard at the SAIF, IIT, Mumbai, India.

Synthesis of Schiff bases and Copper Complexes

Five Schiff bases were synthesized by the condensation of Thiophene-2-carboxaldehyde and Pyrrole-2-carboxaldehyde with 2-Aminophenol, 2-Amino-4-nitrophenol, 2-Amino-4-methyl-phenol. Synthesis and characterization of ligands were reported in our previous work (A. A. Shanty, et al. 67-73).

Thiophene-2-carboxaldehyde and 2-aminophenol (TA)

Thiophene-2-carboxaldehyde and 2-amino-4-nitrophenol (TNA)

Thiophene-2-carboxaldehyde and 2-amino-4-methylphenol (TMA)

Pyrrole -2-carboxaldehyde and 2-aminophenol (PA)

Pyrrole -2-carboxaldehyde and 2-amino-4-nitro phenol (PNA)

Synthesis of Copper (II) Complexes

A solution of cupric acetate in methanol was added to the solution of the Schiff bases, TA, TNA, TMA, PA, PNA, in methanol. The solution was refluxed for three hours at 60°C. The precipitate was formed on slow evaporation of the solvent. The product was washed with cold methanol and petroleum ether before drying over phosphorous pentoxide in desiccators.

DNA Binding Experiments

Absorption Spectral Studies

The UV-Visible absorption spectroscopic method is used to study the DNA binding nature of Schiff base ligands and their Cu (II) complexes. The DNA concentration per nucleotide was measured spectrophotometrically by using known molar extinction coefficient value $6600M^{-1}$ cm^{-1} at 260 nm. The absorption titrations were carried out in Tris–HCl buffer (5 mMTris– HCl/50 mMNaCl, pH 7.1) at 25°C by keeping the concentration of ligands and complexes constant and varying the concentration of the HS-DNA while maintaining the total volume constant (3 mL). To measure the

absorbance of the complex and to eliminate the absorbance of HS-DNA itself, equal quantity of HS-DNA was added to both the complex solution and the reference solution. The magnitude of spectral perturbation is an evidence for the extent of binding. From the absorption data, the intrinsic binding constant (K_b) was calculated by a plot made between [DNA] / (ϵ_a-ϵ_f) and [DNA] (L. H. Abdel Rahman, et al. 79-95 and 18-31), (V. Narendrula, et al. 1317-29).

Voltammetric Studies

Differential Pulse Voltammetric studies were performed on an Electrochemical Analyser (CH instrument, Austin, TX) which is a three electrode system with platinum electrode as the working electrode, a platinum wire as the auxiliary electrode and Ag/AgCl as the reference electrode. Platinum electrode was mechanically polished with aqueous slurries of alumina (50 nm) on a flat pad prior to surface modification. After polishing, it was rinsed ultrasonically with absolute ethanol to remove residual alumina particles from the surface and then cleaned with a piranha solution (H_2O_2:H_2SO_4=1:3v/v) for 10 minutes. Following this mechanical process, an electrochemical cleaning process was carried out using Cyclic Voltammetry performed from 0 to 1500 mV in a 0.5 M sulphuric acid solution at a scan rate of 100mV/s until a stable cyclic vol-tammogram was obtained.

All the electrochemical measurements were carried out at room temperature in a 10 mL electrolytic cell by using 5 mMTris–HCl/50 mMNaCl buffer (pH 7.1) as the supporting electrolyte. Solutions were deoxygenated by purging with N_2 prior to the measurements. The working electrode was cleaned after every electrochemical assay. The voltammograms of $1x10^{-5}$ M solution of complexes were recorded in absence of DNA. The procedure was then repeated for systems of 10 ml of a mixture containing constant concentration of the complexes and varying the concentration of DNA (M. D. A. Maria, et al. 105-116).

Circular Dichroism (CD) Spectral Studies

The Circular dichroism spectrum have been utilized as a powerful tool for exploring the chiral aspect of compounds. CD spectra of HS DNA in the presence and absence of metal complexes were obtained in Tris–HCl buffer (pH=7.1) containing 50 mMNaCl at room temperature by using a Jasco Circular Dichroism Spectropolarimeter (CS/PPG/CD/018) equipped with a Peltier temperature control device at 25 ± 0.1°C with a 0.1 cm path length cuvette. The spectra were recorded in the region of 220–320 nm for fixed concentrationof DNA ($1x10^{-5}$ M) and varying the concentration of complexes (A. Patra, et al. 156-63).

α-Amylase Inhibition Assay

α-Amylase inhibitory activity was determined by Dinitrosalicylic acid (DNSA) method as reported earlier with slight modification (G. L. Miller 426-28). The total assay mixture composed of 500 μL of amylase (in 0.05 M sodium phosphate buffer (pH = 6.9) and test compounds (at different concentrations of 50-200 μM) was incubated at 37°C for 10 min. After pre-incubation, 500 μL of 1% starch solution in the above buffer was added to each tube and again incubated at 37°C for 15 min. The reaction was terminated with 1.0 mL DNSA reagent, placed in a boiling water bath for 5 min, and cooled to room temperature. The reaction mixture was then diluted by adding 10 ml of distilled water and the absorbance was measured at 540 nm. The control amylase represented 100% enzyme activity and did not contain sample. Acarbose was used as a standard inhibitor and it was assayed at above mentioned test sample concentrations. The maltose liberated was deter-

mined with the help of standard maltose curve and the activities were calculated according to the following equation (P. Sudha, et al. 11-15) and (A.V. Gusakov, et al. 2011).

$$\text{Activity} = \frac{\text{Conc. of maltose liberated x enzyme used in mL}}{\text{Mol: Wt of maltose x time (min) x dilution factor}}$$

$$\% \text{ Inhibition} = \frac{\text{Absorbance of control} - \text{Absorbance of sample}}{\text{Absorbance of control}} \text{X100}$$

plots. For the study, 200 μL of the sample was incubated with α-amylase. Concentration of the starch (substrate) was varied from 0.2 to 5 mg/mL. The mixture was then incubated for 10 min at 37°C and then boiled for 5 min after the addition of 1.0 mL of DNS to stop the reaction. The amount of reducing sugars released was determined spectrophotometrically using a maltose standard curve and converted to reaction velocities. A double reciprocal plot (1/V versus 1/(5F)) where V is reaction velocity and (5F) is substrate concentration was plottedand the type (mode) of inhibition of the samples on α-amylase activity was determined (D. L. Nelson and M. M. Cox 2008).

Results and Discussion

Synthesis and Characterization

All copper complexes are coloured, non-hygroscopic and stable at room temperature. These complexes are insoluble in water and common organic solvents but are soluble in DMF and DMSO.

The IR spectra of all copper complexes show strong band in the range 1568–1594 cm^{-1} assigned to the υ(C = N) vibration. Compared to the spectra of free ligands [υ(C = N) 1608-1650 cm^{-1}], it shifts to lower frequency by 15–20 cm^{-1} and supports the coordination of the υ(C = N) group. The involvement of deprotonated phenolic moiety in the complexation process is confirmed by the shift of υ(C–O) stretching band to a lower frequency to the extent 10–20 cm^{-1} (K. Nakamoto 1963). The molar conductance values for all copper complexes are in the range 3-20 $Ohm^{-1}cm^2$ mol^{-1} in DMSO and are in accordance with those reported for non-electrolytes in this solvent (E. Akila, et al. 15-19). Magnetic moment μ_{eff}) values of all copper(II) complexes were found to be in the range from 1.7-1.9 BM corresponding to one unpaired electron and this is an indication of monomeric compounds with Square pyramidal or Square planar geometry (S. T. Syed and K. Geetha 40-48). The electronic spectra of all copper complexes were recorded in DMSO (10^{-4} and 10^{-2}M) in the range 900-220 nm. The band in the wavelength ranges 21,833 - 14,619 cm^{-1} corresponds to d–d transition (B. Subhra, 115-21).

The EPR spectra of the copper (II) complexes in polycrystalline state at 298 K and in DMF at 77 K were recorded in the X-band, using 100-kHz

modulation frequency and 9.1 GHz microwave frequency. The spectra of $[Cu(TA)_2H_2O]\cdot H_2O$ and $[Cu(TMA)_2]\cdot H_2O$ complexes show an isotropic spectrum with g_{iso}= 2.10 and 2.12 at room temperature. All other copper(II) complexes $[Cu(TNA)_2]\cdot 2H_2O$,$[Cu(PA)_2\cdot H_2O]\cdot 2H_2O$ and $[Cu(PNA)_2]\cdot 3H_2O$ displayed axial spectra in the polycrystalline state at 298 K with $g\parallel$ and $g\perp$ values. The variation in the $g\parallel$ and $g\perp$ values indicates that in the solid state, the geometry of the compounds is affected by the nature of coordinating ligands (K. Jayakumar, et al. 28-36). These compounds with axial behaviour in polycrystalline state show $g\parallel > g\perp > 2.0023$, which is consistent with a $d_{x^2-y^2}$ ground state in a square planar or square pyramidal geometry. In DMF solution, for all the copper complexes $[Cu(TNA)_2]\cdot 2H_2O$($g\parallel$ =2.277 and $g\perp$ = 2.076), $[Cu(TMA)_2]\cdot H_2O$($g\parallel$ =2.298 and $g\perp$ =2.065), $[Cu(PA)_2 H_2O]\cdot 2H_2O$($g\parallel$ =2.24 and $g\perp$ = 2.065) and $[Cu(PNA)_2]\cdot 3H_2O$($g\parallel$ =2.25 and $g\perp$ = 2.06), four well resolved hyperfine lines are observed inthe parallel region due to coupling of the electron spin with the nuclear spin (^{63}Cu, I = 3/2), the splitting arenot well differentiable in the perpendicular region. In frozen DMF, $[Cu(TA)_2H_2O]\cdot H_2O$ reveals three sets of resonances at low, mid and high fields corresponding to g_x, g_y and g_z respectively. From the peak positions, the g values evaluated are g_x = 2.02, g_y = 2.07 and g_z = 2.39. Hyperfine structure was not resolved in both parallel and perpendicular regions. The calculated g values provide valuable information on the electronic ground state of the ion. If $g_z > g_y > g_z$, and the quantity of R {$R = (g_y - g_x)/(g_z - g_y)$} is greater than unity, the ground state is (d_z^2) and if R is less than unity, the ground state is ($d_{x^2-y^2}$). For $[Cu(TA)_2 H_2O]\cdot H_2O$, the value of 'R' (0.173) indicates $d_{x^2-y^2}$ as ground state suggesting a rhombic structure (K. Jayakumar, et al. 50-56) and (B. N. Figgis 1996).

To determine the thermal stability and chemical composition of Cu(II) complexes, Thermogravimetric analysis has been performed in a temperature range of 50-800°C in nitrogen atmosphere at a heating rate of 10°C/min. Copper complexes $[Cu(TA)_2H_2O]\cdot H_2O$ and $[Cu (PA)_2 H_2O]\cdot 2H_2O$ decomposed in three stages. The first estimated mass loss observed in the temperature range of 80-110°C is due to the loss of lattice water molecules. The second mass loss in the temperature range 130-220°C corresponds to the presence of one coordinated water molecule. The third step was found in the temperature range of 223–600°C corresponding to the loss of organic molecules. All other copper complexes, $[Cu(TNA)_2]\cdot 2H_2O$, $[Cu (TMA)_2]H_2O$ $[Cu(PA)_2 H_2O]\cdot 2H_2O$ and $[Cu (PNA)_2]\cdot 3H_2O$ showed mass loss in the temperature range 74-135°C corresponding to the presence of lattice water molecules. Above this temperature, a gradual weight loss occurs due to decomposition of organic ligands (N. Kavitha and P.V. Anantha Lakshmi 457-66).

Electronic Spectral Studies

Electronic Absorption Spectroscopy is an effective technique to study the binding mode and extent of binding of metal complexes with DNA (P. J. Cox, et al. 6054-62). The absorption spectra of copper complexes (1×10^{-5}M) in Tris-HCl buffer pH 7.1 in the absence (R=0) and presence of increasing amount of DNA are represented in Figure-1 (a) - 5 (a). The binding mode of the synthesized copper complexes to DNA is characterized by the change in absorbance. The absorption spectra of Cu (II) complexes showed absorbance in the range 350-450 nm. Upon increasing the concentration of HS-DNA, change in absorbance is effected, resulting in hypochromism indicating an intercalative way of binding between DNA duplex and complexes. Hypochromism is observed due to the presence of aromatic chromophore which might facilitate the interaction of the

complexes with the HS-DNA bases through noncovalent π-π* interactions (S. Kashanian, et al. 1314-48). When the complexes intercalate to the base pairs of HS-DNA, the π* orbital of the intercalatedligand in the complexes can couple with π orbital of the DNA base pairs, and then decreasing the π-π* transition energies. The coupling π orbital was partially filled by electrons, thus decreasing the transition probabilities and concurrently resulting in hypochromism. Planar complexes containing aromatic heterocyclic ligands could stack among the DNA base pairs.

In order to elucidate the binding strengths of these complexes, the intrinsic binding constant K_b was calculated by monitoring the changes of absorbance with increasing amounts of HS-DNA. The K_b (intrinsic binding constant) is calculated from a plot of [DNA]/ (ϵ_a-ϵ_f) Vs [DNA] using the equation:

$$[DNA] / (\epsilon_a-\epsilon_f) = [DNA]/ (\epsilon_b-\epsilon_f) +1/K_b (\epsilon_b-\epsilon_f),$$

where [DNA] is the concentration of DNA in base pairs. ϵ_a = the apparent coefficient =Aobsd/[complex], ϵ_f = the extinction coefficients of the free metal complexes, ϵ_b = the extinction coefficients of the free metal complexes in the fully bound forms. The binding constant K_b was calculated by the ratio of slope to the intercept. The magnitude of K_b value gives the extent of binding (N. H. Campbell, et al. 209-22).

A plot of [DNA] / (ϵ_a-ϵ_f) versus [DNA] for the titration of DNA with complexes for binding constant are represented in Figure-1(b) - 5(b). The binding constant values obtained for Cu(II) complexes are represented in Table-1. The order of K_b values obtained for the synthesized complexes are as follows:

$[Cu(TA)_2H_2O]\cdot H_2O(1.1x10^5) > [Cu(TNA)_2]\cdot 2H_2O$ $(5.2x10^4) > [Cu(TMA)_2]\cdot H_2O$ $(4.2x10^4) > [Cu(PA)_2H_2O]\cdot 2H_2O$ $(4.1x10^4) > [Cu(PNA)_2]. 3H_2O$ $(2.1x10^4)$. These results indicate that $[Cu(TA)_2 H_2O]\cdot H_2O$ complex has more affinity to bind to DNA than other copper complexes. This study also shows that the binding affinity of complexes is higher than that of ligands.

The binding constant values fall in the range 10^4-10^5 for all ligands and complexes and they are comparable with but still lower than that of the standard intercalator Ethidium bromide (1×10^7 M^{-1}) (V. Rajendiran, et al. 8208-21). These results

Table - 1: Binding Constant (k_b) M^{-1} for Schiff base Ligands and Complexes

Ligand	Binding constant (k_b) M^{-1}	
	Ligand	Cu(II) complex
TA	7.6×10^3	1.1×10^5
TNA	9.9×10^3	5.2×10^4
TMA	1.7×10^4	4.2×10^4
PA	2.3×10^4	4.1×10^4
PNA	7.7×10^3	2.1×10^4

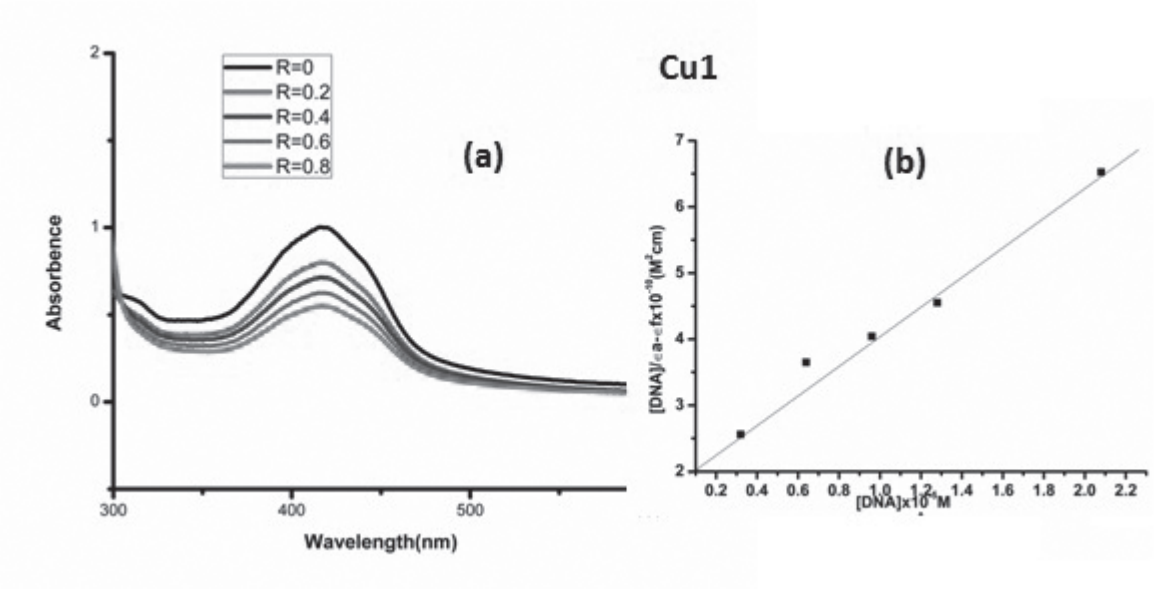

Figure - 1: a) Absorption spectra of [Cu $(TA)_2$ $H_2O]\cdot H_2O$](1.5x10^{-5} M) in Tris-HCl buffer of pH 7.1 in the absence (R=0) and presence (R= 0. 2, 0. 4, 0.6, & 0.8) of increasing amount of DNA, R= [DNA] / [Complex](b) A plot of [DNA]/ (ϵ_a-ϵ_f) Vs [DNA])

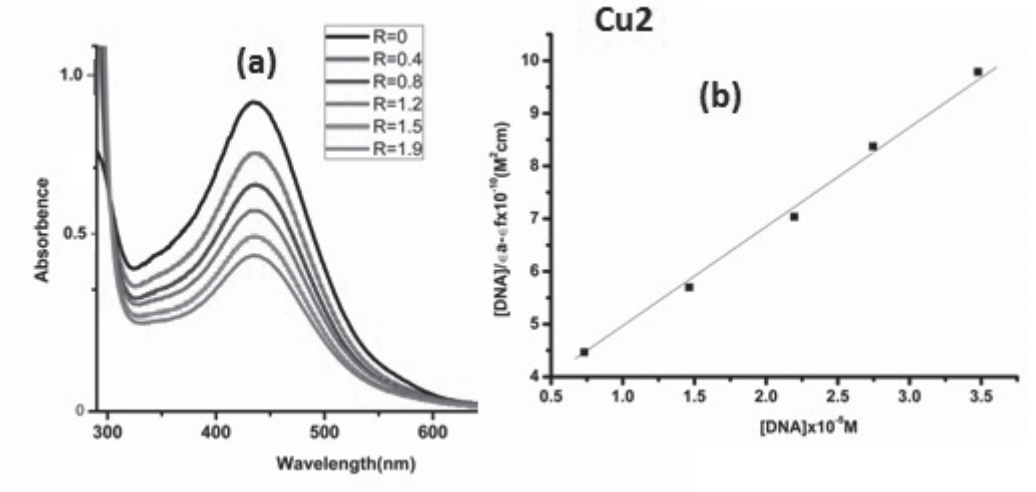

Figure - 2: (a) Absorption spectra of [Cu $(TNA)_2]\cdot 2H_2O$(1.5x10^{-5} M) in Tris-HCl buffer of pH 7.1 in the absence (R=0) and presence (R= 0. 4, 0. 8, 1.2, 1.5, & 1.9) of increasing amount of DNA,R= [DNA] / [Complex]. (b) A plot of [DNA]/ (ϵ_a-ϵ_f) Vs [DNA])

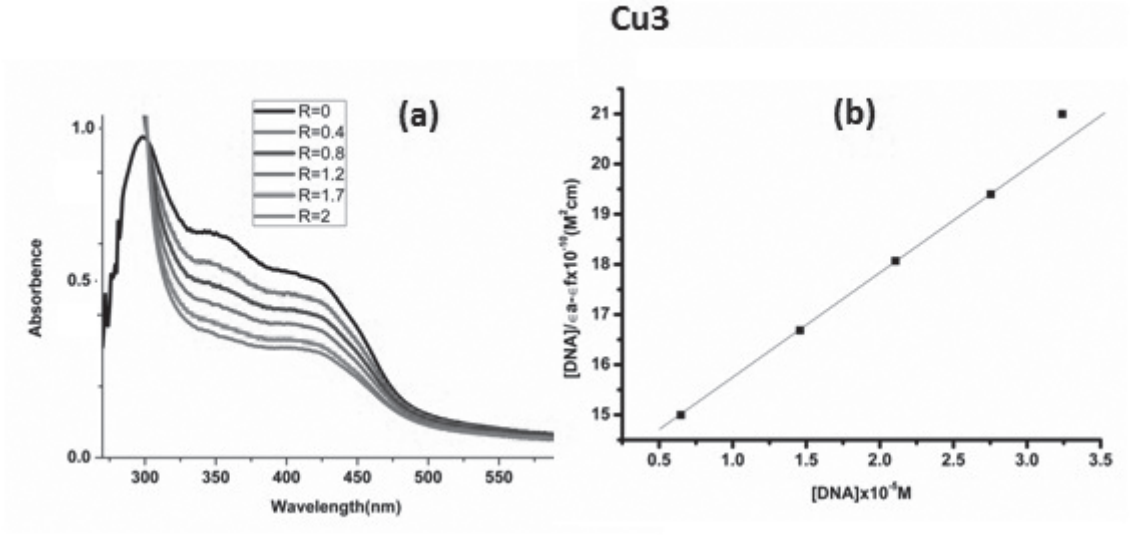

Figure - 3: (a) Absorption spectra of [Cu $(TMA)_2]\cdot H_2O$(1.5x10^{-5} M) in Tris-HCl buffer of pH 7.1 in the absence (R=0) and presence (R= 0. 2, 0. 4, 0.8, 1.2, 1.7 & 2) of increasing amount of DNA, R= [DNA] / [Complex](b) A plot of [DNA]/ (ϵ_a-ϵ_f) Vs [DNA])

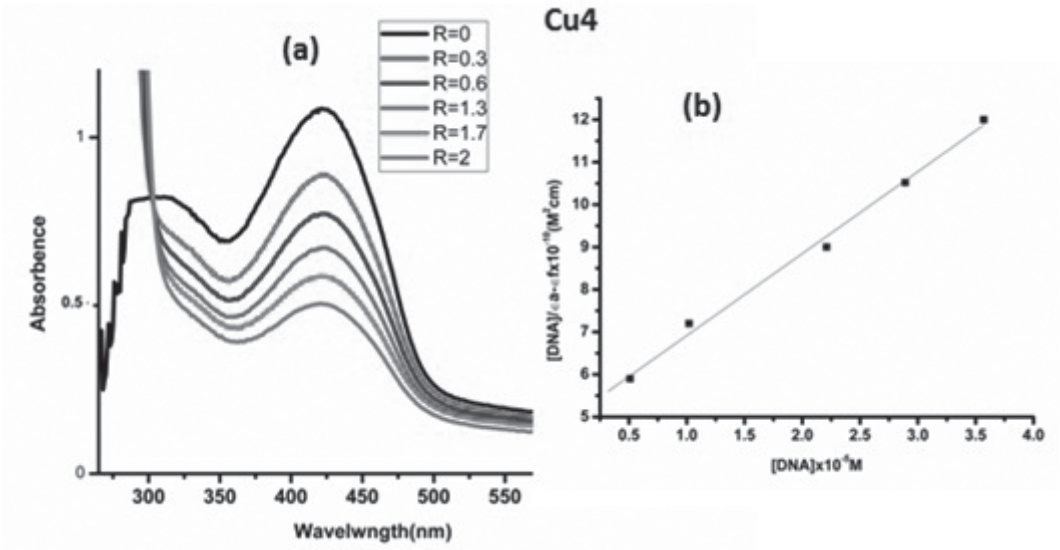

Figure - 4: (a) Absorption spectra of [Cu $(PA)_2$ $H_2O]\cdot 2H_2O$(1.5x10^{-5} M) in Tris-HCl buffer of pH 7.1 in the absence (R=0) and presence (R= 0. 2, 0. 3, 0.6, 1.3, 1.7 & 2) of increasing amount of DNA, R= [DNA] / [Complex](b) A plot of [DNA]/ (ϵ_a-ϵ_f) Vs [DNA])

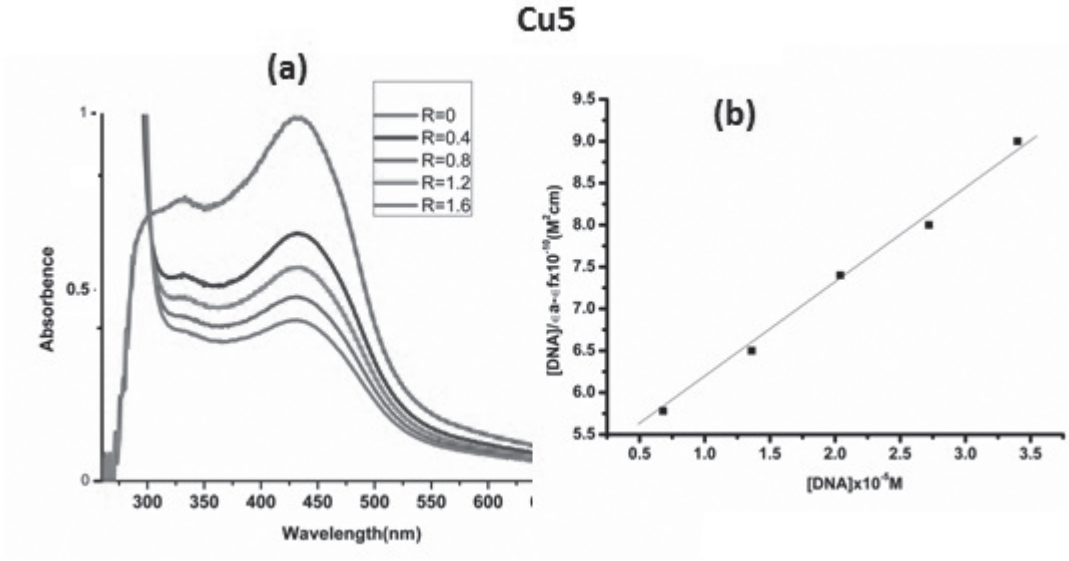

Figure - 5: (a) Absorption spectra of [Cu $(PNA)_2$]·$3H_2O$($1.5x10^{-5}$ M) in Tris-HCl buffer of pH 7.1 in the absence (R=0) and presence (R= 0. 4, 0. 8, 1.2 & 1.6) of increasing amount of DNA, R= [DNA] / [Complex](b) A plot of [DNA]/ (ϵ_a-ϵ_f) Vs [DNA])

indicate that all the synthesized compounds strongly interact with DNA by intercalation.

Voltammetric Studies

Recently, electrochemical techniques were used as a simple and rapid method to study DNA interaction with different compounds. One of the advantages of using this technique is the simultaneous determination of multiple oxidation states of the same species as well as mixtures of several interacting species. Differential Pulse Voltammogram (DPV) technique provides the needed high current sensitivity and good peak resolution for the investigation of the interaction between different molecules and the DNA (M. T. Carter and A. J. Bard 7528-30).

DPV experiments were performed to observe the changes in the formal potential as well as the current density during the addition of DNA to the experimental solution of Cu(II) complexes. Differential Pulse Voltammogramof Cu(II) complexes have been collected both in the absence and presence of DNA. The effect of increase of DNA concentration on voltammograms of the studied compounds is presented in Figure-2-6. In the case of all copper complexes, incremental addition of DNA effectively alters both potentials and currents of anodic peaks. Presence of DNA causes a considerable decrease in the volta-mmetric current. The drop of the volta-mmetric currents in the presence of DNA may be attributed to the slow diffusion of the metal complexes bound to higher and slowly diffusing HS - DNA. This in turn indicates the extent of binding affinity of the compounds to DNA. It can be concluded that all synthesized complexes bind to DNA through intercalation, with insertion of the molecule between the base pairs of the DNA strand.

Circular Dichroism

Additional evidence for DNA interaction was obtained from circular dichroism (CD) spectral studies. CD spectroscopy is an optical technique

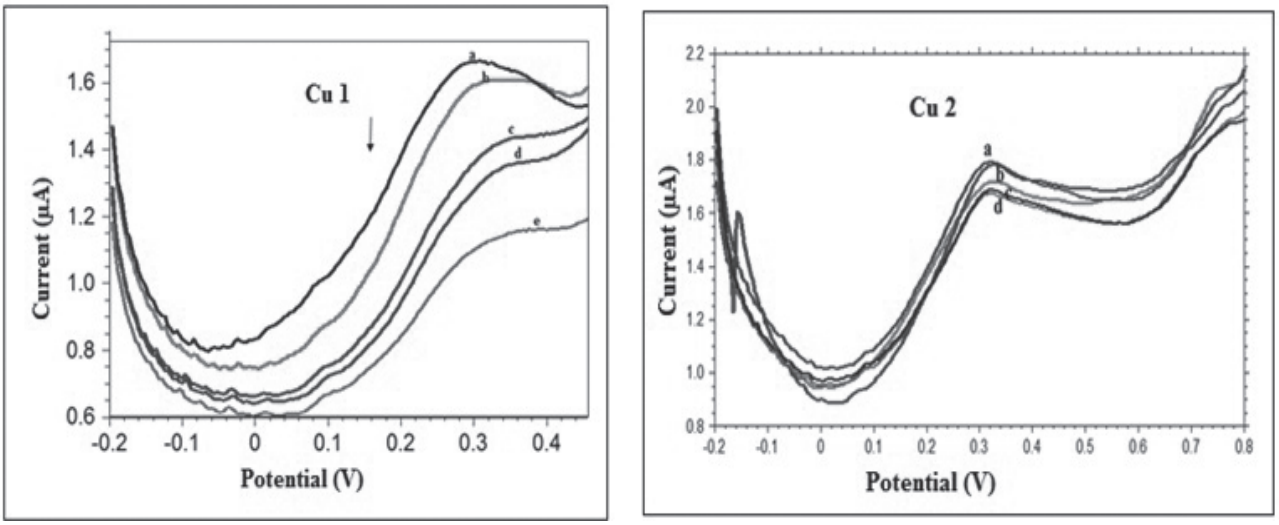

Figure - 2 and 3: Differential pulse voltammogram of Cu 1 = [Cu (TA)$_2$H$_2$O]·H$_2$Oand Cu 2 = [Cu(TNA)$_2$]·2H$_2$O(1.5×10^{-5} M) in Tris-HCl buffer of pH 7.1 in the absence (a) and presence (b, c and d) of increasing amount of DNA.

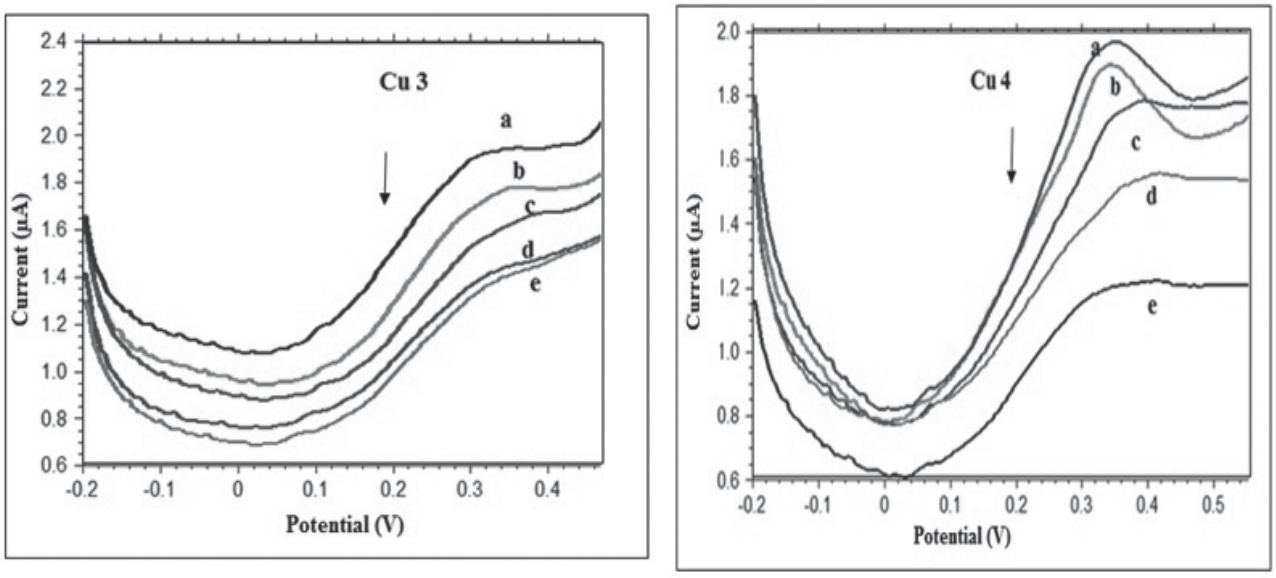

Figure - 4 and 5: Differential pulse voltammogram of Cu 3 = [Cu (TMA)$_2$]·H$_2$Oand Cu 4 = [Cu(PA)$_2$H$_2$O]·2H$_2$O(1.5×10^{-5} M) in Tris-HCl buffer of pH 7.1 in the absence (a) and presence (b, c and d) of increasing amount of DNA.

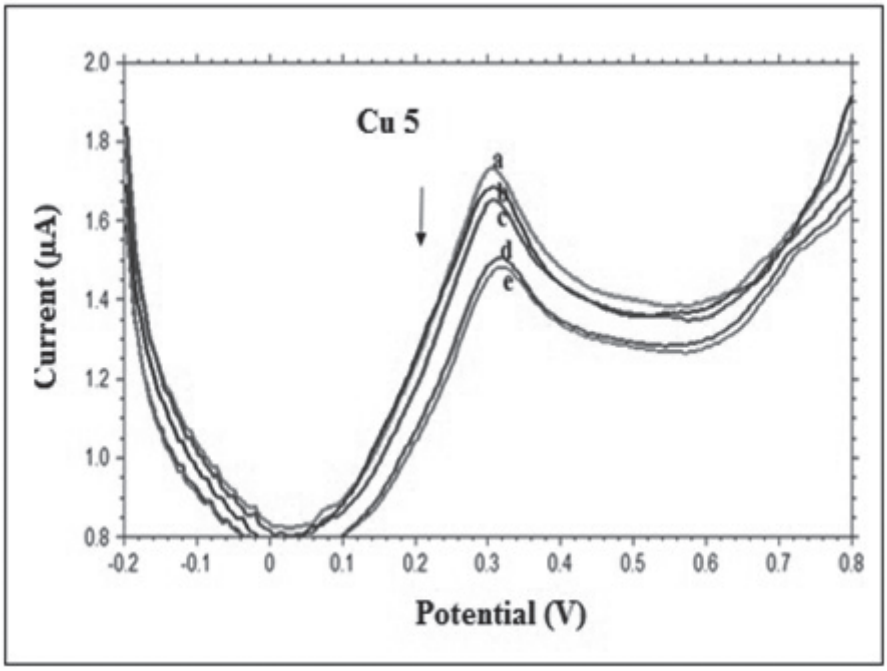

Figure - 6: Differential pulse voltammogram of Cu 5 = [Cu $(PNA)_2]\cdot 3H_2O$ and Cu 6 =$[Cu(PMA)_2]\cdot H_2O$ (1.5×10^{-5} M) in Tris-HCl buffer of pH 7.1 in the absence (a) and presence (b, c and d) of increasing amount of DNA

that measures the difference in the absorption of left and right circularly polarized light. This technique has been widely used in the studies of structures of nucleic acids and the use of it to monitor conformational polymorphism of DNA. DNA may undergo conformational changes to B-form, A-form, Z-form, quadruplexes, triplexes and other structures as a result of the binding process to different compounds (A. Rodger and B. Norden 1997). The CD spectrum of HS- DNA consists of a positive band at 275 nm that can be due to base stacking and a negative band at 245 nm that can be due to helicity and it is also characteristic of DNA in a right-handed B form (Yu-Ming Chang, et al. 3394-413). CD spectra of HS-DNA in the UV region show a distinct change in the spectral band corresponding to the B-DNA conformation. Groove binding or electrostatic interaction between the small molecules and the DNA causes less or no perturbation on the base stacking and helicity bands, whereas a classical intercalation enhances both CD bands (Z. H. Xu, et al. 77-83). The observed decrease in the positive DNA dichroic signal is likely due to a transition from the extended nucleic acid double helix to the more denatured structure (L. Milne, et al. 102-09). It should be noted that hydrophobic base stacking in oligomers and polymers result in close contacts and Coulombic interactions give rise to intense CD bands corresponding to each base transition (B. Macias, et al. 441-51). So the intercalated complexes which disrupt interactions between DNA bases and weaken base stacking and decrease the intensities of CD bands. Reductions in molar ellipticity in the negative band (245nm) when complexes are present are related to destabilization and helix unwinding.

The conformational changes of HS-DNA induced by the synthesized Cu(II) complexes were monitored by CD spectroscopy in Tris-buffer at pH = 7.1 at room temperature. The CD spectrum of HS-DNA exhibits two bands, a positive band at 275 nm due to base stacking and a negative band at 243 nm due to right-handed helicity. When all copper complexes were incubated with HS-DNA, the CD spectra of HS-DNA undergo significant changes in both positive and negative bands represented in Figure-7-11. In all compounds, the intensity of the positive band decreased and that of negative band increased. The decreased intensity in the positive band may be due to the intercalation of the complexes and has an effect on the π-π stacking of DNA base pairs. The increased intensity in the negative band suggests that the complexes can unwind the DNA helix and lead to some loss of helicity, which induces a more A-like conformation in DNA. This result remarks a loss of the typical chirality of HS-DNA after its interaction with synthesized compounds, in agreement with helix unwinding after intercalation. These changes also suggest that the stacking mode and the orientation of base pairs in DNA were disturbed with the binding of the complexes, and certain conformational changes, such as the conversion from a more B-like to a more A-like structure within the DNA molecules has happened. These observations clearly indicate that the binding mode of all the compounds should be intercalative.

α-Amylase Activity

α-Amylase activity of the synthesized compounds was evaluated *in vitro* by amylase inhibition assay using DNS method. The results of the α-amylase activity studies of Cu(II) complexes are given in Table-2. In the case of

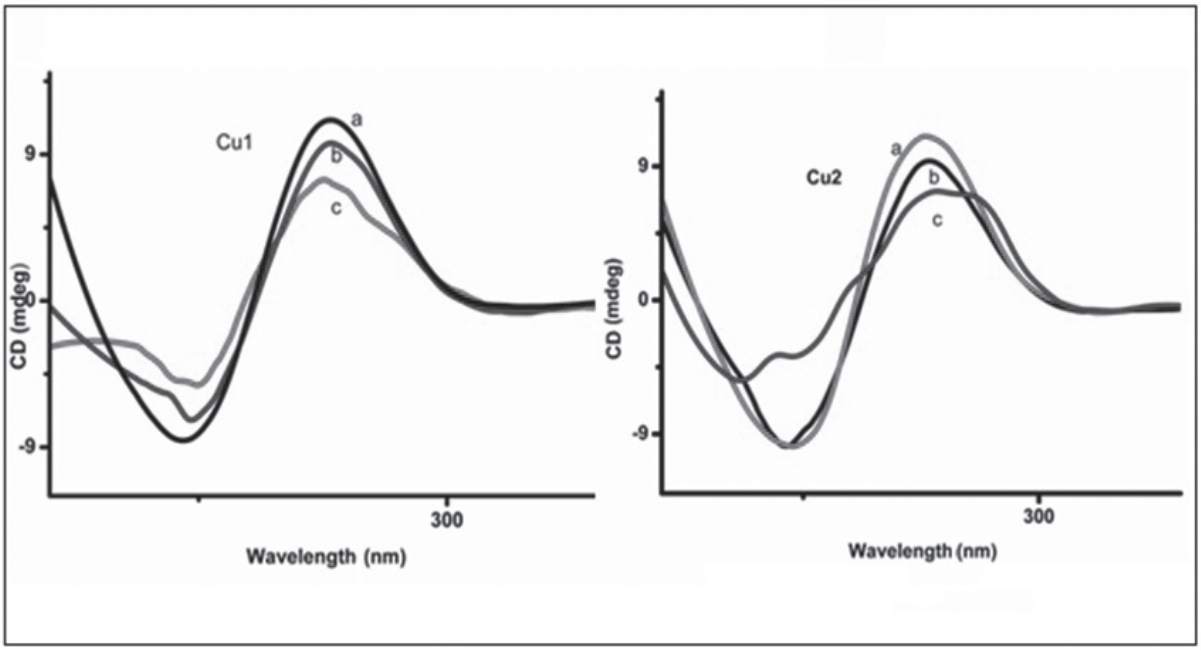

Figure - 7-8: CD spectra of HS-DNA (1×10^{-5} M) in Tris-HCl buffer of pH 7.1 in the absence (a) and presence (b and c) of Cu1 = $[Cu(TA)_2H_2O]\cdot H_2O$ and Cu2 = $[Cu(TNA)_2]\cdot 2H_2O$

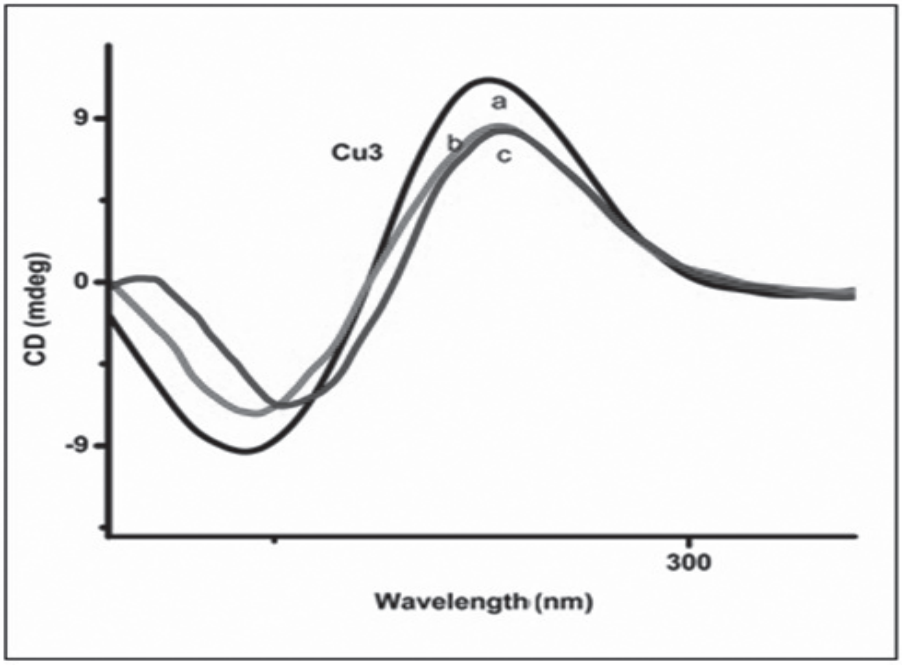

Figure - 9: CD spectra of HS-DNA (1×10^{-5} M) in Tris-HCl buffer of pH 7.1 in the absence (a) and presence (b and c) of Cu3 = $[Cu(TMA)_2]\cdot H_2O$

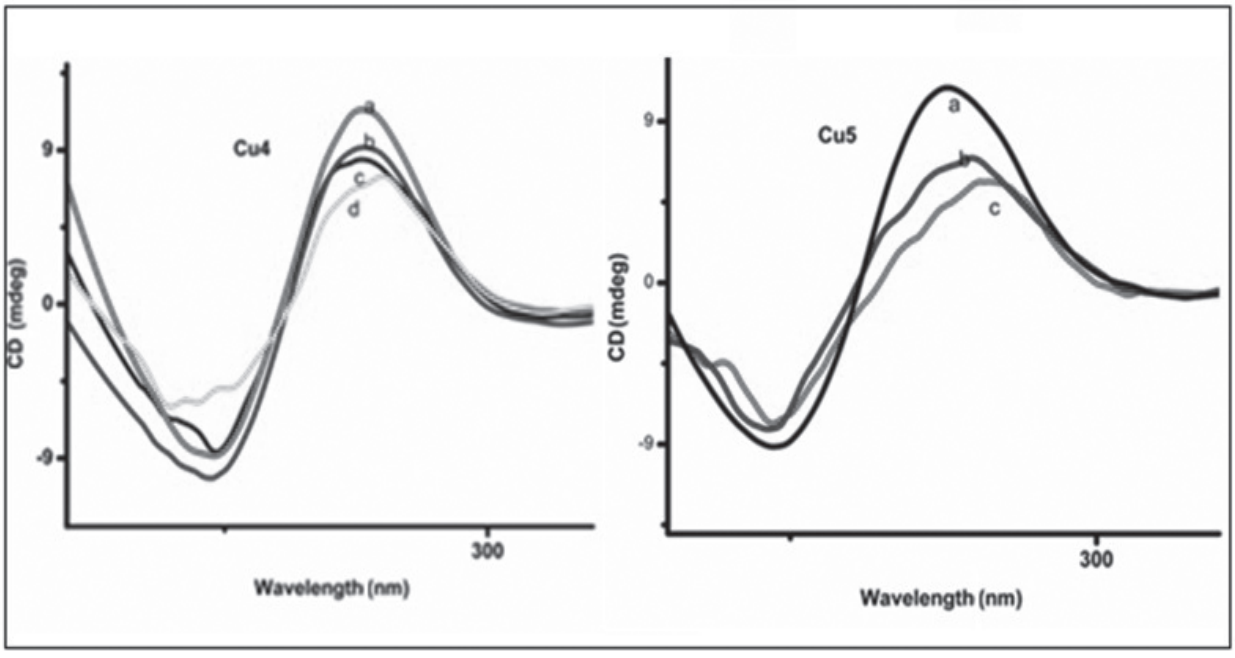

Figure - 10-11: CD spectra of HS-DNA (1×10^{-5} M) in Tris-HCl buffer of pH 7.1 in the absence (a) and presence (b and c) of Cu4 = $[Cu(PA)_2H_2O]\cdot 2H_2O$ and Cu5 = $[Cu(PNA)_2]\cdot 3H_2O$

synthesized compounds, $[Cu(TMA)_2]\cdot H_2O$ complex shows amylase inhibition. This compound showed lower amylase inhibition activity than that of standard amylase inhibitor acarbose (IC_{50} value - 0.13 μM). In the action media, salvation behaviour of synthesized compounds and acarbose are different. This may be a reason why $Cu(TMA)_2]\cdot H_2O$ complex showed lesser amylase inhibition activity compared to that of acarbose (R. A. Thesignu and R. A. Natarajan 2007). All other copper complexes enhance α-amylase activity. IC_{50} value of that compound which shows inhibition was also determined. IC_{50} value of $[Cu(TMA)_2]\cdot H_2O$ is 90.45 μM. Lower IC_{50} value indicates greater inhibition activity. Inhibition of enzymes such as α-amylase involved in the hydrolysis of carbohydrates has been exploited as a therapeutic approach for controlling postprandial hyperglycemia (Y. A. Lee, et al. 287). The inhibition activity of α-amylase was extended and might be responsible for decreasing the rate of glucose absorption and concentration of postprandial serum glucose (N. Ramasubbu, et al. 2517). This effect would delay the degradation of starch and oligosaccharides, which would in turn cause a decrease in the absorption of glucose and consequently inhibit the increase in postprandial blood glucose. In the human species, α-amylase is present in both salivary and pancreatic secretions. This enzyme is responsible for cleaving large malto-oligosaccharides to maltose.

Table - 2: α-Amylase Inhibitory Activity of Cu(II) Complexes (200 μM)

Compounds	OD at 540 nm	Conc.of Maltose liberated (mg)	Activity (mmoles/ml/min)	% Activity	% Inhibition
Control	0.2068	0.140	0.0013	100.00	0.00
$[Cu(TA)_2H_2O]\cdot H_2O$	0.3768	0.260	0.0024	185.76	-85.76
$[Cu(TNA)_2]\cdot 2H_2O$	0.3866	0.270	0.0025	192.90	-92.90
$[Cu(TMA)_2]\cdot H_2O$	0.1167	0.053	0.0005	37.87	62.13
$[Cu(PA)_2H_2O]\cdot 2H_2O$	0.3321	0.230	0.0021	164.32	-64.32
$[Cu(PNA)_2]\cdot 3H_2O$	0.2760	0.190	0.0018	135.75	-35.75

Mode of Inhibition

Kinetic studies were carried out to identify the mode of inhibition of $[Cu(TMA)_2]\cdot H_2O$ using Lineweaver-Burk plot. Figure-14 shows that the straight lines intercept at a single point in the second quadrant. This indicates that this compound inhibits α-amylase enzyme non competitively. The noncompetitive mode of inhibition obtained from the Lineweaver-Burk plot points to the fact that the active components in

$[Cu(TMA)_2]\cdot H_2O$ complex do not compete with the substrate for binding to the active site rather the inhibitors bind to a separate site on the enzyme to retard the conversion of disaccharides to monosaccharides [48]. Kinetic parameters: Michaelis-Menten constant (K_m) and the maximum reaction velocity (V_{max}) for$[Cu(TMA)_2]\cdot H_2O$ complex are presented in Table-3. In $[Cu(TMA)_2]\cdot H_2O$,V_{max} decreases but K_m remained the same.

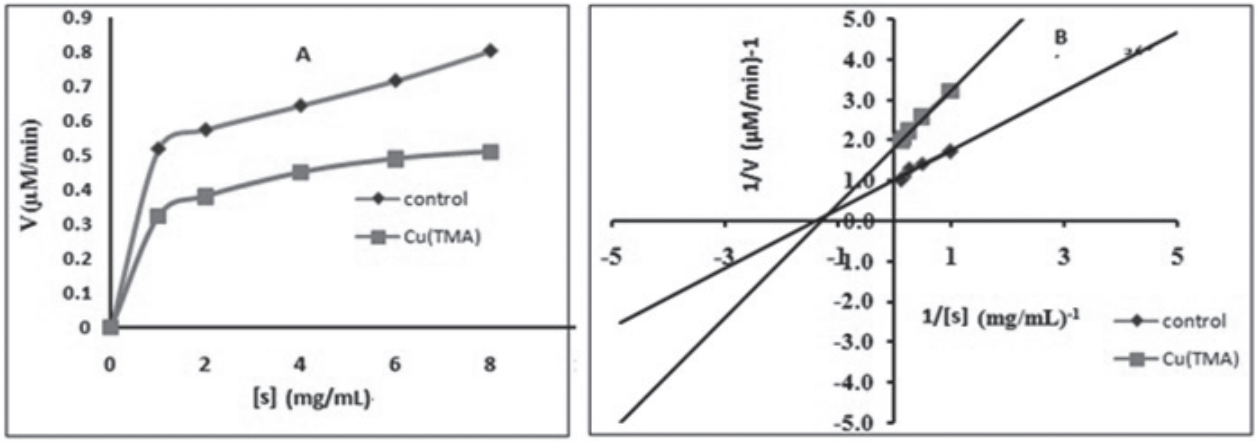

Figure - 12: Mode of inhibition of α-amylase by $[Cu(TMA)_2]\cdot H_2O$ (A) Michaelis-Menten plot and (B) Lineweaver-Burk plot

Table - 3: Kinetic Parameters K_m and $V_{max}$of $[Cu(TMA)_2]\cdot H_2O$

Compound	K_M	V_{Max}	IC_{50} (µM)
Control	0.7279	0.9991	-
$[Cu(TMA)_2]\cdot H_2O$	0.7228	0.5509	90.45

Conclusion

In conclusion, we have successfully synthesized five new Cu(II) Schiff base complexes and characterized them using various spectroscopic methods. Magnetic moment values of all copper complexes give an indication of square pyramidal or square planar structure. UV-Vis, EPR and Thermogravimetric data confirmed square pyramidal structure for $[Cu(TA)_2H_2O]\cdot H_2O$ and $[Cu(PA)_2H_2O]\cdot 2H_2O$ complexes and square planar structure for all other $[Cu(TNA)_2]\cdot 2H_2O$, $[Cu(TMA)_2]\cdot H_2O$ and $[Cu(PNA)_2]\cdot 3H_2O$ copper complexes. The complexes have been also employed to bind HS-DNA and such binding ability has been explored using diverse techniques. It is concluded that all these studies proved the HS-DNA binding of the complexes through the intercalation mode. Amongst all of them, $[Cu(TA)_2H_2O]\cdot H_2O$ complex, reveals the strongest DNA binding affinity. The amylase inhibition activity of Cu(II) complexes has also been studied. $[Cu(TMA)_2]\cdot H_2O$ complex is found to be an effective noncompetitive inhibitor of α-amylase.

References

A. A. Wasfi, et al. *International Journal of Pharmaceutics*, vol. 6, 2015, pp. 386-389.

A. M. Ahmed and M.A.M. Ibrahim. *Journal of Basic and Applied Sciences,* vol. 4, 2015, pp. 119-133.

A. Patra, et al. *Polyhedron*, vol. 1, 2013, pp. 156-163.

A. Rodger and B. Nordén. 3rd ed., *Oxford University Press,* Oxford; New York, 1997.

A. V. Gusakov, et al. *International Journal of Analytical Chemistry,* 2011, doi.org/10.1155/2011/283658.

A.A. Shanty, et al. "Synthesis, Characterization and Biological Studies of Schiff bases derived from Heterocyclic Moiety." *Bioorganic Chemistry,* vol. 70, 2017, pp. 67-73.

"American Diabetes Association (ADA)." *Diabetes Care*, vol. 27, 2004, pp. 94-102.

B. Macýas, et al. *Journal of Inorganic Biochemistry,* vol. 101, 2007, pp. 441-451.

B. N. Figgis. "Introduction to Ligand fields" *Interscience,* New York, 1996.

B. S. Creaven, et al. *Inorganica Chimica Acta,* vol. 363, 2010, pp. 4048-4058.

B. Subhra, et al. *Structural Chemistry,* vol. 19, 2008, pp. 115-121.

C. Mala, et al. *Inorganic Chemistry,* vol. 46, 2007, pp. 3072-3082.

D. L. Nelson and M. M. Cox, Lehninger. *Principles of Biochemistry,* 5th ed., W. H. Freeman, New York, USA, 2008.

E. Akila, et al. *International Journal of Inorganic and Bioinorganic Chemistry,* vol. 2, 2011, pp. 15-19.

G. Kumar, et al. *International Journal of Engineering, Science and Technology*, vol. 3, 2011, pp. 1630-1635.

G. L. Miller. *Analytical Chemistry,* vol. 31, 1959, pp. 426-428.

G. W. Zhang, et al. *Journal of Agricultural and Food Chemistry,* vol. 61, 2013, pp. 2638-2647.

I. A. Ogunwande, T. Matsui, T. Fujise, and K. Matsumoto. *Food Science and Technology Research,* vol. 13, 2007, pp. 169.

K. Jayakumar, et al. *Polyhedron.,* vol. 75, 2014, pp. 50-56.

---. *Spectrochim. Acta Mol. Biomol. Spectrosc.*, vol. 139, 2015, pp. 28-36.

K. Nakamoto. "Infrared Spectra of Inorganic and Coordination Compounds." *Wiley-Inter Science,* 2nd ed., 1963.

K. Rishu, et al. *Scientific Reviews and Chemical Communications,* vol. 3, 2013, pp. 1-15.

L. H. Abdel Rahman, et al. *International Journal of Nanotechnology,* vol. 2, 2015, pp. 79-95.

---. *Int. J. Nano. Chem.,* vol. 2, 2015, pp. 79-95.

---. *Journal of Photochemistry and Photobiology B: Biology,* vol. 160, 2016, pp. 18-31.

L. Milne, et al. *Archives of Biochemistry and Biophysics*, vol. 304, 1993, pp. 102-109.

L. Xiaoquan et al. *Talanta.,* vol. 73, 2007, pp. 444-450.

M. D. A. Maria et al. *Journal of Chemical and Pharmaceutical Research, Res.,* vol. 11, 2015, pp. 105-116.

M. T. Carter and A. J. Bard. *Journal of the American Chemical Society,* vol. 109, 1987, pp. 7528-7530.

N.H. Campbell, et al. *Journal of Medicinal Chemistry,* vol. 55, 2011, pp. 209-222.

N. Kavitha and P.V. Anantha Lakshmi. *Journal of Saudi Chemical Society,* vol. 21, 2017, pp. 457-466.

N. Ramasubbu, et al. *European Journal of Medicinal Chemistry,* 2004, pp. 271, 2517-2529.

P. J. Cox, et al. *Journal of Medicinal Chemistry*, vol. 16, 2009, pp. 6054-6062.

P. Sudha, et al. *BMC Complementary and Alternative Medicine,* vol. 11, 2011, pp. 11-15.

R. A. Thesingu and R. Natarajan. *Spectrochim. Acta Molecular and Biomolecular Spectroscopy*, 2014, pp. 127-292.

S. Kannan, et al*. Chem.,* vol. 692, 2007, pp. 3380-3391.

S. Kashanian, et al. *DNA Cell Biology*, vol. 31, 2012, pp. 1314-1348.

S. Shinde, et al. *Organic Communications*, vol. 7, 2014, pp. 60-67.

S. T. Syed and K. Geetha. *Indian Journal of Advances in Chemical Science, vol. 4,* 2016, pp. 40-48.

T. Aboul-Fadl, et al. *European Journal of Medicinal Chemistry.* vol. 45, 2010, pp. 4578-4586.

T. Alessio, et al. *Dalton Transactions,* vol. 42, 2013, pp. 11220-11226.

V. Narendrula, et al. *Journal Fluorescence,* vol. 26, 2016, pp. 1317-1329.

V. Rajendiran, et al. *Inorganic Chemistry,* vol. 46, 2007, pp. 8208-8221.

Synthesis and Characterization of Imidazole In-built Small Organic Compounds as Effective Antibacterial, Antifungal, Antioxidant Agents, Toxicity Assessment and Theoretical Evaluation for Promising In-vitro Enzyme Activity/ Anti-Viral/ADMET Parameters

G. Anjali Krishna
Research Scholar, Department of Applied Chemistry
Cochin University of Science and Technology
Kalamassery, Cochin-682022
Kerala, India, Email: anjalianju123krishna@gmail.com

T. M. Dhanya
Research Scholar, Department of Applied Chemistry
Cochin University of Science and Technology
Kalamassery, Cochin-682022
Kerala, India, Email: mdhanyat@gmail.com

Dr. Shanty A. A.
Assistant Professor, Department of Chemistry
St. Teresa's College (Autonomos) Ernakulam
Cochin-11, Ernakulam, Kerala, India
Email: shanty.sheen@gmail.com, shantyaa@teresas.ac.in.

Dr. P.V. Mohanan
Professor, Department of Applied Chemistry
Cochin University of Science and Technology
Kalamassery, Cochin-22, Ernakulam, Kerala, India
Email: mohan@cusat.ac.in

Abstract

A flexible class of imidazole based Schiff base ligands (1-2) were synthesized in present study via conventional approach. The synthesized compounds were taken for structural characterizations such as elemental analysis, UV-visible spectra, infrared spectra, ^{1}H NMR, ^{13}C NMR and LC-MS spectroscopy. The in-vitro antibacterial and antifungal activity of synthesized compounds have been tested in microorganisms like *Escherichia coli, Pseudomonas aeruginosa, Bacillus subtilis, Staphylococcus*

Contd... to next page

Keywords: *Schiff Base, Antibacterial, Antifungal, Antioxidant, and Molecular Docking.*

aureus, Aspergillus niger, Candida albicans by agar disk diffusion method. Imipenem and Miconazole were selected as reference drugs. The antioxidant activity of synthesized compounds was also screened by 1,1-diphenyl-2-picrylhydrazyl (DPPH) method. The structure activity relationship between the compounds has been investigated. The IC_{50} value of synthesized compounds was evaluated using α-Tocopherol as a standard antioxidant and promising outcomes were obtained. Encouragingly, all the compounds are generally non-toxic, to human breast adenocarcinoma cell lines (MCF-7). The in-vitro biological possibilities of these compounds were additionally endorsed through molecular docking studies. Additionally, in-silico ADMET studies were determined for all compounds.

One of the fascinating and appealing areas of modern medical science is Schiff base chemistry. The good ligands known as Schiff bases, which contain the azomethine group (-C=N-), were named after the Italian chemist Hugo Schiff in 1864. They are created when a primary amine is condensed with an aldehyde or ketone under particular conditions (A. Juan, et al. 467-73). There are several biological uses for Schiff bases with a diazole and phenol ring, including antifungal (A. A. Shanty, et al. 67-73), anti-oxidant (M. A. Mokhales, et al. 85-96), anti-bacterial (K. V. Shuvaev, et al. 4583-86), anticancer (Z. Bingchang, et al. 13620-31), anti-inflammatory (A. K. Pandey, et al. 41-43), and antipyretic (R. P. Chinnasamy, et al. 342-47). Particularly, imidazole, a subclass of the azole family that contains two nitrogen atoms, serves as the structural core of a variety of natural compounds and biological frameworks (K. Shalini et al. 1-36). They stand out for having a wide range of toxicological characteristics and playing a crucial role in several biochemical cycles (H. Bhawar, et al. 189-194) and (F. Bellina, et al. 4571-624).

As a result, illnesses brought on by bacteria or fungi are commonly considered normal, and the fatality rate associated with microbial diseases increases over time (M. Patra, et al. 6350-58). Because bacteria are resistant to anti-toxins, the primary cause of infectious diseases including cholera, pneumonia, influenza, typhoid, tuberculosis, measles, and others is the lack of restorative care (B. Naureen, et al. 129946). Therefore, it is required to develop new antibacterial drugs. Therefore, experts have been researching new antimicrobial drugs to enhance bacterial and fungal blockage for the past several years (C. M. da Silva, et al. 1-8). On the other hand, antioxidant agents primarily act as electron acceptors or hydrogen donors at the responsive site to neutralize free radicals. They can serve as cancer-preventive agents because of their well-known capacity to protect organisms and cells from damage brought on by oxidative stress. New compounds that are either integrated into existing compounds or obtained from common sources and may provide active chemicals to counteract the effects of oxidative stress on cells are inspiring researchers in a variety of fields (C. M. da Silva, et al. 1-8), (A. C. Bustamante, et al. 5445-59), (N. Dharmaraj, et al. 3617-24), and (C. Basu, et al. 3617-24). In the literature, several mechanisms and synthesis methods for evaluating the antioxidant activity of heterogeneous ring derivatives employing hydrogen peroxide (H_2O_2), nitric oxide (NO), and DPPH radicals have been described (Halliwell 23-27). Numerous natural and synthetic antioxidants have been studied, and a variety of methods have been used to assess their antioxidant ability (K. L. Liao, and M.C. Yin 2266-70). Therefore, it is crucial to understand how these antioxidant molecules function (M. Kumar, et al. 322-28). Therefore, more thought must be given to the development

of novel beneficial drugs to counteract the influence or injury caused by free radicals (K. Tsai, et al. 1465-72), C. S. Rivas, et al. 330-38), (T. S. Kamatchi, et al. 16428-43), and (J. K. Barton, et al. 2172-76). Additionally, there are currently very few reports on imidazole-related Schiff bases' strong antibacterial and antioxidant activity. Therefore, the idea of synthesizing tiny chemical molecules with an imidazole unit is currently of tremendous interest to researchers.

Therefore, in this regard, we have made an effort to create two novel heterocyclic imidazole-based Schiff bases that can inhibit the growth of microbes and act as powerful antioxidants to reduce damage from free radicals (A. A. M. Abdel-Aziz 614-26) and (A. Prakash and D. Adhikari 1891-96). Here, we have announced the traditional methods for creating imidazole-derived organic compounds, steps 1-2, and have screened their efficacy in antibacterial, antifungal, antioxidant, and toxicity tests in-vitro. Additionally, in this work, we have determined a docking study of compounds to connect them with their future scope as in-vitro enzyme and antiviral activities and assessed the binding energy which was compared with imidazole containing known drugs. For the drug likeness prediction, in-silico ADMET parameters were executed for each molecule simultaneously.

2. Experimental Section

2.1 Materials and Physical Measurements

From Sigma Aldrich, we obtained 4-amino-phenol, 2-amino-4-methyl phenol, and imidazole-2-carboxaldehyde. All of the compounds employed were of the highest purity and weren't further purified before usage. The solvents employed were either 99% pure or had undergone recognized research procedures (Vogel's 1989). Thermo Scientific Evolution 220 spectrophotometer was used to capture electronic spectra in methanol in the 200-800 nm region. Using KBr pellets, FT-IR spectra of the compounds were taken on a JASCO-4100 spectrometer in the 400–4000 cm^{-1} range. The elemental analysis of all the compounds was carried out using an Elementar Vario EL III CHN analyzer. Using a Bruker AMX 400 FT-NMR Spectrometer, DMSO-d_6 as the solvent and TMS as the internal standard, ^{1}H and ^{13}C NMR spectra were captured. For routine LC-MS testing, a Waters 3100 Mass Detector using the ESI technique was utilized.

2.2 Synthesis of Schiff bases: *1H-Imidazole-2-carboxaldehyde and 5-Methyl-3H-imidazole-4-carboxaldehyde derivatives* (1-2)

A solution of imidazole carboxaldehyde (10 mmol) in 20 mL methanol was progressively added before a suitable quantity of matching aromatic amines (10 mmol) was added. To speed up the reaction, a few drops of glacial acetic acid were added to the previously mentioned combination. For 12 hours, the matching coloured solutions were refluxed with constant stirring. At room temperature, the produced colourful solutions progressively dissipated. After being washed numerous times in different solvents, the product was dried in a vacuum over anhydrous $CaCl_2$ after the coloured precipitate was recrystallized from methanol. Utilizing TLC, the compound's purity was evaluated.

2.2.1 Synthesis of Schiff base of imidazole-2-carboxaldehyde and 4-amino phenol: *4-[(1H-Imidazole-2-ylmethylene)-amino]-phenol* (1)

Equimolar amounts of 4-amino phenol and imidazole-2-carboxaldehyde were combined, heated under reflux for 12 hours, and then combined. The resulting yellow solution eventually started to dissipate. After adding anhydrous ether, a brown precipitate was formed that was later recrystallized from methanol and dried. Additionally, the compound's purity was examined.

Brown Solid. Yield 85%, mp 213°C. UV-Vis spectrum, nm: 289 (π-π*), 340 (n-n*). IR spectrum, υ, cm^{-1}: 3400 (O-H), 1622 (-HC=N), 1587 (-C=N ring). ^1H NMR (300 MHz, DMSO-d_6) δ in ppm: 9.57 (s, 1H, imine), 8.38 (s, 2H, imidazole ring), 6.78-7.22 (m, 4H, aromatic ring); ^{13}C NMR (100 MHz, DMSO-d_6) δ in ppm: 163.69 (C=N), 157.06 (C-OH), 142.64 (ArC), 137.07 (Imidazole C), 125.43; 125.13 (Imidazole C), 122.90; 122.65 (ArC), 116.63;116.28 (ArC). MS (m/z): 187.07 (M^+). Anal. calc. for $C_{10}H_9N_3O$ (%): C, 65.16; H, 5.05; N, 23.45, O, 7.45. Found: C, 64.16; H, 4.85; N, 22.45, O, 8.55.

2.2.2 Synthesis of Schiff base of imidazole-2-carboxaldehyde and 2-amino-4-methyl phenol: *2-[(1H-imidazole-2-ylmethylene)-amino]-4-methyl-phenol* (2)

Equimolar amounts of 2-amino-4-methyl phenol and imidazole-2-carboxaldehyde were combined, then refluxed for 12 hours in methanol. At room temperature, the solution steadily evaporated. The resultant yellow coloured precipitate was repeatedly washed with methanol, and then the pure chemical was recrystallized.

Yellow Solid. Yield 81%, mp 221°C. UV-Vis spectrum, nm: 296 (π-π*), 363 (n-n*). IR spectrum, υ, cm^{-1}: 3400 (O-H), 1624 (-HC=N), 1589 (-C=N ring). ^1H NMR (300 MHz, DMSO-d_6) δ in ppm: 9.78 (s, 1H, imine), 7.80 (s, 2H, imidazole ring), 6.49-7.26 (m, 3H, aromatic ring), 2.07 (s, 3H, methyl); ^{13}C NMR (100 MHz, DMSO-d_6) δ in ppm: 162.03 (C=N), 148.99 (C-OH), 138.78 (ArC), 136.71 (Imidazole C), 131.04 (ArC), 128.26 (ArC), 124.06 (ArC), 122.96;122.64 (Imidazole C), 117.05 (ArC), 21.15 (Methyl C). MS (m/z): 201.4 (M^+). Anal. calc. for $C_{11}H_{11}N_3O$ (%): C, 64.08; H, 4.91; N, 22.23, O, 7.95. Found: (%): C, 64.98; H, 5.01; N, 21.23, O, 7.35.

2.3 Antibacterial/Antifungal Activity

2.3.1 Agar Disk Diffusion Method

The agar disk diffusion method was used to carry out antibacterial screening on synthetic compounds. The agar disk diffusion method is typically used to assess how well synthetic compounds work against a particular bacterium. An agar plate was first incubated with microbes, followed by paper disks of compounds. This method is used to determine the best compound to use against a new or drug-resistant pathogen. One virgin colony was put aseptically into 10 mL of nutritional broth, which was then heated to 37°C. *Escherichia coli, Pseudomonas aeruginosa*, *Bacillus subtilis*, and *Staphylococcus aureus* bacteria were uniformly swabbed onto each of the sterile MHA plates. On PDA plates, fungus colonies including *Aspergillus niger* and *Candida albicans* were swabbed. On the disc covering the agar plates, test samples in the amount of 20 L were added. The PDA was retained for an appropriate 48 hour time for growth while the MHA plates were incubated at 37°C for 18 hours. After incubation, the inhibitory zones surrounding each plate were measured in terms of their diameter in cm. As reference medications, Imipenem and Miconazole were employed, and methanol served as the control solvent. Each test was run three times or in duplicates (E. A. Elzahany, et al. 210-22).

2.3.2 Minimum Inhibitory Concentration (MIC)

2.3.2.1 Resazurin based Microtiter Dilution Assay (RMDA)

The minimal concentration at which an antibiotic will prevent a microbe from growing visibly during 24 hour incubation is known as a "MIC." The smallest concentration that will stop microbial growth after being cultivated on antibiotic-free media is the bactericidal or fungicidal concentration. Here, RMDA was used to record a

quantitative assessment of the test compound's antimicrobial activity. 96-well HiMediamicrotitre plates were used for RMDA under specific conditions. 100 L of test materials that had been dissolved in sterile water were loaded up on the main row of microtiter plates. 50 L of Luria stock was placed in each of the microtitre plate wells. By starting to transfer 50 L of the test material from the main row to the succeeding wells in the next line of a comparable segment such that each well has 50 L of test material in increasing concentrations, two-fold sequential dilution (across the column) was acknowledged. Each well contained a 2 L marker solution of resazurin. Finally, 10 L of the microbial suspension was taken and then added to each well to achieve a final concentration of 5×10^6 CFU/mL. Each plate was liberally coated in stick film to prevent the drying of the microbial culture and to ensure that the bacteria didn't become dried out. A total of three controls were present on each microtitre plate: (a) a segment containing Imipenem/Miconazole as a positive control, (b) a segment containing all solutions minus the test substance, and (c) a segment containing all solutions minus the microbiological solution minus 10 L of Luria broth. The plates underwent 24 hours of hatching at 37°C. Then someone outside noticed the well's exterior colour shift. Any shift in colour from purple to pink or colourlessness was seen favourably. The MIC value was determined as the lowest sample concentration at which there was no change in colour. All of the tests were administered in triplicate. For the MIC of the test substance, average values were established (K. Shanker, et al. 205-211).

2.4 Antioxidant Activity Screening

2.4.1 DPPH Radical Scavenging Assay

In the current study, the 1,1-diphenyl-2-picrylhydrazyl (DPPH) radical scavenging screening determined the antioxidant activity of the synthesised compounds (1-2). The spectrophotometric mechanism of DPPH tests led to the quenching of stable coloured radicals. It demonstrates how antioxidants can still scavenge free radicals even in complex biological combinations. The decrease in absorbance at 517 nm, which corresponds to the DPPH free radical, can be used to screen the produced compounds for their ability to scavenge free radicals. The colourless DPPH-H product is produced when a coloured free radical combines with a scavenger DPPH. As a stock solution, each sample (1-2) was dissolved in methanol (mg/mL). To prevent deterioration from light, it was stored in the refrigerator wrapped with foil. A suitable amount of compounds were quantitatively transferred from the stock solutions to the DPPH solution (1 mg/100 mL) and brought up to the volume of 3 mL using methanol. After 20 minutes, a UV-Vis spectrophotometer was used to measure the test compounds' absorbance at 517 nm. For comparison purposes, the same absorbance measurements were also taken with a control solution that contained DPPH and methanol but no test samples. Tocopherol was utilized as the reference. Assays are repeated in duplicate for every sample. The following phrase (P. Kavitha, et al. 159-68) can be used to get the radical scavenging percentage.

% DPPH radical scavenging = 100 x [(Absorbance of sample blank–Absorbance of sample + DPPH)/ Absorbance of sample blank]

By utilizing linear regression analysis to plot a curve between concentrations and % inhibition, it was possible to determine the concentration of the compound needed to scavenge the DPPH radical. For each molecule that demonstrated the required activity, the IC_{50} (half maximal inhibitory concentration) value, the sample concentration needed to scavenge 50% of DPPH free radicals was determined from the graph.

2.4.2 H_2O_2 Radical Scavenging Assay

Hydrogen peroxide (H_2O_2) might go into the human body through the internal breaths of smoke or haze and eye or skin contact. H_2O_2 starts lipid peroxidation by the quick deterioration into oxygen and water and this might deliver hydroxyl radicals (OH^-) and cause DNA harm in the body. The capacity of prepared compounds to scavenge H_2O_2 can be assessed by setting up a solution of H_2O_2 (30 mM) in phosphate buffer (40 mM pH 7.4). The concentration of H_2O_2 was determined at 230 nm using a UV-Vis spectrophotometer. The mixtures in a methanol-water solvent were added to H_2O_2 and absorbance at 230 nm in every 10 minute up to 1 hr was recorded. A clear solution containing phosphate buffer or methanol-water without H_2O_2 and a control solution without all compounds were likewise taken. The level of hydrogen peroxide scavenging is determined as follows (B. H. Babu, et al. 272-77).

% H_2O_2 radical scavenging = 100 x [(Absorbance of control–Absorbance of test)/Absorbance of control]

The required concentration of compound to scavenge H_2O_2 radical was obtained from a graph by plotting a curve between concentrations and % inhibition.

2.4.3 NO Radical Scavenging Assay

NO radical is produced in natural tissues by the method of the specific enzyme nitric oxide synthase. The compound sodium nitroprusside is known to deteriorate in aqueous arrangements at physiological pH (7.2) conveying NO radical. Additionally in presence of oxygen, NO radical gives out nitrates and nitrites. Sodium nitroprusside (20 mL) dissolved in 0.5mL phosphate buffer (30 mL pH 7.4) was mixed with 0.5 mL of samples at different concentrations. The mixture was then incubated at 25°C for 2 hr. After incubation, 0.5 mL of the solution was taken out and mixed with 0.5 mL of Griess reagent (M. N. Peyrat-Maillard, et al. 709-16). The absorbance of the samples was estimated at 546 nm. The amount of nitric oxide (%) scavenging was obtained from the following expression.

% NO radical scavenging = 100 x [(Absorbance of control–Absorbance of sample)/Absorbance of control]

The minimum concentration of compound to scavenge NO radical was obtained from a graph by plotting a curve between concentrations and % inhibition.

2.5 In-vitro Cytotoxicity

2.5.1 MTT Assay

Mouse 3T3L1 preadipocytes cells were permitted to fill in Dulbecco's Modified Eagle's Medium (DEM) and spread in 96 well plates at a thickness of 5 x 10^3 cells/well and incubated at 37°C in presence of 5% CO_2 for 24 h preceding the addition of prepared compounds. The cells were then treated with various concentrations (10, 50, 100, 150 and 200 μM) of mixtures disintegrated in DMSO and incubated at 37°C for 24 h in presence of 5% CO_2. The triplicatewas done. After 24 hr, a grouping of 50 μg/well MTT was added and incubated in a CO_2 incubator. The functioning solution of MTT was ready in Hank's Balanced Salt Solution (HBBS) without phenol red. After 2-3 h, the formazans framed were seen under a phase contrast magnifying lens. The crystal was solubilized by adding DMSO and further incubated at 20 min at 37°C in dark. After solubilisation, the plate was read at anabsorbance of 570 nm. Control tests were cells without any treatment. The percentage (%) cell viability of control cells was kept at 100% (M. Houdkova, et al. 56-62). The general cell viability (%) was determined as,

% cell viability = (100-Absorbance of treated / Absorbance of control) x 100

2.6 Molecular Docking Study

The molecular docking approach can be utilized to display the association between a small molecule and a protein at the nuclear level, which permits us to describe the behaviour of small molecules in the active site of target proteins just as to clarify basic biochemical processes (B. J. McConkey, et al. 845-55). In the present work, we would like to elucidate the docking parameters of synthesized compounds toward potent enzyme and antiviral activity 5 (PDB ID: 1HD2) and severe acute respiratory syndrome coronavirus 2 (PDB ID: 6WTT) were selected for checking enzyme activity and antiviral activity, respectively which were downloaded from the RCSB protein data bank. Docking software is preferred to collect proteins from a protein data bank with a resolution of no more than 2.5 A°. The unwanted moieties like water or hetero atoms associated with the enzyme were cleaned using Pymol Visualization software. The structure of synthesized compounds was optimized using Density Functional Theory based on the B3LYP method along with the 631G (d, p) basis set. The optimized structures were visualized using Chemcraft version 1.6 packages and Gauss View version 5.0.9 with proper 3D orientation (G. G. Mohamed and Z. H. Abd El-Wahab 1059), (R. Dennington, et al. 2009), and (G. M. Morris, et al. 2785). Thus we obtained the energy, bond angle and bond length parameters via DFT calculations. The synthesized compounds were converted to PBD files using Open Babel software and to PDBQT files using Autodock 4.2 software. The docking algorithm provided with Auto Dock Vina was utilized to look for the best docked conformation among compounds and proteins. The conformations with the most favourable free binding energy were chosen for investigating the interactions between the target receptor and compounds by the Discovery studio visualizer.

2.7 In-silico ADMET Prediction Study

To be viable as a drug, a powerful molecule should arrive at its target in the body in adequate concentration, and stay there in a bioactive form long enough for the normal biologic process to happen. Drug development involves the evaluation of absorption, distribution, metabolism, excretion and toxicity progressively earlier in the discovery process, at a stage when considered

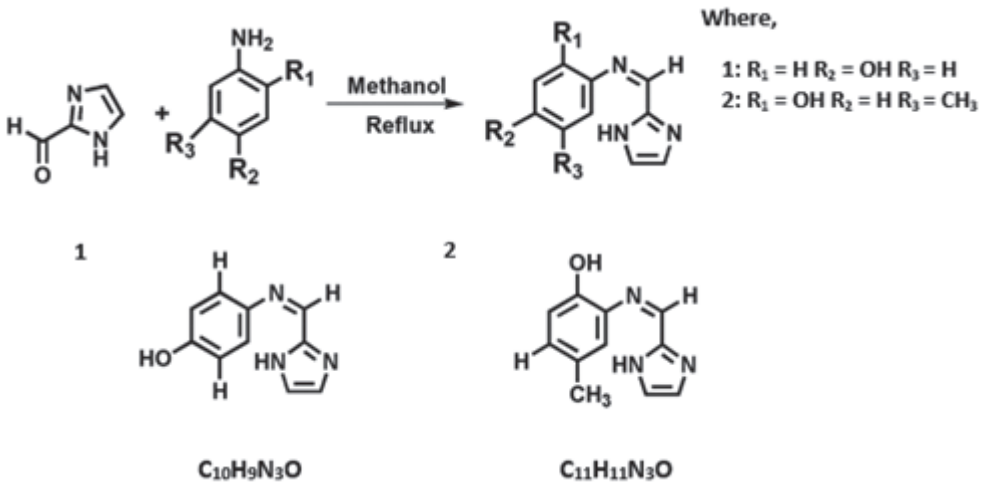

Scheme 1 - Synthesis of Schiff bases 1-2

compounds are numerous but access to the physical samples is restricted. Here, we present the new Swiss ADMET web tool that gives free access to a pool of quick yet powerful predictive models for physicochemical properties, pharmacokinetics, drug-likeness and medicinal chemistry (C. A. Lipinski, et al. 3-25). ADMET prediction requires a model, to sum up a set of unseen drugs that are structurally distant from the known drug set. The results from in-silico ADMET prediction analysis propose that the obtained compounds follow the Lipinski rule of 5 for parameters like molecular weight (MW), octanol/water partition coefficient (Clog P), number of hydrogen bond donors (HBD) and number of hydrogen bond acceptors (HBA) (P. Ertl, et al. 3714-17). Drug-likeness model score was calculated by Molinspiration software (www.molinspiration.com).

3. Results and Discussion

The synthesized imidazole based Schiff bases, 1–2 are provided in Scheme 1. All the non-substituted imidazole derivatives were characterized well and obtained good yields. All the Schiff bases are crystalline, coloured and non-hygroscopic in nature. Compounds were completely miscible in solvents such as chloroform, methanol, DMF and DMSO but insoluble in water. Melting points were in the range of 213–225°C. Thin layer chromatography (TLC) was used to monitor the progress of the reaction in hexane: ethyl acetate (9:1).

3.1 Antibacterial/Antifungal Activity Screening

The Agar disk diffusion method was followed for the screening of the antimicrobial activity of synthesized compounds. First, we investigated the antibacterial property of compounds and microorganisms used for the analysis including *Escherichia coli* and *Pseudomonas aeruginosa*, *Bacillus subtilis* and *Staphylococcus aureus*. Among them, *Escherichia coli*, *Pseudomonas aeruginosa*is gram negative and *Bacillus subtilis* and *Staphylococcus aureus* are gram positive pathogens. The MIC value was evaluated for compounds that showed better antibacterial activity. Imipenem was used as reference antibiotic. The antibiogram of synthesized compounds is shown in Figure-1, where the labels IP and IMP in the plate were assigned to compounds 1-2, respectively. The disk diameter of the zone of inhibition and the MIC values for the synthesized compounds are presented in Tables-1 and 2. Compound 1 showed better activity on the bacteria *Escherichia coli*, while 2 showed some moderate activity. Also, compounds 1 and 2 resulted in the best activity against *Pseudomonas aeruginosa* while compounds 1 and 2 showed some moderate activity against *Staphylococcus aureus*. Coming to *Bacillus subtilis*,

Table-1: Antimicrobial activities of Schiff bases

Microbe	Zone of Inhibition (cm)	
	1	**2**
Escherichia coli[a]	1.5	0.7
Pseudomonas aeruginosa[a]	1.2	0.9
Bacillus subtilis[b]	0.9	1.0
Staphylococcus aureus[b]	0.9	1.2
Aspergillus niger[c]	0.8	-
Candida albicans[c]	1.0	0.9

'-' No activity, a - Gram negative, b - Gram positive bacteria, and c - Fungal species

compounds 1-2 exhibited significant activity. From the results, all the Schiff bases exhibited remarkable effects against four bacterial strains. Although, compound 2 is the best candidate for antibacterial assay.

Next, we considered the same compounds for antifungal screening. Miconazole was used as the reference drug. *Aspergillus niger* and *Candida albicans* were the selected antifungal strains used for the analysis. Compound 2 has outstanding performance against the fungal species with a higher zone of inhibition. Compound 1 was active against *Aspergillus niger* while compounds 1 and 2 were found to be active against *Candida albicans*. All the compounds registered comparable activity against the reference standards. The contradictions in the adequacy of different compounds against selected organisms rely either on the impermeability of the cells of the organisms or contrasts in the ribosomes of microbial cells.

Inhibition of microbial development was not seen with *Escherichia coli*, conceivably because of the presence of an external defensive layer called lipopolysaccharide. The external layer gives an extra fortress to the cell lines, restricting the concentration of test compound gushing through the bacterial cell wall (C. B. Arjun, 33-37). In addition, the inactivity of compounds towards the fungal species is mainly because of the simulated environment. Hence, we concluded that imidazole incorporated molecules hold great promise to discover new antimicrobial agents.

Table-2: MIC values (mg/mL) for the Schiff bases

Microbe	1	2	Imipenem	Miconazole
Escherichia coli	0.040	0.035	0.10	-
Pseudomonas aeruginosa	0.025	0.08	0.05	-
Bacillus subtilis	0.20	0.10	0.15	-
Staphylococcus aureus	0.35	0.15	0.05	-
Aspergillus niger	-	0.25	-	0.15
Candida albicans	0.10	0.065	-	0.10

3.2 Antioxidant Activity

In-vitro antioxidant activity for all synthesized compounds was experimentally done by DPPH, H_2O_2 or NO method. A graph was plotted against concentration versus % of inhibition for all compounds via the DPPH method is depicted in Figure-2. The calculated IC_{50} value for each compound by three methods is tabulated (Table-3) and compared with a natural antioxidant α-Tocopherol. Experiments were repeated thrice for accuracy.

In the set of three imidazole linked organic compounds, all the compounds showed better radical scavenging activity. All three methods are more suitable for the better activity of samples which was retrieved from IC_{50} values. The DPPH

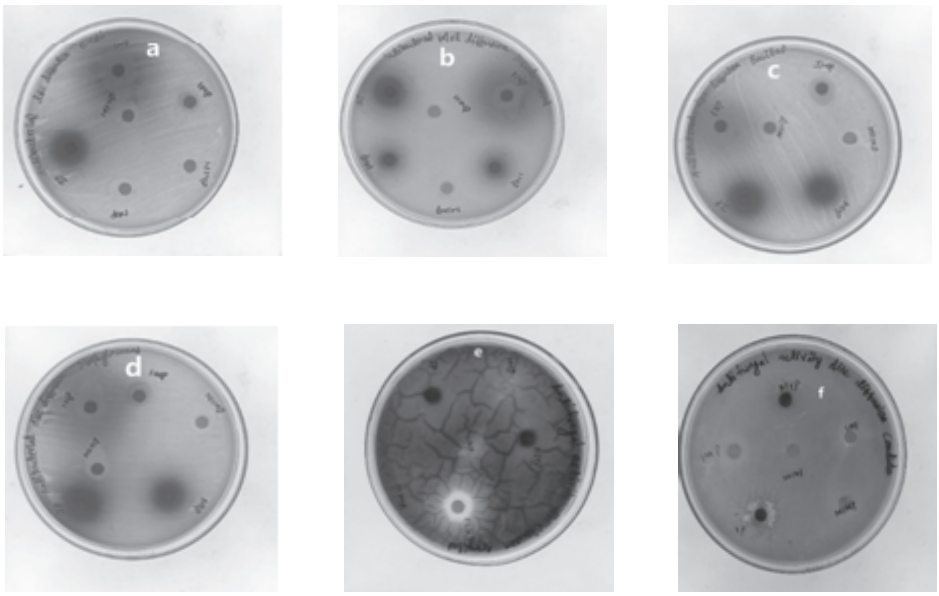

'a'- Escherichia coli, 'b'- Pseudomonas aeruginosa, 'c'- Bacillus subtilis, 'd'- Staphylococcus aureus, 'e'- Aspergillus niger, ' f '- Candida albicans

Figure-1: Antibiogram of 1-2 Schiff bases

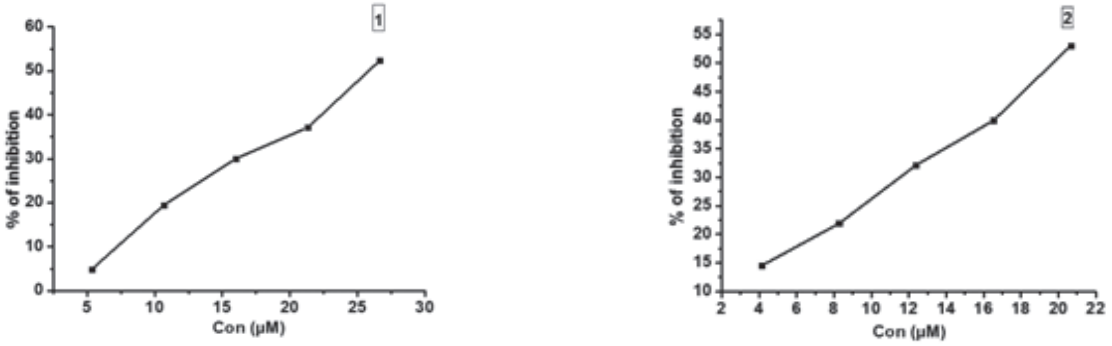

Figure-2: Antioxidant Activity of Schiff bases 1-2 by DPPH method

Table-3: Radical scavenging capacities of compounds with IC_{50} values by DPPH, H_2O_2 and NO method

Compound	IC_{50} (μM) Methanol-Water Media (Fixed Reaction Time, 30 min)		
	DPPH	H_2O_2	NO
1	26.04 ± 0.003	28.05 ± 0.001	30.05 ± 0.006
2	20.07 ± 0.001	26.87 ± 0.003	25.98 ± 0.007
α-Tocopherol	221.5 ± 0.002	248.50 ± 0.001	236.05 ± 0.003

method is a somewhat little more best method with lower IC_{50} values for all compounds rather than other methods. A lower IC_{50} value is advisable for better antioxidant activity. The presence of a hydroxyl group in its structure is the reason for the selective activity. Also, the starting compounds have a hydroxyl group in their structure, so we find out the IC_{50} values of all starting materials such as aldehydes and substituted phenols, and saw IC_{50} values in the region of 60-80 μM which was quite higher than synthesized compounds again confirming the biological significance imine functionality within it. The compounds inhibit the DPPH radical in a concentration dependent way. Phenolic compounds may ionize in methanol due to the high dielectric constant of methanol resulting in the abstraction of H^+ forming phenoxide ion. The phenoxide ion is a strong electron donor than phenol and can rapidly donate its electrons to the DPPH radical (L. Jing, et al. 5744-47). The result indicates that all the synthesized compounds have lower IC_{50} values than that of the standard compounds and compound 2 with one methyl group showed higher activity than compound 1. Among them, nitro substituted compounds have shown very weak radical scavenging activity since it is an electron withdrawing group. Proton donation followed by electron delocalization in the aromatic ring and the presence of an imine group hence supported the better antioxidant activity and structure activity relationship in compounds (M. Leo-poldini, et al. 288-306).

3.3 In-vitro Cytotoxicity

Cell viability is the prominent parameter in order to check whether cells converts MTT into purple coloured formazan compounds with absorbed in the 570 nm region. When the cells die, they lose the ability to convert MTT into formazan. The percentage cell viability results of imidazole inbuilt organic compounds (Table-4) against 3T3L1 cells by MTT assay indicates that all are non to mild toxic in four different concentrations. All the ligands exhibited 100% cell viability against normal 3T3L1 cells. Compounds 1 and 2 showed low toxicity even at lower and higher concentrations.

Table-4: Cytotoxicity studies of the synthesised compounds by MTT Assay

Compound	Cell	10 μM	50 μM	100 μM	150 μM	200 μM
1	3T3L1	100	100	100	100	100
2	3T3L1	100	100	100	100	100

3.4 Molecular Docking Studies

Molecular docking studies is a theoretical approach done prior to the experimental sections in order to understand the capacity of compounds to act as biological agents. Here, we need to analyse the in-vitro enzyme activity and antiviral properties of all compounds against the proteins, 1HD2 and 6WTT. The optimized structures of compounds 1-2 (Figure-3) were docked into the active site of the proteins and evaluated the binding scores. In-vitro enzyme activity was compared with a reference standard α-Tocopherol which is a natural antioxidant and antiviral properties were compared with a set of imidazole bearing five FDA approved drugs used for the treatment of various viral diseases (Table-5).

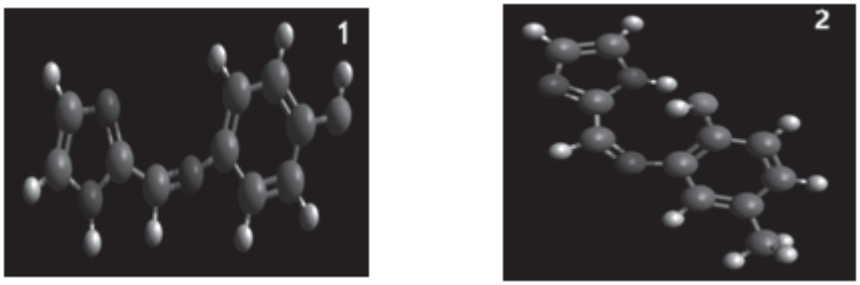

Figure-3: Optimized structures of Schiff bases 1-2

Table-5: Binding scores of compounds towards the enzyme 1HD2

Compound	Binding score (Kcal/mol)	Interaction of amino acid residue
1	-5.5	H-bond, electrostatic
2	-6.1	H-bond, electrostatic
α-Tocopherol	-3.9	H-bond, electrostatic

The compounds were superimposed in the active site of the enzyme as shown in Figure-4. The compounds are capable of binding with the 1HD2 enzyme thereby activating the enzyme more effectively than the natural antioxidant, α-Tocopherol. 1HD2 human enzyme is not that active to fight against free radicals formed due to some oxidative cleavages inside the tissues and will result in diabetic condition. So our synthesized compounds are able to enhance the activity by binding with the active site of protein thereby reducing the risk of diabetes. The lower the binding energy, the higher the possibility of synergic interaction between synthesized compounds and target enzyme. Hence all the compounds bearing the OH group could interact more effectively in the active pocket of the enzyme and thereby enhancing its activity. The methyl rich compound gives better binding energy as compared to others due to an additional alkyl interaction. Finally, strong hydrogen bonding and hydrophobic interactions for all compounds with the target protein was noticed (Figure-5).

Figure-4: The Compounds 1-2 are present in the binding cavity of enzyme

Figure-5: 2D Interaction diagram for all compounds

Evaluation of the potency of compounds as antivirals has been done in SARS-CoV-2 (COVID-19). Five sets of FDA approved drugs, Acyclovir (-6.3 Kcal/mol), Ganciclovir (-6.8 Kcal/mol), Penciclovir (-6.6 Kcal/mol), Valaciclovir (-7.0 Kcal/mol) and Deoxyguanosine (-7.5 Kcal/mol) were taken for the comparative study since they possess imidazole unit. The docking results of six synthesized compounds exhibited a good docking score and interacted with binding pockets of amino acids in 6WTT (Figure-6) in a similar fashion. The ligand-protein interactions of synthesized compounds are highlighted in Table-6. Our designed compounds formed hydrogen bond with amino acid chains like GLN:107, ASN:84, PRO:108 and GLN:83. Among the H-bond interactions, GLN:107 and ASN:84 are common to the majority of compounds. Finally, we could reach the conclusion that all the synthesized compounds exhibited the best docking score and will act as the best antiviral candidates in the future for curing viral attacks more effectively than standard drugs.

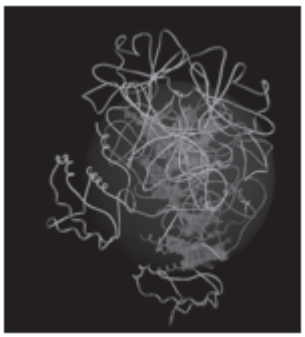

Figure-6: Active site of protein 6WTT

Table-6: Binding scores and possible interactions of synthesized compounds 1-2 with 6WTT

Compound	Binding Energy (Kcal/mol)	Hydrophobic interaction	Residues involved in Hydrogen bond formation
1	-6.2	PRO:108, VAL:202, ILE:249, HIS:246	GLN:107, ASN:84
2	-7.1	THR:201, GLU:240, GLY:109, ILE:249, ASN:180, VAL:202, ILE:200, GLN:83, GLN:107, GLN:110, ASP:245	PRO:108, ASN:84

3.5 In-silico ADMET prediction study

The compounds need to achieve clinical progress because of their inadequate absorption, distribution, metabolism, elimination and toxicity but many compounds failed to have it. So, a theoretical study of synthesized compounds 1-2 was carried out for evaluation of ADMET properties and the values obtained are tabulated (Table-7). Polar surface area (Mol PSA), number of stereo centres (n-SI), molecular volume (Mol V), blood brain barrier (BBB), the logarithm of compound aqueous solubility (Clog S), drug model score (DMS) and Lipinski's rule of five (MW ≤ 500, Clog P ≤ 5, HBD ≤ 5 and HBA ≤ 10) were examined. All the synthesized compounds showed significant permeation and none of the compounds violated Lipinski's rule of five. Hence, the synthesized compounds satisfy the standard for orally active drugs and can be additionally exceptional as oral drug candidates. The results of this in-silico ADME prediction analysis propose that the obtained compounds follow the computational assessment and thus indicate a pharmacologically active framework that should be considered on progressing further potential hits. All the compounds were shown better drug-likeness scores.

Table-7: Pharmacokinetic parameters (ADMET) of synthesized compounds 1-2

Entry	Mol PSA (A^2)	n-SI	Mol V (A^3)	BBB	Clog S	MW (g/mol)	Clog P	HBD	HBA	DMS
1	47.43	0	173.74	4.41	-0.97	187.07	0.99	2	3	-0.70
2	45.66	0	196.33	4.56	-1.27	201.09	1.93	2	3	-0.70

4. Conclusion

In this present work, we synthesised and characterized three imidazole based organic compounds. We applied the conventional method for the synthesis with significant yield. The biological evaluation of compounds was performed and the antibacterial, antifungal and antioxidant capacities of compounds were investigated. In particular, antimicrobial studies exhibited the best results for the synthesized compounds. Some compounds are specific toward the antifungal activity as shown by their efficacy against different fungal species. Also, almost all the synthesized compounds exhibited excellent antioxidant properties due to the presence of the hydroxyl group in the aromatic ring hence supporting the structure activity relationship. In-vitro cytotoxicity studies showed that all compounds are non-toxic in nature. A theoretical approach for the prior evaluation of in-vitro enzyme activity and antiviral properties of all the compounds could be done via molecular docking studies and favourable binding scores were obtained. In-silico ADMET prediction and drug likeness model score were performed. From the inferences, the synthesized compounds could act as a better drug candidates in the future and be useful for the investigation of new biological agents.

Conflict of Interest

The authors have declared no conflict of interest.

Acknowledgement

All the authors are thankful to Cochin University of Science and Technology, Kerala, India for providing the Senior Research Fellowship. Authors also acknowledge to Dr. Susmita De, Cochin University of Science and Technology, Kerala, India for optimization studies.

Appendix A. Supplementary Data

UV-Vis, FT-IR, ^{1}H NMR, ^{13}C NMR and LC-MS spectra of the Schiff bases 1-2 are provided in the supplementary information.

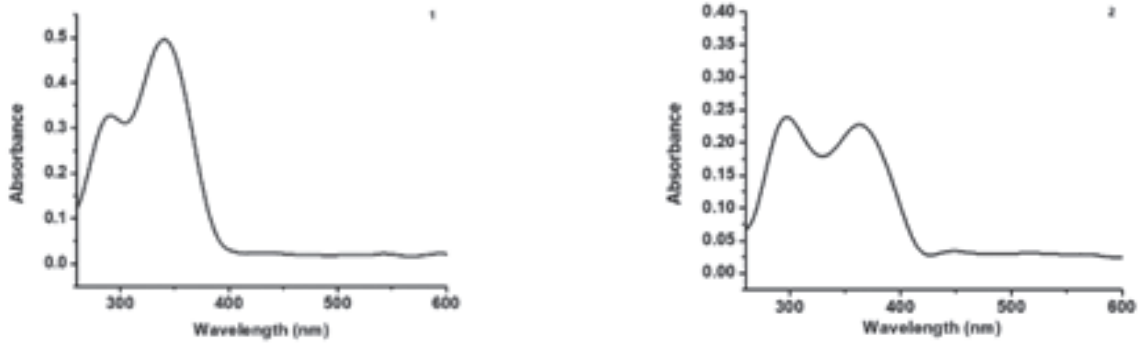

Figure-S1: UV-visible spectra of Schiff bases 1-2

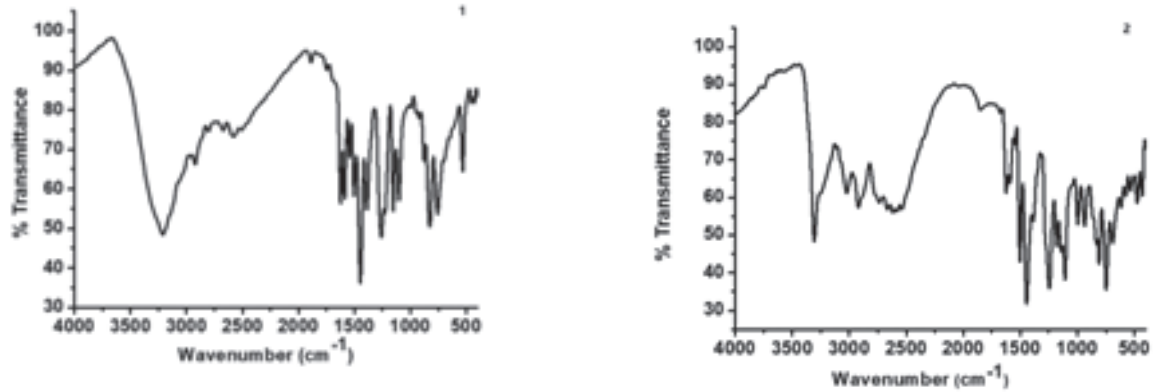

Figure-S2: FT-IR spectra of Schiff bases 1-2

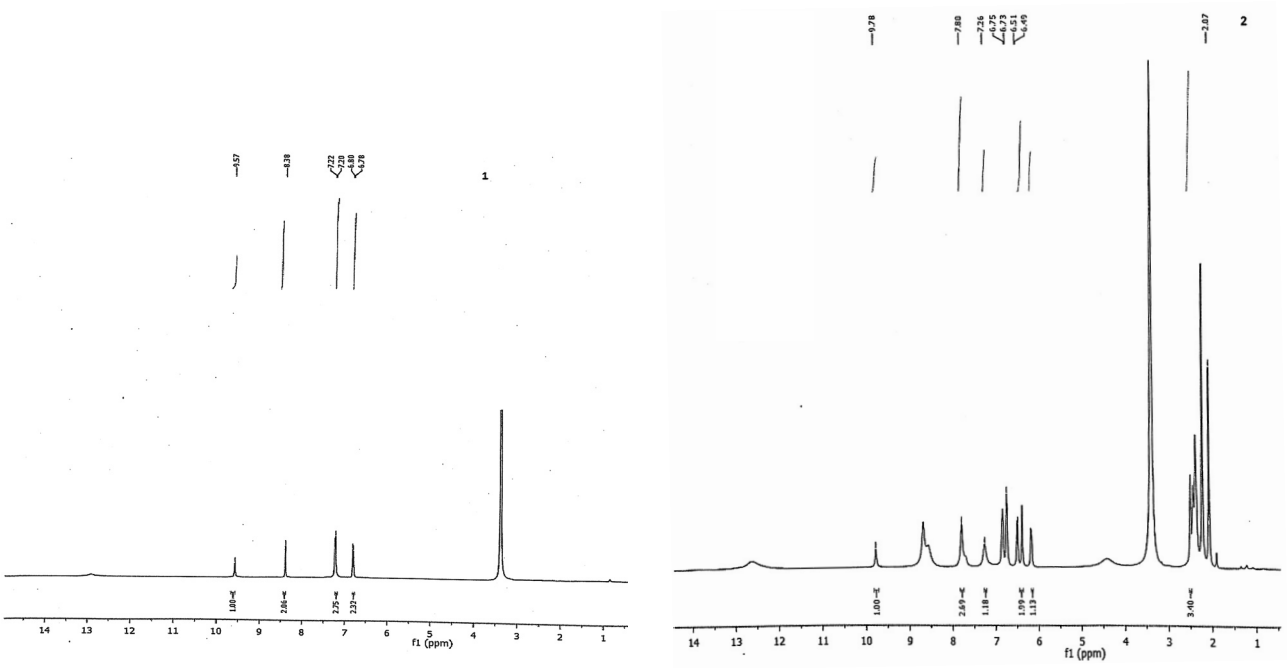

Figure-S3: ^{1}H NMR Spectra of synthesized compounds 1-2

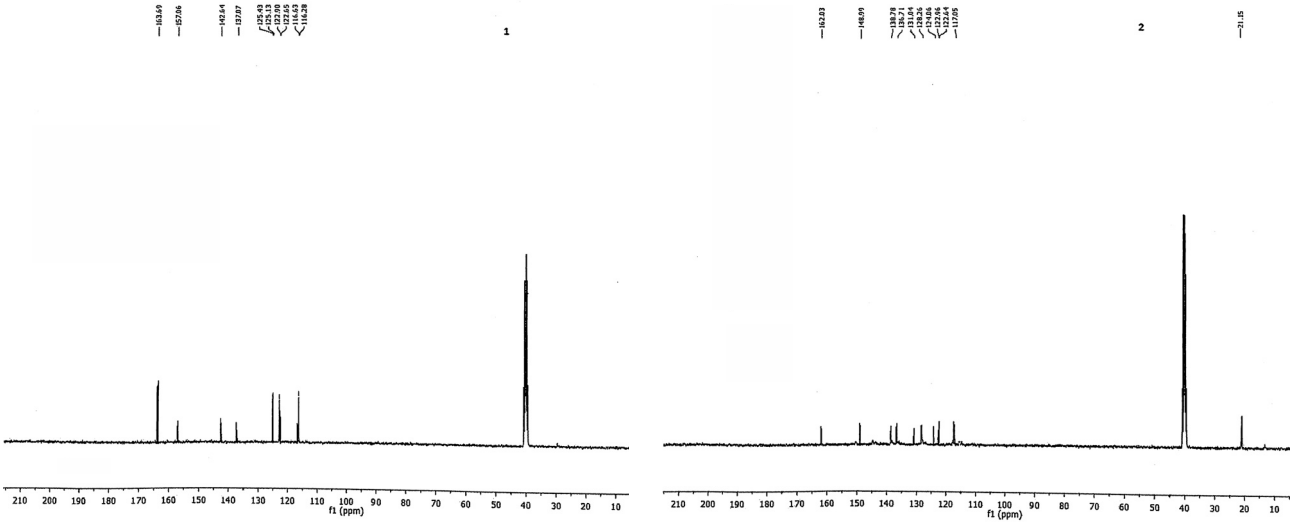

Figure-S4: ^{13}C NMR Spectra of synthesized compounds 1-2

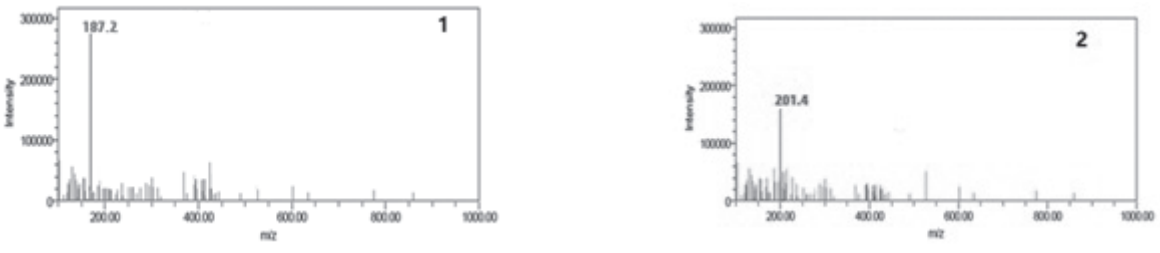

Figure-S5: LC-MS Spectra of synthesized compounds 1-2

References

A. Juan, et al. "Synthesis, Characterization and Antibacterial Activity of a Tridentate Schiff Base Derived from Cephalexin and 1, 6 - Hexanediamine and its Transition Metal Complexes." *Journal of Medicinal Chemistry*, vol. 6, 2016, pp. 467–473.

A. Prakash and D. Adhikari. "Application of Schiff bases and their metal complexes-A Review." *International Journal of Che-mical Technology*, vol. 3, 2011, pp. 1891-1896.

A.A. Shanty, et al. "Synthesis, Characterization and Biological Studies of Schiff Bases Derived from Heterocyclic Moiety." *Bioorganic Chemistry*, vol. 70, 2017, pp. 67-73.

A.A.M. Abdel-Aziz. "Novel and Versatile Methodology for Synthesis of Cyclic Imides and Evaluation of Their Cytotoxic, DNA Binding, Apoptotic Inducing Activities and Molecular Modeling Study." *European Journal of Medicinal Chemistry*, vol. 4, 2007, pp. 614–626.

A.C. Bustamante, et al. "Antioxidant activity of butyl- and phenyl-stannoxanes derived from 2-, 3- and 4-Pyridinecarboxylic Acids." *Molecules*, vol. 15, 2010, pp. 5445-5459.

A.K. Pandey, et al. "Anti-Inflammatory Activity of Novel Schiff Bases by In Vitro Models." *Bangladesh Journal of Pharmaco-logy*, vol. 12, 2017, pp. 41-43.

B. Naureen, et al. "Iron (III) and zinc (II) Monodentate Schiff Base Metal Complexes: Synthesis, Characterisation and Biological Activities." *Journal of Molecular Structure,* vol. 1231, 2021, p. 129946.

B.H. Babu, et al. "Antioxidant and Hepatoprotective Effect of Acanthus Ilicifolius." *Fitoterapia,* vol. 72, 2001, pp. 272-277.

B. Halliwell and J.M.C. Gutteridge "Free radicals in Biology and Medicine." *Oxford University Press,* 1999, 3, pp. 23-27.

B.J. McConkey, et al. "The Performance of Current Methods in Ligand-Protein Docking." *Current Science*, vol. 83, 2002, pp. 845–855.

C. Basu, et al. *Polyhedron,* vol. 26, 2007, pp. 3617-3624.

C.A. Lipinski, et al. "Experimental and Computational Approaches to Estimate Solubility and Permeability in Drug Discovery and Development Settings." *Advanced Drug Delivery Reviews,* Rev. 23, 1997, pp. 3-25.

C.B. Arjun, et al. "Schiff Base Complex of Cu (II) with Antibacterial and Electro-chemical Study." *American Journal of Chemistry*, vol.10, 2020, pp. 33-37.

Carlos M. Da Silva, et al. "Schiff Bases: A Short Review of Their Antimicrobial Activities." *Journal of Advanced Research*, vol.2, 2011, pp. 1–8.

C.S. Rivas, et al. "An Easy and Fast Test to Compare Total Free Radical Scavenger Capacity of Foodstuffs." *PCA,* vol. 11, 2000, pp. 330–338.

E.A. Elzahany, et al. "Synthesis, Characterization and Biological Activity of Some Transition Metal Complexes with Schiff Bases Derived from 2-Formylindole, Salicyladehyde, and N-amino Rhodanine." *Australian Journal of Basic and Applied Sciences,* vol. 2, 2008, pp. 210–222.

F. Bellina, et al. "Synthesis and Biological Activity of Vicinal Diaryl-Substituted 1H-Imidazoles." *Tetrahedron*, vol. 63, 2001, pp. 4571–4624.

G.G. Mohamed and Z.H. Abd El-Wahab. "Spectroscopic and Biological Activity Studies on Tridentate Schiff Base Ligands and Their Transition Metal Complexes." *Spectrochimica Acta Part A,* vol. 61, 2005, p. 1059.

G.M. Morris, et al. "AutoDock4 and AutoDockTools4: Automated docking with Selective Receptor Flexibility." *Journal of Computational Chemistry,* vol. 30, 2009, p. 2785.

H. Bhawar, et al. "Synthesis and Evaluation of Some New Imidazole Derivatives for Their Anti-Microbial and Anti-Inflammatory Activities." *AJP Tech.,* vol. 4, 2014, pp. 189-194.

J.K. Barton, et al. "Tri-s (phenanthroline) ruthenium (II): stereo selectivity in binding to DNA." *Journal of the American Chemical Society,* vol. 106, 1984, pp. 2172–2176.

K. Shalini, et al. "Imidazole and its Biological Activities: A Review." *Der Chemica Sinica,* vol. 1, 2010, pp. 1-36.

K. Shanker, et al. "Ru (II) Complexes of N4 and N2O2 Macrocyclic Schiff base ligands: Their Antibacterial and Antifungal Studies." *Spectrochimica Acta Part A: Molecular and Biomolecular Spectroscopy,* vol. 73, 2009, pp. 205–211.

K. Tsai, et al. "Oxidative DNA Damage in Human Peripheral Leukocytes Induced by Massive Aerobic Exercise." *Free Radical Biology and Medicine,* vol. 31, 2001, pp. 1465–1472.

K.L. Liao and M.C. Yin. "Individual and Combined Antioxidant Effects of Seven Phenolic Agents in Humanerythrocyte Membrane Ghosts and Phosphatidylcholine Liposome Systems: Importance of the Partition Coefficient." *Journal of Agricultural and Food Chemistry*, vol. 48, 2000, pp. 2266-2270.

K.V. Shuvaev, et al. "Mn II 12 Supramolecular Array with Four Independent Spin-Coupled Subunits." *European Journal of Inorganic Chemistry*, vol. 29, 2010, pp. 4583–4586.

L. Jing, L. Chang, C. Yun-Fen, Y. De-Yu, S. Cui-Rong, The Antioxidant Effect of Imine Resveratrol Analoguesbioorg." *Medicinal Chemistry Letters*, vol. 22, 2012, pp: 5744-5747.

M. Houdkova, et al. "Evaluation of Antibacterial Potential and Toxicity of Plant Volatile Compounds using New Broth Micro dilution Volatilization Method and Modified MTT Assay." *Fitoterapia*, vol. 118, 2017, pp. 56-62.

M. Kumar, et al. "Synthesis, Characterization and Antioxidant Activities of Schiff Bases are of Cholesterol." *Journal of Saudi Chemical Society,* vol. 21, 2017, pp. 322–328.

M. Leopoldini, et al. "The Molecular Basis of Working Mechanism of Natural Polyphenolic Antioxidants." *Food Chemistry,* vol. 125, 2011, pp. 288–306.

M. Patra, et al. "Small Organometallic Compounds as Antibacterial Agents." *Dalton Transactions*, vol. 41, 2012, pp. 6350-6358.

M.A. Mokhles, et al. "Synthesis, Anticancer Activity and Molecular Docking Study of Schiff Base Complexes Containing Thiazole moiety." *Journal of Applied Sciences*, vol. 5, 2016, pp. 85–96.

M.N. Peyrat-Maillard, et al. "Determination of the Antioxidant Activity of Phenolic Compounds by Coulometric Detection." *Talanta,* vol. 51, 2000, pp. 709-716.

N. Dharmaraj, et al. "Ru (II) Complexes Containing Biden date Schiff Bases and Their Antifungal Activity." *Transition Metal Chemistry*, vol. 26, 2001, pp. 105-110.

P. Ertl, et al. "Fast Calculation of Molecular Polar Surface Area as a Sum of Fragment-Based Contributions and Its Application to the Prediction of Drug Transport Properties." *Journal of Medicinal Chemistry*, vol. 43, 2000, pp. 3714-3717.

P. Kavitha, et al. "Synthesis, Structural Characterization, Fluorescence, Antimicrobial, Antioxidant and DNA Cleavage Studies of Cu (II) Complexes of Formyl Chromone Schiff Bases." *Spectrochimica Acta Part A,* vol. 102, 2013, pp. 159–168.

R. Dennington, et al. "Molecular Docking of Selective Binding Affinity of Sulfonamide Derivatives as Potential Antimalarial Agents Targeting the Glycolytic Enzymes: GAPDH, Aldolase and TPI (Eds.)." *Gauss View*, Version 5.0.8, Dennington, Semichem Inc., Shawnee Mission, 2009, R, KS.

R.P. Chinnasamy, et al. "Synthesis, Characterization, and Analgesic Activity of Novel Schiff Base of Isatin Derivatives." *Journal of Advanced Pharmaceutical Technology and Research*, vol. 1, 2010, pp. 342–347.

T.S. Kamatchi, et al. "The Effect of Incorporating Carboxylic Acid Functionalities Into 2, 22-Bipyridine on the Biological Activity of the Complexes Formed: Synthesis, Structure, DNA/Protein Interaction, Anti-Oxidant Activity And Cytotoxicity." *RSC Advances*, vol. 7, 2017, pp. 16428–16443.

"Vogel's Textbook of Practical Organic Chemistry." 5th ed., *Longmans*, London, 1989.

Z. Bingchang, et al. "Antitumor Activity of a Trans-Thiosemicarbazoneschiff Base Palladium (II) Complex on Human Gastric Adenocarcinoma Cells." *Europe PMC,* vol. 8, 2017, pp. 13620-13631.

Self-Propagated High-Temperature Synthesis of Nanomanganese Chromite and Its Characterization

Dr. Sr. Stella K.A.
Assistant Professor, Department of Chemistry
St. Xavier's College for Women, Aluva
Palace Road,Aluva-683101
Ernakulam, Kerala, India
Email: stellagrace@stxaviersaluva.ac.in

Abstract

Nanosized manganese chromite powders ($MnCr_2O_4$) have been prepared by Self-propagated High-temperature Synthesis (SHS) using metal nitrates and urea as fuel. The resulting powders were characterized by X-ray diffraction and the crystallite size calculated from the XRD line broadening (27.73 nm). The microstructure of the sintered discs was studied using Scanning Electron Microscopy (SEM) and the band gap was calculated using UV-Visible spectra. The temperature-resistance characteristics of this spinel-type material were found to exhibit a negative temperature coefficient of resistance.

Keywords: *Manganese Chromite, SHS, Nano Size, Negative Temperature Coefficient of Resistance, and Spinels.*

Modern technology is attracted by nanostructured materials. At the nano-size levels, materials exhibit unusual physical and chemical properties. The magnetic behaviour of $MnCr_2O_4$ nanoparticles was also reported in 2006 (R.N. Bhowmil and Ranganathan 2006). Spinel chromite is represented by the formula unit ACr_2X_4 (A = Mn, Co, X = O, S). Chromites are one of the classes which exhibit typical magnetic properties like ferrimagnetism (N. Mufti, et al.). Chromite materials synthesized by conventional ceramic methods have a very low surface area. The preparation of materials by the classical solid-state reactions requires a high calcination temperature and a long-time mechanical milling process (Whipple and A. Wold). However, to produce nanosized chromite particles, some techniques such as chemical co-precipitation (K.S. De, et al.), sol-gel method (D. Bokov, et al.), etc., have been developed. The synthesis method reported here is the SHS technique which offers great potential in the preparation of chromites (A.C.F.M. Costa, et al.) and (S. Sundar Manoharan and N.R.S. Kumar). This synthesis is also known as combustion synthesis (R.M. Thankachan and B. Raneesh). This method holds many advantages over conventional methods; saving energy, environmental protection, the substitution of raw materials with cheaper ones for synthesizing the same products and the high purity of products are some of them (A. Huczko, et al.). The $MnCr_2O_4$ synthesized by the SHS method is crystalline and has high chemical homogeneity and purity as evident from the XRD pattern. The microstructure of sintered $MnCr_2O_4$ has been studied by Scanning Electron Microscopy (SEM) and the resistance *vs*. temperature graph is plotted which shows a negative temperature coefficient of resistance for $MnCr_2O_4$.

Experimental

Nanosized spinels of Manganese chromite with nominal composition $MnCr_2O_4$ were prepared by combustion reaction using urea as the fuel. The starting materials were Manganese nitrate, Chromium nitrate, and urea. The stoichiometric composition of metal nitrates and urea were calculated using the total oxidizing and reducing valency of the components which serve as the numerical coefficient for the stoichiometric balance so that the equivalence ratio is unity and the energy released is maximum (S. Sundar Manoharan and Kashinath C. Patil). The precursors were placed in a beaker and heated to a temperature above 300°C, until the ignition took place, producing $MnCr_2O_4$ as foam. The powder was characterized by X-ray diffraction. Scherrer's equation was used to calculate the average crystallite size from X-ray line broadening (S.R. Jain, et al.). FT-IR spectra were also recorded. The powder was mixed with a PVA binder and a small amount of Bi_2O_3 was also added as a sintering aid. The green compacts were made by pressing the granules in a uniaxial press, to a size of a diameter of 10mm and thickness of 2mm discs. The pellets were sintered at 1373, 1473, 1523, and 1573K for 3 hours in an air atmosphere. The furnace was allowed to cool at a controlled rate of 275K per minute up to 1273K. The phase purity of the sintered $MnCr_2O_4$ was analysed using XRD. Scanning electron microscopy was used for the microstructural characterization of the sintered discs. And the electrical characteristics were monitored by measuring resistance vs. temperature studies using calibrated silicon oil baths (Fluke Hart Scientific Model No. 7340).

Results and Discussion

The XRD patterns of the samples $MnCr_2O_4$ [ICDD 33-892 before and after calcination are given in Figure-1. The data demonstrate the formation of

phase pure spinel products even before the calcination process. The crystallite size of $MnCr_2O_4$ was calculated from X-ray line broadening (using Scherrer's equation) at 20 nm and for the calcined powder, the crystallite size was increased to 22 nm. Thus, by the SHS method, it is possible to prepare phase pure nanosized $MnCr_2O_4$ without sintering at high temperatures as in the case of a compound prepared by the solid-state method.

Single-phase crystal in manganese chromites has been confirmed by a characteristic XRD pattern (Figure - 2(A)) which was compared with the previously reported structure (H.P. Klug and L.E. Alexander). XRD pattern of the powder and the sintered sample (Figure-2(B)) shows single-phase cubic structured manganese chromite. The crystallite size calculated from X-ray line broadening using Scherrer's equation was 27.73 nm.

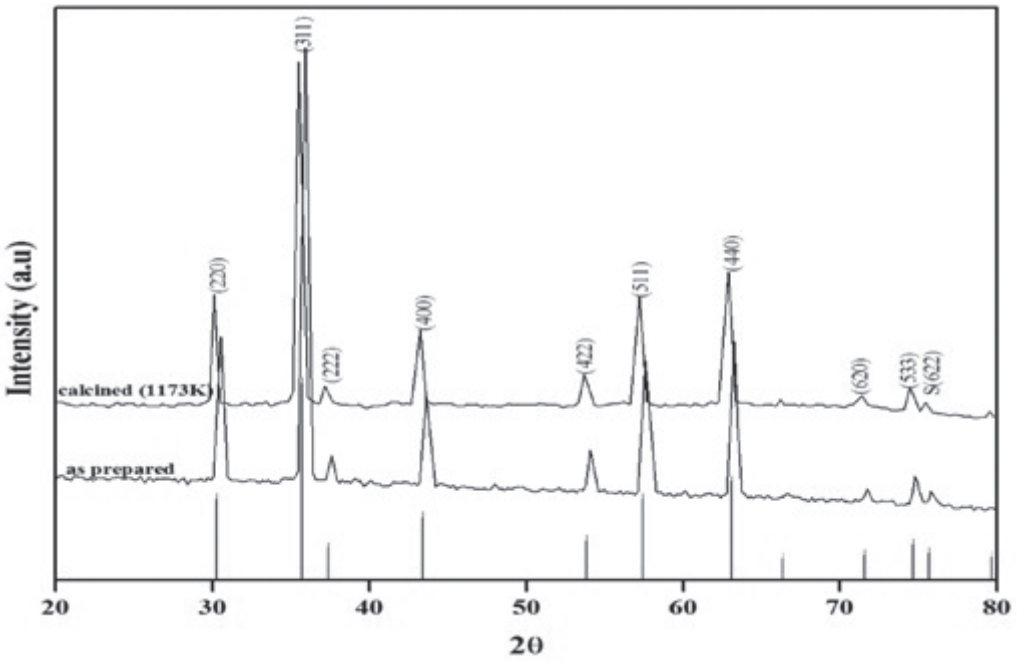

Figure - 1: XRD Patterns of the $MnCr_2O_4$ powder synthesized by SHS

[Match ICDD 33-892]

FT-IR spectra of manganese chromite is given in Figure-3 which shows characteristic absorption bands around 600 and 500 cm^{-1} due to M-O and Cr-O stretching frequencies, respectively.

Discussion

The UV-Visible spectrum of $MnCr_2O_4$ was recorded for a wavelength range of 300-900nm (Figure-4). The spectra of the Mn-Cr-O systems consisted of four absorption maxima due to various ligand field transitions. These peaks are compatible with the literature reported earlier (B. Dutta and D. Pal). The band gap energy calculated is around in the range of 1.87–3.69 eV.

The SEM microstructure obtained for a sintered sample at 1473 K is given in Figure-5. It is seen that uniformly sized grains are formed during

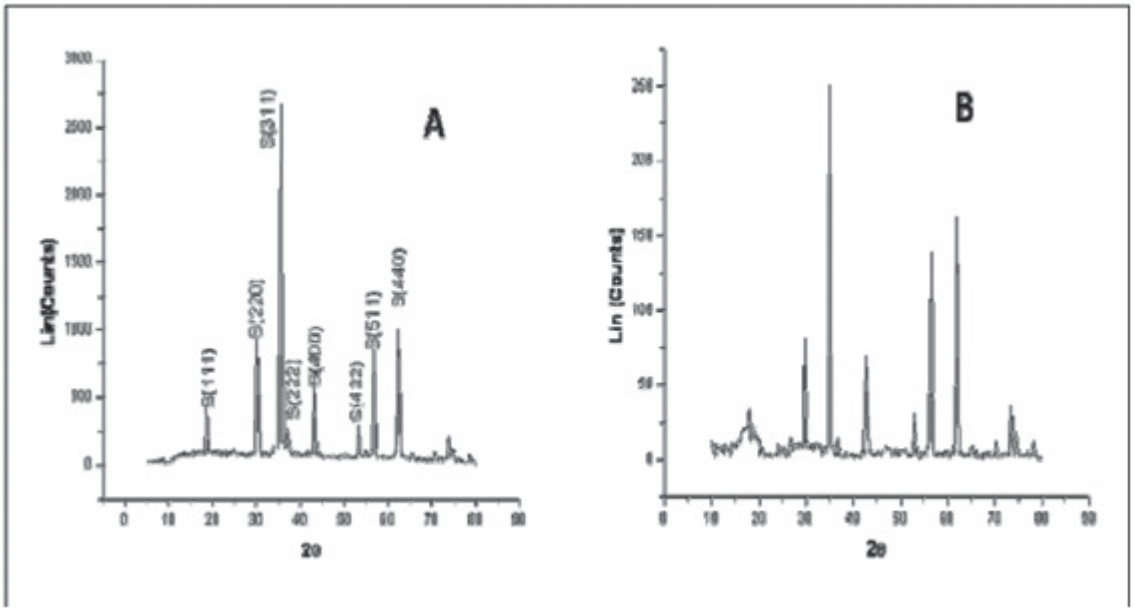

Figure - 2: (A) X-ray Diffraction pattern for the powder specimen, (B) XRD pattern for sintered specimen at 1473K

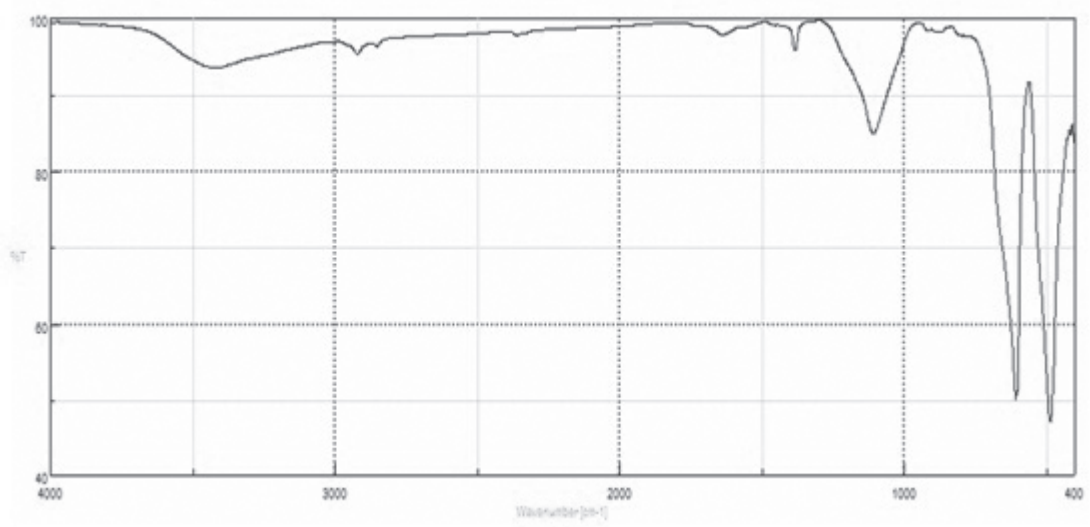

Figure - 3: FT-IR Spectra of $MnCr_2O_4$ powder

sintering. On careful observation, we can see the tetrahedral and octahedral nature of the spinel.

The relationship between resistance and temperature was studied and shown in Figure-6 which shows the negative temperature coefficient characteristics of the material. Resistance decreases with the increase of temperature which confirms the NTC characteristics.

Conclusion

The synthesis by combustion reaction was favourable to obtain crystallite powders with nanosized particles of manganese chromite. The X-ray line broadening confirmed the nature of nanosized particles. $MnCr_2O_4$ pellets sintered at different temperatures and the image of the pellet at 1473K showed a fine-grained microstruc-

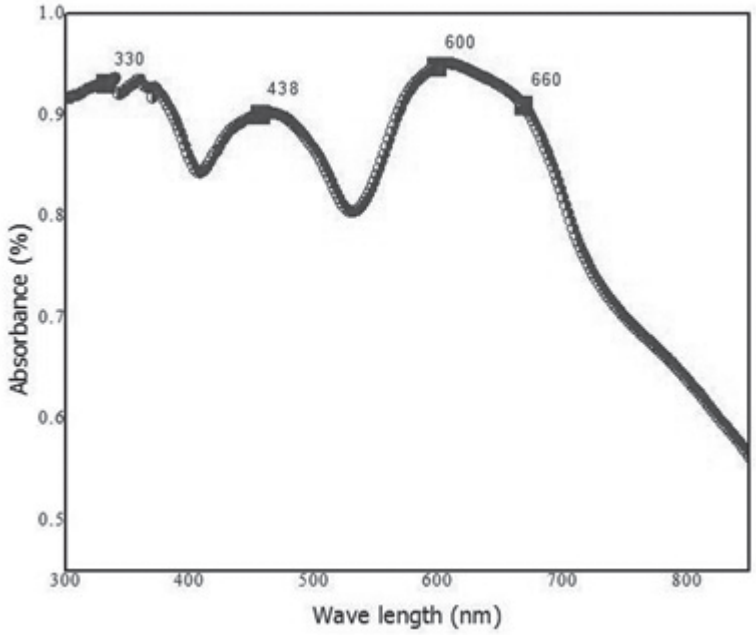

Figure - 4: The plot of absorbance vs wavelength with major absorption peaks in $MnCr_2O_4$

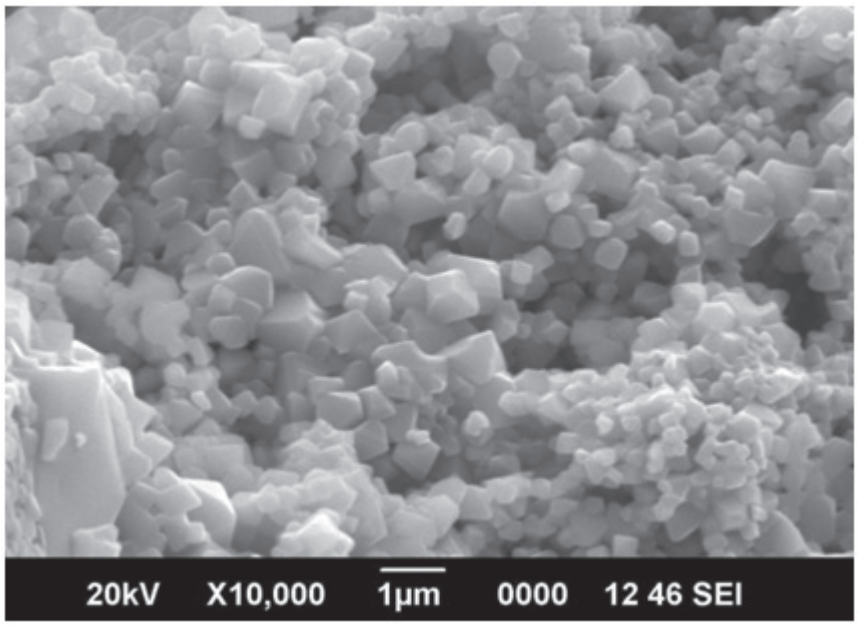

Figure - 5: Scanning electron micrograph of $MnCr_2O_4$ specimen sintered at 1473K

ture with uniform grain growth. The presence of Mn and Cr in the sample was confirmed by the IR spectrum. UV-Visible spectrum measurements were taken to find band gap energy. A graph of resistance against absolute temperature (K) was plotted which shows the negative temperature coefficient characteristics of the material. In summary, the study reveals that the $MnCr_2O_4$ pre-

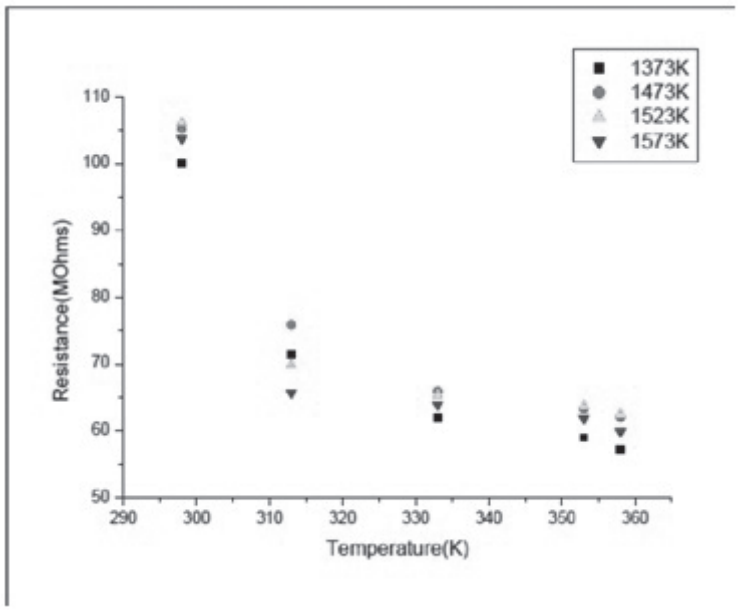

Figure - 6: Relationship between resistance and absolute temperature (K) for the $MnCr_2O_4$ spinel

pared by self-propagated high-temperature synthesis has all the characteristics of $MnCr_2O_4$ prepared by the conventional method and also has comparatively good results.

Acknowledgement

I appreciate the support of the Centre of Materials for Electronics Technology (C-MET) Thrissur, Kerala, India for helping me to carry out this project.

Declaration of Interest Statement

I declare that I have no known competing financial interests or personal relationships that could have appeared to influence the work reported in this paper.

References

A. Huczko, et al. "Self-propagating High-Temperature Synthesis (SHS) of Crystalline Nanomaterials." *Journal of Crystal Growth*, February 2014, pp. 1-5, doi.org/10.1016/j.jcrysgro. 2014.02.049.

A.C.F.M. Costa, et al. "Preparation of Nano-structured $NiFe_2O_4$ Catalysts by Combustion Reaction." *Journal of Materials Science,* 41, August 2006, pp. 4871-4875, doi.org/10.1007/s10853-006-0048-1.

B. Dutta and D. Pal. "Absorption and Raman Spectroscopy: Ferrimagnet Spinel $MnCr_2O_4$." *AIP Conference Proceedings,* vol. 2115, July 2019, 030369; pp. 1-4, doi.org/10.1063/1.5113208.

D. Bokov, et al. "Nanomaterial by Sol-Gel Method: Synthesis and Application." *Advances in Materials Science and Engineering,* December 2021 pp. 1-21, doi.org/10. 1155/2021/5102014.

H. P. Klug and L.E. Alexander. "X-ray Diffraction Procedures." *Wiley*, Newyork, EUA, p. 491, 1962.

K. S. De, et al. "Electrical Properties of the $CuCr_2O_4$ Spinel Catalyst." *Journal of Solid State Chemistry*, 43, July 1982, pp. 261-266, doi.org/10.1016/0022-4596(82) 90238-9.

N. Mufti, et al. "Magnetodi Electric Coupling in $MnCr_2O_4$ Spinel." *Journal of Magnetism and Magnetic Materials,* vol. 321, June 2009, pp. 1767-1769. doi.org/10.1016/j.jmmm. 2009.02.023.

R. M. Thakachan and B. Raneesh. "Synthesis of Inorganic Nanomaterial." *Elsevier Ltd.*, pp.185-211, 2018. doi.org/10.1016/C2 016-0-01718-7.

R. N. Bhowmil and Ranganathan. "Lattice Expansion and Non-Collinear to Collinear Ferrimagnetic order in a $MnCr_2O_4$ Nano-particle." *Physical Review Journals,* B73, 144413, April 2006, pp. 1-9, doi.org/ 10.1103/PhysRevB. 73.144413.

S. Sundar Manoharan and Kashinath C. Patil. *Journal of the American Ceramic Society,* 75, April 1992, pp. 1012-15, doi.org/10. 1111/ J.1151-2916.1992.TB 04177.X.

S. Sundar Manoharan and N.R.S. Kumar. "Preparation of Fine Particle Chromites: A Combustion Approach." *Materials Research Bulletin,* 25, February 1990, pp. 731-738, doi: 10.1016/0025-5408(90) 90201-c.

S. R. Jain, et al. "A New Approach to Thermochemical Calculations of Condensed Fuel-Oxidizer Mixtures." *Combustion and Flame*, vol. 40, 1981, pp. 71-79, doi.org/ 10.1016/0010-2180(81) 90111-5.

Whipple and A. Wold. "Preparation of Stoichio Metric Chromites." *Journal of Inorganic and Nuclear Chemistry*, vol. 24, January 1962, pp. 23-27, doi.org/10.1016/0022-1902 (62)80064-5.

Kaolinite as a Low Temperature Binder for Porous Ceramic SiC Foam

Dr. Resmi V.G.
Assistant Professor
Department of Chemistry
Mahatma Gandhi College
Thiruvananthapuram
Email:resmiviswanadhan@gmail.com

Dr. Annu Raju
Assistant Professor, Department of Chemistry and
Centre for Research
St. Teresa's College (Autonomous)
Science Block, Ernakulam
Email: annukaramayil@gmail.com

Dr. C.K. Simi
Assistant Professor
Department of Chemistry
Mahatma Gandhi College, Thiruvananthapuram
Email: cksimi@gmail.com

Dr. Rajan T.P.D.
Senior Principal Scientist, CSIR – National Institute for
Interdisciplinary Science and Technology
Thiruvananthapuram
Email: tpdrajan@niist.res.in

Abstract

In the present study, low temperature fabrication of porous ceramic SiC foams via burnt-out method has been carried out with varying composition of urea formaldehyde resin as a porogen and kaolin clay as a low temperature binder. During sintering, the kaolinite clay transformed to mullite phase. It acted as the bonding material between SiC particles and the polymer porogen burned off into gases and left pores in respective places. The characteristics of in-situ reaction derived bonding phases and their composition, microstructural evolution, open porosity and pore size distribution of porous SiC ceramics were studied. Porous SiC fabricated from 60 volume percent UF resin porogen added system showed 48% open porosity. The compressive strength increased from 5 to 13 MPa with the poreformer content varying from 40 to 60 volume percent.

Keywords: *Kaolinite, Porogen, Sintering, Mullite, and Porosity.*

Macroporous SiC ceramics have been exploited in numerous applications in the area of molten metal and hot gas filters, catalytic support, thermal insulators, refractory material etc., due to its potential advantages including low density, high mechanical strength, thermal and chemical stability (W. Chi, et al. 869-74), (J. She, et al. 2852-54), and (Yan Ma, et al. 253-55). The properties of porous ceramics strongly depend on the processing methods adopted, porosity content and microstructure characteristics. Various methods developed for the processing of porous SiC are replica, gel casting, reaction sintering, oxidation bonding, partial sintering and by carbothermal reduction method (J. She, et al. 2852-54), (Jung-Hye Eom, et al. 220-42), and (Atanu Dey, et al. 223-30). One of the simple and inexpensive methods used for the synthesis of porous SiC ceramic was oxide bonding technique because it does not require any sophisticated equipment and delicate instrumentation (Sumin Zhu, et al. 595-597). Various low temperature sintering agents reported are silica, mullite, cordierite, alumina, etc., that can be directly added to the starting material, or can be formed during the in-situ reaction bonding process (Jung-Hye Eom, et al. 220-42), (Atanu Dey, et al. 223-30), and (Sumin Zhu, et al. 595-597, 115-18). Among this, mullite possesses higher melting point (>1800°C) and lower oxygen diffusion coefficient so that mullite bonded porous SiC exhibit better high-temperature stability and oxidation resistance when compared to other bonding phases such as silica and alumina (Permeability and Nano-partilce Filtration Assessement of Cordierite - Bonded Porous SiC Ceremics, 18362-72).

In recent years, several investigations were reported on the synthesis of mullite-bonded porous SiC ceramics. Mullite is usually synthesized from the starting materials SiO_2 which reacts with - $\langle Al_2O_3$ at temperatures over 1410°C (Kwang-Young Lima, et al. 6827-34). Mullite bonded porous SiC ceramics were fabricated in air by the in situ reaction of cristobalite $\langle Al_2O_3$ at 1400–1550°C using graphite as poreformer (Permeability and Nano-partilce Filtration Assessement of Cordierite - Bonded Porous SiC Ceremics, 18362-72). A reactive processing method was successfully adopted to fabricate mullite bonded porous SiC ceramics by using calcined kaolin, $Al(OH)_3$, and SiC (Shuqiang Ding, et al. 2095-2102). Porous mullite bonded SiC ceramics were fabricated by the infiltration of mullite liquid precursor into the SiC porous compacts followed by sintering at 1300–1500°C in air using petroleum coke powder as poreformer (Wu S., et al. 1579-82).

In the present study, in order to realize the low-temperature fabrication of porous SiC ceramics, kaolin clay was added to bond SiC particles and urea formaldehyde resin is added as the porogen. The characteristics of in-situ reaction derived bonding phases and their composition, microstructural evolution, open porosity and pore size distribution of porous SiC ceramics were studied.

Experimental Procedure

Materials and Sample Preparation

Commercially available α-silicon carbide particles (hexagonal SiC polytype 6H, Grindwell Norton) with size of 42 μm (particle size analysis) and kaolinite clay were chosen as the starting material for this work.

Synthesis of Urea Formaldehyde Resin

Urea-formaldehyde resin is an amino resin which is included in the class of thermosetting resins. It can be prepared by the reaction between urea and formaldehyde. The synthesis takes place in two stages. First step involves the preparation of methylol-urea (MU) solution which is the monomer. For the preparation of the MU solution, urea

and formaldehyde were taken in a 1:4 ratio; 45g of urea was dissolved in 250 ml formalin (37% formaldehyde); and pH was adjusted to 9 by the addition of 3.5 ml 4% NaOH solution. In this stage, urea is hydroxyl methylolated by the addition of formaldehyde. This involves a series of reactions that lead to the formation of mono-, di-, and trimethylolureas. The reaction between urea and formaldehyde is pH dependent. The formation of mono, di and tri trimethylolureas take place at a pH ratio of 9:3:1. At our reaction pH, only mono derivative is formed. The second stage is the condensation of the monomer methylol urea to a low molecular weight polymer. The rate of condensation reaction very much depends on pH. Also in order for the condensation reaction to take place, the ratio of urea and formaldehyde should be 1:2. So at the time of condensation reaction, the required amount of urea was added to make the desired ratio. The pH was adjusted to 5 by the addition of dil. HNO_3 for the condensation reaction. This results in the formation of low molecular weight urea formaldehyde resin. Heating of this polymer at 100-120°C leads to further condensation and produces a high molecular weight UF resin.

Clay Coated SiC Using Polyester as Binder

In this process, SiC powder was dispersed in a solution of polyester resin (standard FRP laminating resin) in acetone where in the polyester content was 1% of the SiC powder. The solvent was evaporated, while stirring, to give a semi-dried product. The semi-dried product was then added in small quantities to clay powder (15% of SiC) in a glass mortar and simultaneously mixed by using a pestle. The mix was finally dried at a temperature of 120°C for 2 hr. The dried powder thus obtained was stable in aqueous medium as well as in non-aqueous solvent such as acetone. Only a small amount of clay was found to be separated. SEM revealed that clay particles were adhering to the SiC particles. Urea-formaldehyde resin is an amino resin which is included in the class of thermosetting resins. It can be prepared by the reaction between urea and formaldehyde.

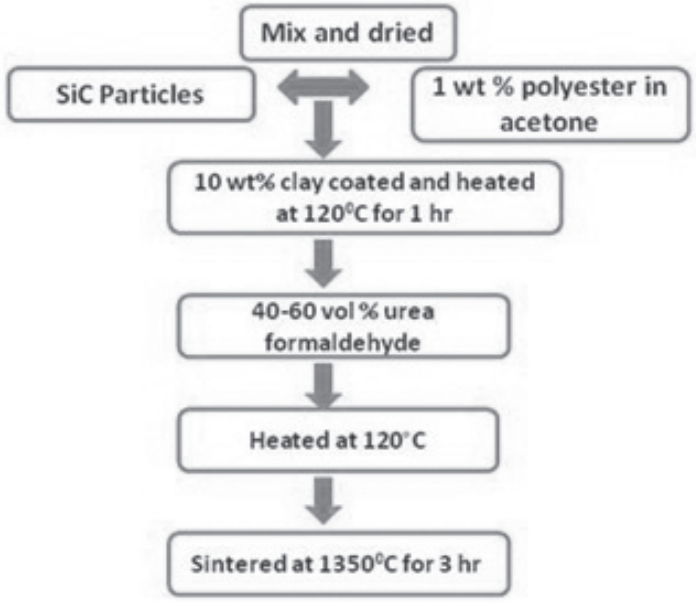

Figure - 3.1: Processing step for clay bonded porous SiC ceramics

Varying compositions of urea formaldehyde with respect to clay coated SiC were thoroughly mixed and compacted using hydraulic press. The green samples were fired at 200°C-400°C for 2 hrs with a heating rate of 0.5°C/min for 1 hour to eliminate urea formaldehyde resin. Finally the samples were heated up to 1350°C with a heating rate of 5°C/min for 3 hrs. Figure-3.1 shows the processing steps involved in the preparation of clay bonded porous SiC ceramics.

3.2 Characterization Methods

The thermal analysis (TG/DTA) of pore former was carried out upto 1000°C with a heating rate of 10°C/min in air using the Hitachi (STA 7300) simultaneous thermal analysis system, for identifying the burnt-out temperature of porogen occurring during sintering of SiC preforms. Bulk density and open porosity were determined by Archimedes method using water as the liquid medium. The sintered porous samples were grinded using a mortar and the crystalline phases of the obtained mullite bonded porous SiC ceramics was identified by X-ray diffractometry (XRD, PW-1700, Philips Co.) using Cu$K_{\acute{a}}$ radiation. The diffraction patterns for the porous sintered samples were obtained for the 2 angles from 20°-80° at a scan speed of 0.05°. Microstructures and morphologies were examined by Scanning Electron Microscopy (Zeiss and Jeol SEM). The chemical constituents and its approximate percentage distribution were determined using Energy Dispersive X-ray Spectroscopy (selected region analysis), EDS (Hitachi SU6600). The compressive strength of sintered porous SiC ceramics having dimension 10 mm diameter and length of 15 mm at room temperature was measured by a Universal Testing Machine (Instron 1195) and with a crosshead speed of 1 mm/min. Five specimens were tested to obtain the average compressive strength. The pore size distribution of the porous specimen was measured by mercury porosimetry (Quantachrome Instruments Co. Ltd., Pore Master).

Figure-3.2 shows the SEM image of clay coated SiC particles, it shows that the clay was well coated over the SiC particles. These clay particles acted as binding agents during the sintering process.

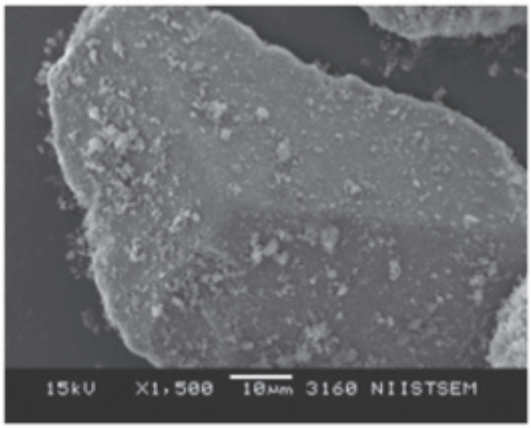

Figure - 3.2: SEM Micrograph of clay coated SiC particles

Figure-3.3 shows the TG–DTA curves of the green powder sample at a heating rate of 10°C/min in air with urea formaldehyde resin as poreformer. It can be observed from the TG curve that there is a rapid weight loss from~ 200 to ~500°C, and a slow weight loss from ~600 to 800°C. The first weight loss upto ~ 500°C was due to the burnout of UF resin present in the sample, whereas the second weight loss was due to the complete oxidation of carbon residue from polymer decomposition. The total of 20% weight loss was observed from the green sample. It is shown in the DTA curve that there are three exothermal peaks, respectively, near ~390°C, ~600°C and at ~1050°C. The peak neat at ~390°C was due to the decomposition of UF resin and at ~600°C was due to the complete oxidation of carbon residue, while the peak at ~1050°C was due to the mullite formation from kaolin.

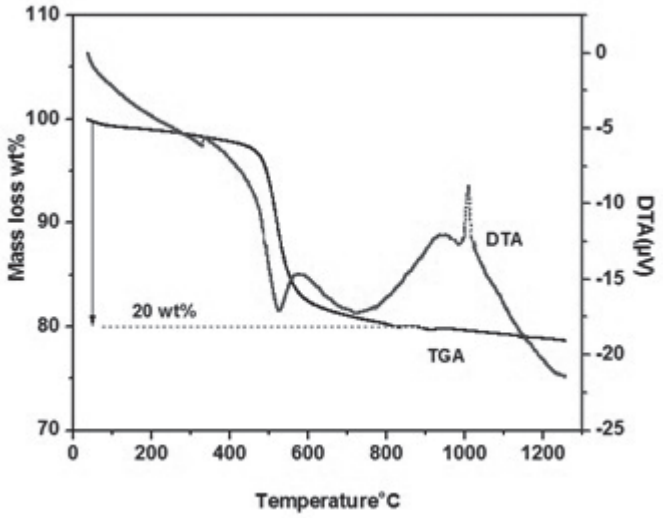

Figure - 3.3: TG–DTA curves of the green powder sample at a heating rate of 10°C/min in air

3.4 Results and Discussion

Figure-3.4 shows the XRD patterns of the kaolin bonded porous SiC ceramics sintered at 1350°C for 3 hours. The porous sample shows the presence of the major crystalline phases such as α-SiC, mullite, α-Al_2O_3 and cristobalite. During the sintering, the mullite is formed from the kaolin and it acts as a good binder for SiC particles.

The effect of UF porogen content on the microstructure of porous SiC ceramics is shown in Figure 3.5 (a). The figure shows typical microstructures of porous SiC samples sintered at 1350°C containing 60 volume percent of UF resin. A number of large pores are observed which originated from the agglomerated porogen, increased with increased UF content. More porogen content led to more agglomeration in the composition and resulted in the increased pore size and the formation of more large pores in the microstructure.

The typical microstructural analysis shows (Figure: 3.5 (b)) the presence of neck growth between SiC particles and mullite formation over the surface of SiC particles. The microstructure

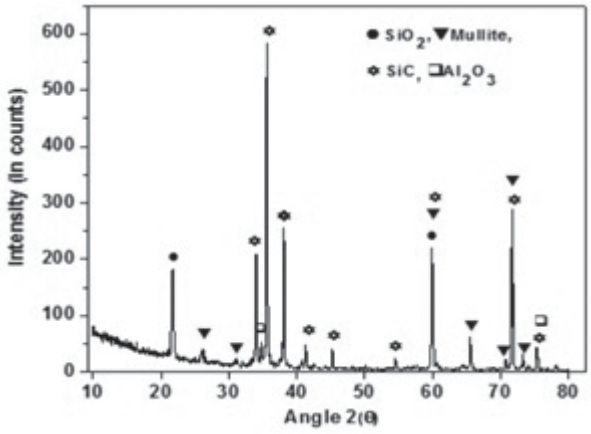

Figure - 3.4: XRD patterns of sintered clay-bonded SiC porous ceramics at a sintering temperature of 1350°C

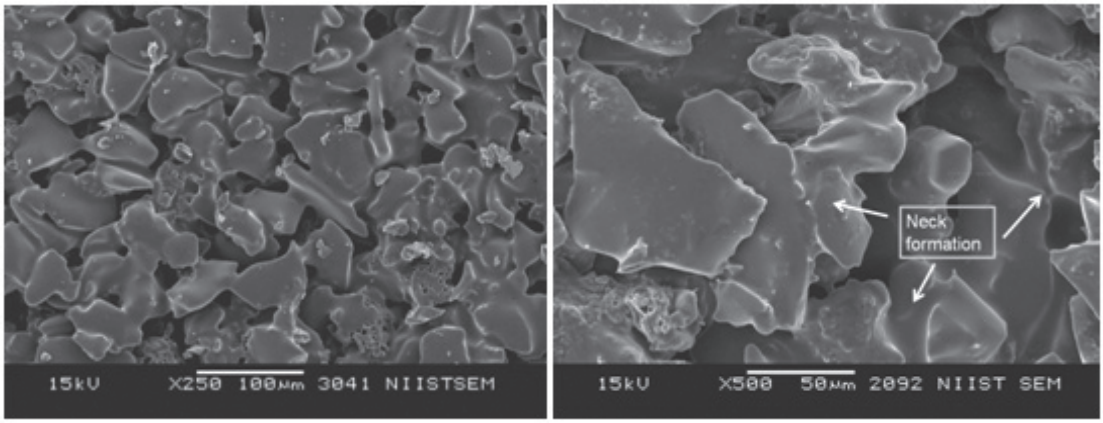

Figure - 3.5: (a) SEM image of Porous SiC ceramics with 60% UF, (b) Neck formation between SiC particles during sintering process.

clearly shows the presence of a viscous phase on the surface of the SiC particles. During sintering, the surface oxidation of SiC leads to the formation of an amorphous SiO_2 layer on the surface of SiC and well-developed bonding necks were seen to be formed between neighbouring SiC particles. With the increase in temperature, this layer softens and a transformative rearrangement of crystalline silica (e.g., cristobalite) could take place at ~1300°C (Yani Jing, et al. 1329-34). The in-situ reaction between cristobalite and alumina from kaolin forms mullite which also acted as strong binder between SiC particles.

Figure-3.6 shows plots of open porosity and bulk density of porous SiC ceramics versus UF resin content. Porogen content has a significant effect on the open porosity and bulk density of porous SiC ceramics. The figure clearly shows that the open porosity increases with the porogen content. It is shown that the open porosity is mainly contributed by stacking particles. Porous SiC fabricated from 60 volume percent UF resin

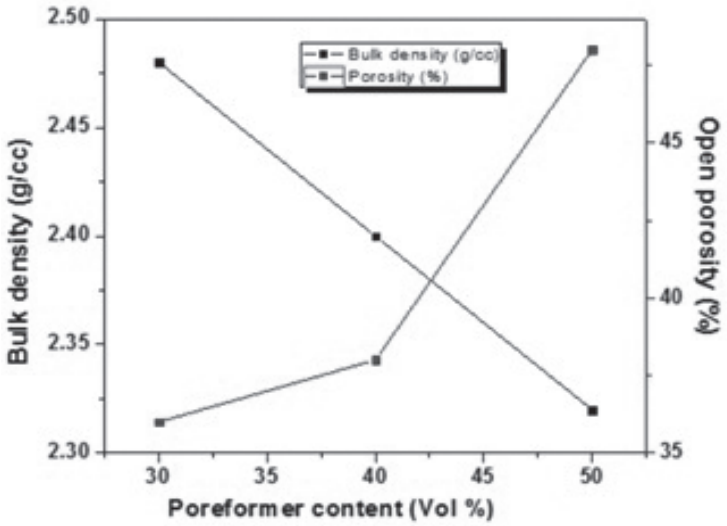

Figure - 3.6: Effect of porogen content on open porosity and bulk density of mullite bonded borous SiC ceramics

porogen added system shows 48% open porosity with bulk density of 2.48 g/cc whereas 40 volume percent porogen added porous SiC ceramics shows an open porosity of 36% with bulk density of 2.32 g/cc.

Figure-3.7 shows the pore size distribution of mullite bonded porous SiC ceramics with 50 volume percent urea formaldehyde porogen addition. It is interesting that the specimens have a unimodal pore size distribution curve. The pore size distribution of porous samples sintered at 1350°C was consistent with the above SEM results very well. The most likely explanation is that a glassy bonding phase was beneficial to forming SiC-based porous ceramics with homogeneous structure. Further, the pores were smaller than the particle size of UF resin, because the oxidation of SiC and the cristobalization were accompanied by volume expansion.

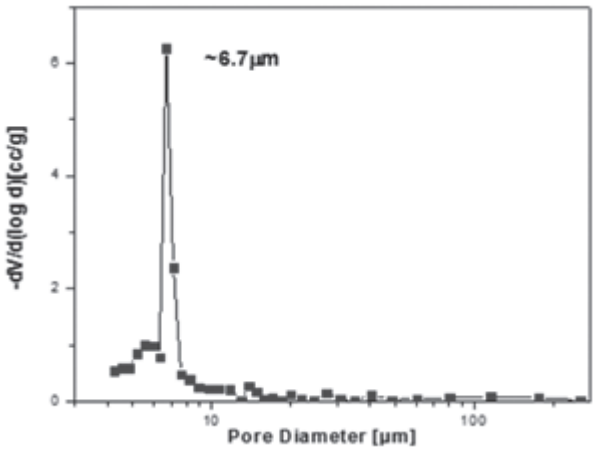

Figure - 3.7: Pore size distribution of porous Sic ceramics by mercury porosimetry analysis

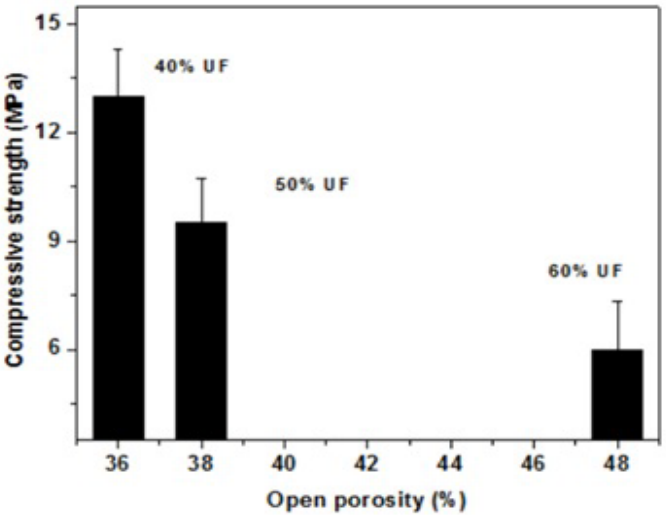

Figure - 3.8: Compressive strength of porous SiC ceramics with varying porogen content

Figure-3.8 shows the variation of compressive strength of mullite bonded porous SiC ceramics as a function of the open porosity percent. The compressive strength increased from 5 to 13 MPa with the poreformer content varying from 40 to 60 volume percent. The increase in porosity caused by adding more poreformer content increased the contact between poreformer in the compacts that leads to high probability of failure of large pores under load. The maximum strength of porous ceramics was 13 MPa with 36% open porosity.

Conclusions

Porous SiC ceramic foams successively fabricated using kaolin acts as low temperature binder and urea formaldehyde as a poreformer. During sintering, the kaolinite clay transforms to mullite phase which acted as the bonding material between SiC particles and the polymer porogen burns off to form pores in respective places. Increase in UF resin has resulted in increase in porosity, however the compression strength is observed to decrease.

Reference

Atanu Dey, et al. "Preparation of Porous SiC Ceramics by an Infiltration Technique." *Ceramics International Journal*, vol. 37, 2011, pp. 223–230.

J. She, et al. "High-Strength Porous Silicon Carbide Ceramics by an Oxidation-Bonding Technique." *Journal of the American Ceramic Society*, vol. 85, 2002, pp. 2852–2854.

Jung-HyeEom, et al. "Processing and Properties of Macroporous Silicon Carbide Ceramics: A Review." *Journal of Asian Ceramic Societies*, vol.3, 2013, pp. 220–242.

Kwang-Young Lima, et al. "Porous Sodium-borate-Bonded SiC Ceramics." *Ceramics International – Journals,* vol. 39, 2013, pp. 6827–6834.

"Permeability and Nanoparticle Filtration Assessment of Cordierite-Bonded Porous SiC Ceramics." *Industrial and Engineering Chemistry Research*, vol. 52, 2013, pp. 18362-18372.

Shuqiang Ding, et al. "Fabrication of Mullite-Bonded Porous Silicon Carbide Ceramics by In Situ Reaction Bonding." *Journal of the European Ceramic Society*, vol. 27, 2007, pp. 2095–2102.

Sumin Zhu, et al. "Low-Temperature Fabrication of Porous SiC Ceramics by Prece-ramic Polymer Reaction Bonding." *Materials Letters*, vol. 59, 2005, pp. 595–597.

Sumin Zhu, et al. "Preparation and Characterization of SiC/cordierite Composite Porous Ceramics." *Ceramics International,* vol. 33, 2007, pp. 115–118.

W. Chi, et al. "Sintering Behaviour of Porous SiC Ceramics." *Ceramics International,* vol. 30, 2004, pp. 869–874.

Wu, S., et al. "Reaction-Forming of Mullite Ceramics Using an Aqueous Milling Medium." *Journal of the American Ceramic Society*, vol. 80, 1997, pp. 1579–1582.

Yan Ma, et al. "Low-Temperature Fabrication and Characterization of Porous SiC Ceramics Using Silicone Resin as Binder." *Ceramics International,* vol. 34, 2008, pp. 253–255.

Yani Jing, et al. "Fabrication and Properties of SiC/mullite Composite Porous Ceramics." *Ceramics International,* vol. 40, 2014, pp. 1329–1334.

A Comparison Study of Alpha Amylase Immobilization on Chitosan-Metal Oxide Composites

Dr. Bindu V. U.
Previously worked as
Assistant Professor (Govt. Guest)
St. Albert's College (Autonomous)
Banerjee Road, Cochin-682018
Ernakulam, Kerala, India
Email: bindukish@gmail.com

Dr. P. V. Mohanan
Professor
Department of Applied Chemistry
Cochin University of Science and Technology
Kalamassery, Cochin-22
Ernakulam, Kerala, India
Email: mohan@cusat.ac.in

Abstract

Chitosan-metal oxide composites, chitosan- Fe_3O_4 (CSM), chitosan-ZnO (CSZ) and chitosan - TiO_2 (CST) were synthesized and intended as suitable supports for immobilization of starch hydrolyzing enzyme, α-amylase. Here α-amylase was chosen as the enzyme to immobilize on these supports due to its wide implementation in industrial applications. The immobilized enzyme, CSZE has shown better immobilization yield of 76%, whereas CSME provides high speed and easy separation from the reaction system due to its magnetic property. The quality of all the immobilized α-amylases were demonstrated and assessed based on its activity and stability. The activity studies demonstrated the substantial improvement in pH and thermal stability of immobilized enzymes. The activation energy (Ea) for the enzymatic reaction was evaluated as 28.23, 23.77 and 25.46 $KJmol^{-1}$ for CSME, CSZE and CSTE, respectively. The kinetic study exhibited the lower substrate affinity of immobilized enzymes in enzymatic reaction compared to the free enzyme attributed to the conformational change of native enzyme upon immobilization. The K_m values for CSME, CSZE and CSTE are 0.65, 0.5 and 0.58 mg / mL respectively, which are higher than that of free enzyme (0.45 mg/mL). The Vmax of free enzyme is decreased from 34.48 μmol mg^{-1} min^{-1} to 16.39 (CSME), 23.81 (CSZE) and 24.39 μmol mg^{-1} min^{-1} as a result of immobilization. The immobilized enzymes have exhibited better storage stability over 6 months and retained more than 50% of their initial activities after 10 cycles of reuse.

Keywords: *Chitosan-Metal Oxide Composite, α-Amylase, Immobilization, Activation Energy, Catalytic Activity, and Maltose.*

An important biopolymer, chitosan, derived from chitin under strong alkaline medium and at elevated temperature was observed as an adequate immobilization carrier due to certain properties such as biocompatibility, biodegradability, non-toxicity and hydrophilicity (X. G. Chen, et al. 269-74) and (M. N. R. Kumar 1-27). Due to its affordability, it is possible for the large-scale production of cheap carriers in the field of enzyme immobilization. The reactive functional groups presented on chitosan such as amino and hydroxyl groups can be chemically modified with some cross-linking agents and enable the coupling of enzymes (B. Krajewska 126-39). This cross-linking of chitosan molecules prevents the direct contact with the enzyme molecules and allows the substrate molecules to reach easily at the catalytic site. Thus chitosan is commonly used as an efficient carrier for enzyme immobilization (G. Spagna, et al. 57-62, 80-89) and (M. Portaccio, et al. 1998).

The amino group in chitosan has pKa of ~ 6.5 which leads to its dissolution in acidic solution, but promote the immobilization of enzyme having isoelectric point less than 6.5. Immobilizations of amylase and cellulase have been successfully reported on chitosan due to the fact that optimum pH of the corresponding enzymes was found to be 5.5 and 5 (S. Heon Lee, et al. 2014) and (C.M. Almeida, et al. 2017). The chitosan can be used as an enzyme carrier in its various forms. Dong et al., observed that immobilized glucose oxidases on the chitosan membrane exhibited excellent stability and reusability (L. Dong, et al. 395-402). Chitosan-gel matrix was found to be an effective carrier for entrapment of biomolecules and resulted in good entrapment efficiencies. Ghanem et al., compared the entrapment of lysine, bovine serum albumin and β-galactosidase in gel beads of chitosan prepared by complexation with tripolyphosphate (A. Ghanem and D. Skonberg 405-13). They observed the controlled release of bioactive compounds and found gel chitosan beads as potential matrix for immobilization. The chitosan beads have been used as an efficient carrier in many immobilization studies (R.S. Juang, et al. 171-77, 187-93), (M. Kamburov and I. Lalov 156-63), and (S. H. Chiou, et al. 265-75). The immobilization of catalase on gluteraldehyde activated chitosan films was shown by Cetinus et al., and also they have mentioned that the immobilized enzyme can be utilized for practical applications.

The introduction of inorganic materials to chitosan offers good mechanical and surface chemical properties and the chitosan-metal oxide composites stand for potent carrier for enzyme immobilization because of their biocompatibility, non toxicity and hydrophilic properties (R. Khan, et al. 207-13) and (A. Kaushik, et al. 676-83) and these have applications in efficacious biosensor fabrication (A. Kaushik, et al. 2013). A novel am-perometric triglyceride biosensor was constructed by Jagriti Narang and coworkers by the covalent co-immobilization of glycerol kinase, lipase and glycerol-3-phosphate oxidase onto the chitosan-ZnO composite film deposited on Pt electrode surface. Raju Khan et al., developed a novel chitosan-TiO_2 bioactive electrode and detected that the immobilization of horseradish peroxidase on chitosan-TiO_2 has shown improved charge transfer resistance (R. Khan and M. Dhayal 2008). Min-Yun Chang et al., investigated the stability and activity of immobilized acid phosphatase onto chitosa-ZrO_2 composite beads (M. Y. Chang and R. S. Juang 2007). Deveci et al., compared the performance of immobilized lipase on chitosan-TiO_2 composite beads by adsorption and covalent binding methods (I. Deveci, et al. 1052-68). Immobilization of pullulanase on chitosan-Fe_3O_4 has been reported and has considered the magnetic chitosan as an effective carrier for enzyme im-

mobilization due to its magnetic property which leads to easy separation of immobilized enzyme from the reaction system by applying an external magnetic field (J. Long, et al. 53-61). Several studies have been reported on the enzyme immobilization onto magnetic chitosan (C. H. Kuo, et al. 2538-45), (L. Zuluaga, et al. 39-43), (L. Zang, et al. 3448-54), (H. Fang, et al. 42-47), and (T. A. Costa-Silva, et al. 16-21).

Amylases are enzymes with attractive industrial applications, which belong to the class of hydrolases. They catalyze the hydrolysis of starch into sugars. In starch processing industries, a large number of commercially available microbial amylases are used for hydrolysis. There have been many reports about the immobilization of amylase and much research has focused on developing polymer based supports (E. Cakmakci, et al. 3-4), (F. Wang, et al. 9374-79), (A. L. Cordeiro, et al. 216-221), (B. Oktay, et al. 386-93), (V. U. Bindu and P.V. Mohanan 1-9), and (Y. Yang and H. A. Chase 145-54). α-amylases (1, 4-α-D-glucanglucanohydrolase) have more importance in the field of biotechnology with applications ranging from food, fermentation, detergent, paper and textile industry (J. Jiang, et al. 600-05). The use of immobilized α-amylase in these industries will reduce the cost of overall enzymes as it can be reused several times, ultimately affecting their economy positively.

Therefore, in this study, we aimed to immobilize α-amylase onto chitosan-metal oxide composites, chitosan-Fe_3O_4 (CSM), chitosan-ZnO (CSZ) and chitosan-TiO_2. We have done the enzyme immobilization studies on these composites. In case of CSZ composite, as a result of centrifugation, undesirable dilution of the sample and the loss of carrier during washing complicate its usage. Support with magnetic core, CSM composite is chosen to avoid these problems. It can be used favourably for high speed separation and for the elimination of mechanical damage by centrifugation. Various parameters such as pH, temperature, contact time and amount of enzyme required for immobilization were optimized so as to acquire immobilized enzymes with maximum activity and stability. The kinetics of the hydrolysis reaction was studied at various substrate concentrations and the kinetic parameters (K_m and V_{max}) were calculated from the Lineweaver - Burke plot. Thermal stability, reusability and storage stability of the immobilized enzymes were also studied.

2. Materials and Methods

2.1. Materials

Diastase α-amylase (1, 4 α-D-glucanglucanohydrolase, EC 3.2.1.1) was acquired from Himedia Laboratories Pvt. Ltd., Mumbai. Soluble starch (potato) was obtained from S.D. Fine-Chem. Ltd., Mumbai. Chitosan (95% degree of deacy-lation) was purchased from Meron Marine Chemicals, Cochin. All other chemicals used were in analytical grade.

2.2. Synthesis of Composites

2.2.1. Chitosan-Fe_3O_4 (CSM) Composite

Chitosan-Fe_3O_4 (CSM) composite was synthesized by reduction–precipitation process, based on the already reported method with slight modification, in which glutaraldehyde was added as the cross-linking agent instead of epoxy chloropropane (C. Cao, et al. 90-97). About 70 mL $FeCl_3$ solution (0.13 mol L-1 in 0.13 mol L-1 HCl) was added into 50 mL of 2% chitosan solution in 1% HCl under continuous stirring for 1hr. Then 30 mL 0.1M Na_2SO_3 solution was added into the colloidal solution and the mixed solution was poured quickly into 40 mL of 12% (v/v) ammonia solution under vigorous stirring at room temperature. The black precipitate suspension was obtained immediately. After that, 5 mL glutaral-

dehyde (25%) was added to the suspension and stirred for 3 hrs in water bath at 60°C in order to stabilize the particles in acid solution. The black precipitate collected with the aid of a magnet was washed several times with distilled water, ethanol and acetone, respectively, then dried in a vacuum oven at 60°C.

2.2.2. Chitosan-ZnO (CSZ) Composite

Firstly, zinc oxide particles were prepared by wet chemical method. About 100 mL 0.9 M aqueous ethanol solution of NaOH was added drop by drop into 100 mL 0.5 M aqueous ethanol solution of zinc nitrate under high speed constant stirring. Then the solution was allowed to settle overnight. The obtained precipitate was washed three times with distilled water and ethanol to remove the by-products and then dried in air atmosphere at about 60 pC (S. Talam, et al. 6). For the preparation of chitosan-ZnO (CSZ) composites, 1 gm ZnO powder was dissolved in 100 mL 1% acetic acid to produce zinc cations. To this solution 1 gm chitosan powder was dissolved under magnetic stirring. Then 1M NaOH was added drop by drop until the solution reached pH 10. The solution was placed in a water bath at 80°C for about 3 hrs. The precipitate obtained was filtered, washed with distilled water several times and then dried in an oven at 50°C for 1 hr (M. M. Abd El Hady 6).

2.2.3. Chitosan- TiO_2 (CST) Composite

About 1 gm nano TiO_2 powder was dissolved in 1% chitosan solution in acetic acid (1% v/v) by sonication. The solution was stirred continuously until clear sol was obtained and after that 1M NaOH solution was added drop wise till the pH of solution became 10. The precipitate formed was heated at 80°C for 5 hrs. Then the precipitate was filtered, washed with excess water and dried in a vacuum oven at 60°C overnight (Y. Haldorai and J. J. Shim 327-33).

2.3. Characterization of Composites

The composites were characterized by FT-IR spectrometry using JASCO FT/IR-4100. Bruker AXS D8 Advance was used for XRD analysis. The TEM images of composites were taken by JEM 2100 having 0.24 nm resolution with an acceleration voltage of 200 kV. Thermograms were obtained using Perkin Elmer, Diamond TG/DTA. The surface areas of the composites were measured using a surface area analyzer (TriStar II 3020 V1.04).

2.4 Preparation of Immobilized Enzyme System

The immobilization of α-amylase was performed by stirring 1 gm each of the composites with enzyme in buffer at room temperature. The immobilization parameters like pH, time and the amount of enzyme for immobilization were optimized. The pH of the immobilization medium varied from 5 to 9, the incubation time varied in the interval from 30-150 minutes and the enzyme concentration from 2 to 20 mg enzyme g^{-1} support. The biocatalyst was then filtered and washed with the same buffer solution. The supernatant and washings were subjected to protein estimation using Folin Ciocalteu's reagent by measuring the absorption at 660 nm in a Thermo Scientific Evolution 201 UV-Visible spectrophotometer (O. H. Lowry, et al. 265-75). The prepared immobilized enzymes were kept in a refrigerator at 4°C for further studies. Immobilization yield (IY) was calculated (Eq. (1)) by measuring the difference in protein concentration of the supernatants before and after immobilization.

$$\textit{Immobilization Yield (IY\%)} = \frac{c_1 - c_2}{c_1} \times 100 \quad (1)$$

where C_1 is the concentration of protein introduced for immobilization and C_2 is the concentration of protein present in the supernatant after immobilization.

The activity yield (Eq. (2)) was determined by measuring the activity of the immobilized en-

zyme and the activity of the initial enzyme used in the immobilization reaction.

ActivityYield (AY%)

$$= \frac{Activity\ of\ Immobilized\ enzyme}{Activity\ of\ free\ enzyme} \times 100 \qquad (2)$$

Immobilization efficiency was calculated using Eq. (3).

$$IE\% = \frac{AY}{IY} \times 100 \qquad (3)$$

2.5. Determination of Activity of Free and Immobilized α-Amylase

The activity of free and immobilized α-amylase was determined by the detection of released reducing sugars from starch using 3, 5 dinitrosalicyclic acid (DNS). The enzymatic reaction was carried out by adding 1 mL of free α-amylase (0.5 mg/mL) or 0.05 gm of immobilized enzyme to 1 mL of 1% starch solution in desired buffer and the system was incubated in a water bath with constant shaking at 30°C for exactly 15 min. The reaction was stopped by adding 1 mL of 3, 5 dinitrosalicylic acid reagent. Incubation was performed in a boiling water bath for 5 min and the reaction tubes were cooled to room temperature. The amount of reduced sugar (maltose) produced was determined spectrophotometrically at 540 nm (N. Jaiswal, et al. 161-67). An enzyme activity unit (EU) was defined as the amount of enzyme liberating 1 ìmol maltose per minute under the assay conditions.

2.6. Optimization of Immobilization Parameters

The optimum pH for maximum activity of free and immobilized enzymes (CSME, CSZE and CSTE) was assayed by incubating the enzyme with starch over a pH range 5-9 at 30°C. The temperature for maximum activity was also assayed by varying the temperature from 30-60°C. In order to test the thermal stability of free and immobilized enzymes, they were subjected to various temperatures ranging from 30-70°C for 1 hr in a water bath. After 1 hr of pre-incubation, both free and immobilized enzymes in buffer were cooled to optimum temperature and enzymatic reaction was performed with the addition of definite amount of 1% starch solution to each reaction medium for a definite time interval.

2.7. Determination of Kinetic Constants

The kinetic parameters were determined by measuring the rates of the reaction at various substrate concentrations ranging from 0.2 to 1.0 mg/mL at optimum temperature and pH. Michaelis constant (k_m) and maximum rate (V_{max}) were calculated from the Lineweaver - Burk plot. This double-reciprocal plot, $^1/_{V_0}$ as a function of $^1/_{S_0}$ gives the y-intercept representing the inverse of V_{max} and the x-intercept of the plot as $-\,^1/_{k_m}$.

2.8. Reusability and Storage Stability

The reusability of the immobilized enzyme was examined by repeated batch experiments maintaining a couple of hours in each cycle. The residual activity of immobilized enzymes at its optimum conditions was measured at fixed time intervals. After each run, the immobilized enzyme was removed, washed with buffer solution and mixed with fresh substrate solution. The reaction was carried out continuously for 10 cycles. The storage stability of immobilized enzymes was studied by calculating their activities after being stored at 4°C in buffer solution for 6 months. The measurement was conducted at regular intervals of time. The activity was compared with initial activity and was represented as percentage relative activity.

3. Results and Discussion

3.1 Characterization Studies

The IR spectrum (Figure-1) of chitosan showed that the absorption band at 3429 cm^{-1} corresponded to combined vibrational frequencies of

hydroxyl and amino functional groups. The peak at 1644 cm^{-1} was related to C=O stretching vibrations of amide and 1540 cm^{-1} to $–NH_2$ bending vibrations. The peak at 1074 cm^{-1} represented the C–O stretching vibrations of primary alcoholic groups in chitosan and the vibrations at 2951 and 2865 cm^{-1} assigned to asymmetric stretching vibrations of $– CH_3$ and $– CH_2$ groups, respectively (D. Zvezdova). For all chitosan-metal oxide composites, the vibrations mentioned above are slightly shifted to lower frequencies, indicating that the complexation of chitosan with metal oxide has taken place through the amino and hydroxyl functional groups presented in it. In case of CSM composite, an additional peak at 577 cm^{-1} was ascribed to Fe–O bond vibrations in magnetite and this peak appeared as a result of electrostatic interaction between positively charged chitosan surface and negatively charged magnetite. This revealed that there was no chemical bonding between chitosan and metal oxide; the metal oxide was only coated by chitosan. This composite has shown other vibrations corresponding to chitosan, but are decreased to lower frequencies and this vibrational change assigned that the amino and hydroxyl groups on chitosan incorporated in the complexation with magnetite (G. Y. Li, et al. 11-18), (Z. Li, et al. 35-43), and (C. Cao, et al. 105-12). The infra red spectrum of CSZ exhibited a new peak at the range of 570 cm^{-1} indicating the stretching vibrations of O–Zn groups. The other peaks showed by this composite that characteristics to chitosan were located in lower frequencies (S. Dhanavel, et al.). In case of CST composite, the absorption band at 520 cm^{-1} ascribed to Ti–O bond vibrations in TiO_2 (I. Deveci, et al. 1052-68). The high intensity of vibration at 1585 cm^{-1} attributed to the interaction of Ti^{4+} in the metal oxide with amino groups of chitosan (P. Norranattrakul, et al. 2013).

The XRD spectra (Figure-2) of chitosan-metal oxide composites have shown the distinctive peaks of chitosan at about 5.5°and 20°, but these peaks were found to be less intense. The strong inter and intramolecular hydrogen bonding existed in the chitosan molecule due to the presence of amino and the hydroxyl groups provided crystalline structure to it. The diminished intensity

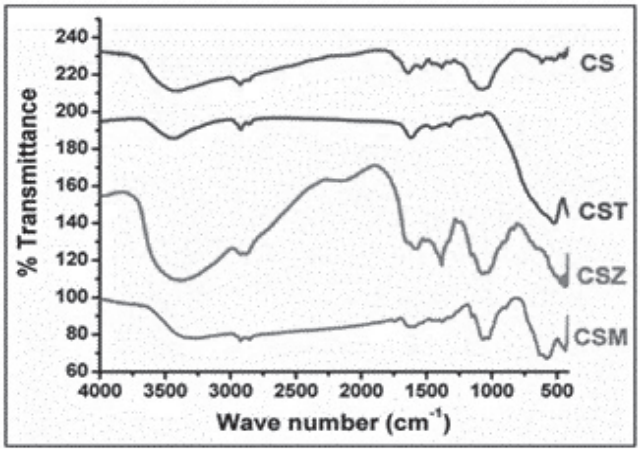

Figure - 1: IR Spectra of CS, CSM, CSZ and CST Composites

of the characteristic peaks of chitosan in the composites indicated that chitosan was successfully modified by the metal oxides. CSM has shown other sharp peaks at 2θ=29.9°, 35.6°, 43.1°, 53.5°, 57.2°, and 62.7° which were assigned to (220), (311), (400), (422), (511) and (440) planes of face centered cubic Fe_3O_4, respectively (JCPDS File No: 75-0033) and revealed its cubic spinel struc-

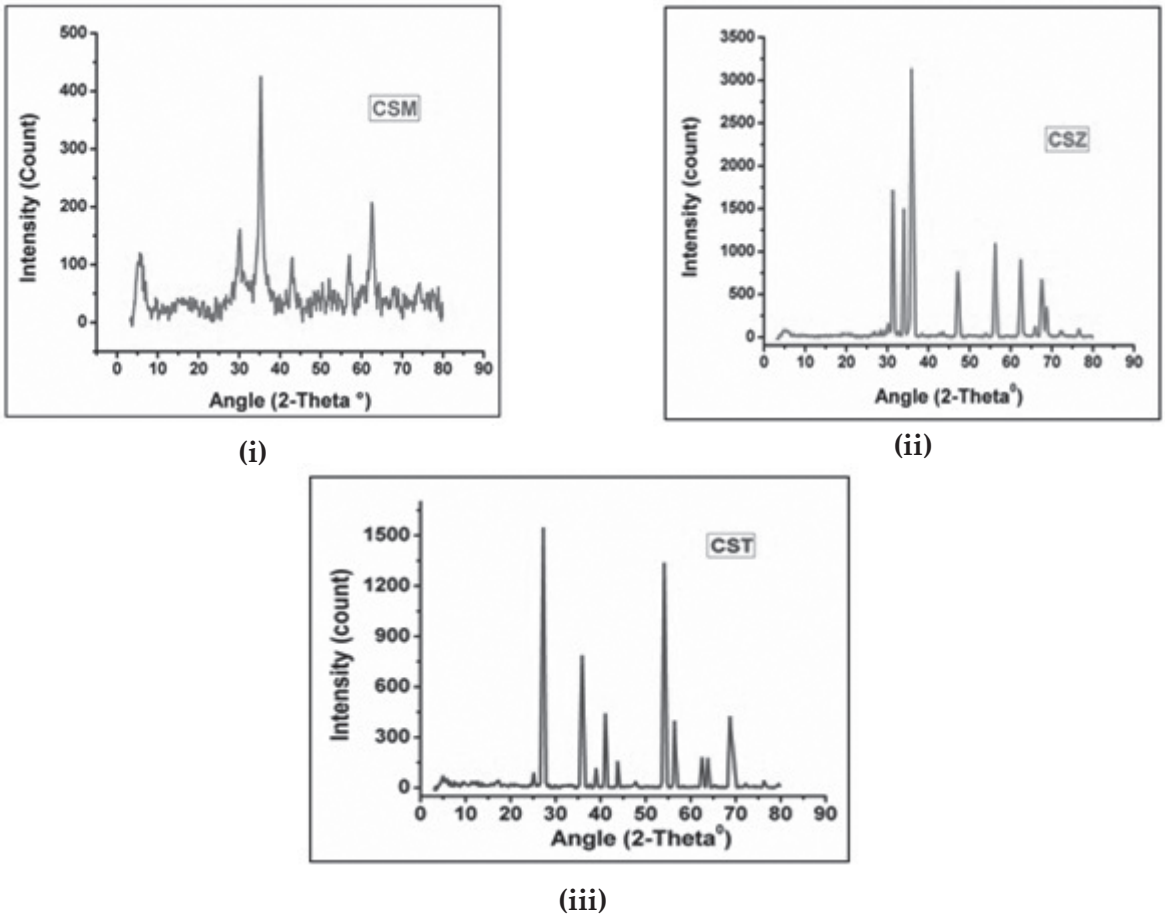

Figure - 2: XRD Spectra of (i) CSM (ii) CSZ and (iii) CST

ture (M. Zhang, et al. 5538-43). In case of CSZ composite, the peaks at 31.7°, 34.36°, 36.2°, 56.59°, 62.7° and 67.90° represented the (1 0 0), (0 0 2), (1 0 1), (1 1 0), (1 03), and (1 1 2) hexagonal planes of ZnO which indicated the Wurtzite structure of ZnO (JCPDS card 36-1451). The diffraction peaks of CST at 26.9°, 36.5°, 39°, 44°, 54° and 55.5° were in good agreement with anatase structure of titanium (JCPDS 21-1272) (T. Theivasanthi and M. Alagar 2013). The average crystalline sizes were evaluated by using Debye–Scherrer equation which was 30 nm for CSM, 25.8 nm for CSZ and 28 nm for CST composites.

The TGA curve (Figure-3) of CSM composite was constituted by three major weight losses, in which the first stage of weight loss of about 8% was attributed to the evaporation of physically adsorbed water. The second and third stages of main weight losses which took place at 200°C – 400°C and 600–730°C can be due to the degradation of primary chains of chitosan and breakdown of cross-linking of chitosan with magnetite. Here we observed that the decomposition of CSM composite occurred at higher temperatures which revealed its higher thermal stability. The cross-linking of magnetite with chitosan and the conformational changes of chitosan increased its thermal stability. The similar thermogram was also reported by Wei Li, et al., in which magnetic chitosan nanoparticles were synthesized by a one-step modified process (W. Li, et al. 57-64). In case of CSZ and CST composites, the first stage of weight loss below 200°C might be due to the loss of adsorbed water and the major weight loss between 200°C and 500°C could have been caused

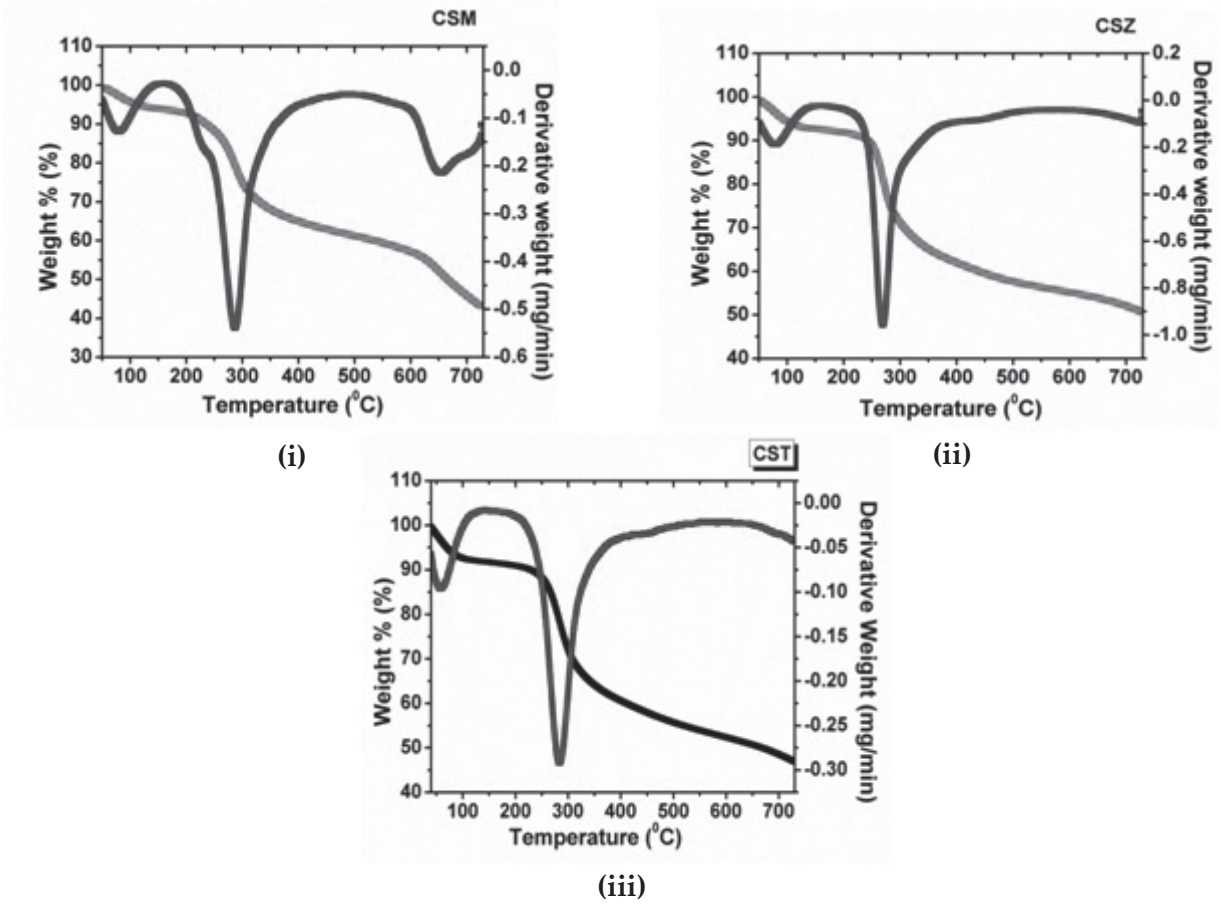

Figure - 3: TGA-DTG Curves of (i) CSM (ii) CSZ and (iii) CST

by the decomposition of the biopolymer and the loss of hydroxyl groups present in the metal oxide. After 500°C there were no remarkable weight losses observed. The thermogram showed that at 700°C, the composites exhibited 45%, 55% and 50% of total weight percentage for CSM, CSZ and CST composites. The interaction between chitosan and the metal oxide contributed high thermal stability to the composites.

The SEM images (Figure-4) have shown that in chitosan matrix, the metal oxide particles were almost evenly embedded into it. Due to the incorporation with the polymer matrix, the metal oxides in the composites were not agglomerated. The average sizes of 30 nm, 20 nm and 25 nm were obtained for CSM, CSZ and CST composites, respectively and these values were in close agreement with that acquired from XRD analysis.

The BET surface areas of chitosan-metal oxide composites are given in Table-1. Among the composites it was found that CSZ composite acquired a higher surface area of 2.4 m^2/g and this provided good sorption ability to it. The decrease of surface area for CSM and CST composites when compared to CSZ may arise from the agglomeration of the metal oxides in the polymer matrix.

3.2 Optimization of α-Amylase Immobilization Conditions

To find out the optimum immobilization condition for the enzyme, we have investigated the effect of pH on the immobilization medium, contact time of support and amount of enzyme taken for immobilization. The effect of immobilization pH on α-amylase activity was investigated by varying the pH ranges between 5 and 9; and the

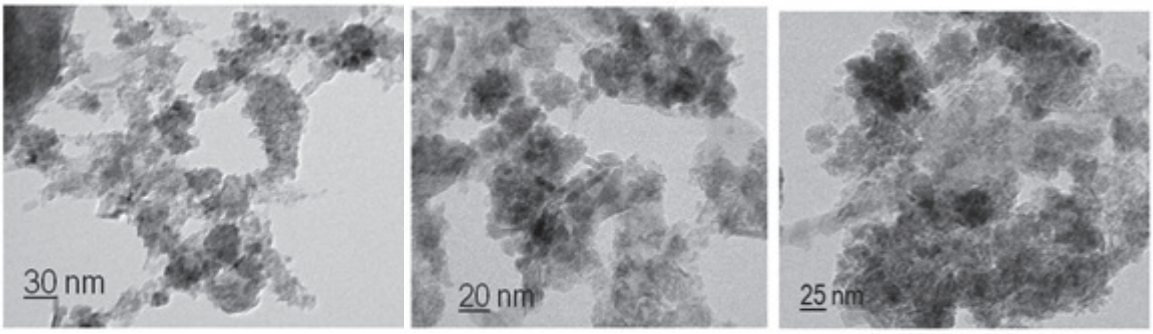

(i) (ii) (iii)

Figure - 4: TEM images of (i) CSM, (ii) CSZ and (iii) CST composites

Table - 1: Surface area of chitosan-metal oxide composites

Composite	Surface Area (m^2/g)
CSM	1.99
CSZ	2.4
CST	1.22

immobilization process was performed for 2 hrs at room temperature. The observations are illustrated in the figure 5a and it showed that the maximum activity acquired by the enzyme was at pH 6 when immobilized on all the three composites CSM, CSZ and CST. At optimum pH 6, there must be significant electrostatic interaction between the support and the enzyme. The strength of interaction was determined by the isoelectric point of enzyme and carrier. The isoelectric point of metal oxides is ~ 6-7 for Fe_3O_4 and TiO_2, ~ 9 for ZnO and that of α-amylase is around 4.6. The pKa of chitosan is ~ 6.5 (J. Nilsen-Nygaard, et al. 552-79) and this value in addition with isoelectric point of metal oxides controls that of whole support. At pH 6, the α-amylase acquires net negative charge and each support may possess net positive charge. This promotes the strong electrostatic interaction between the enzyme and the support and leads to a high enzyme activity. The decreased enzyme activity above and below this pH indicated the poor enzyme adsorption which could be due to the unfavourable charges on the surfaces of the enzyme and the support. When the two surfaces maintained similar charges, electrostatic repulsion existed between them and that led to lower enzyme activity (H. Gustafsson 2013).

The effect of contact time on the activity of immobilized enzyme was given in the Figure-5b. For CSM composite, the maximum enzyme activity was obtained at 120 min of incubation and both CSZ and CST composites exhibited an optimum incubation time of 90 min. The decrease of activity over this optimum incubation time could be due to the multilayer adsorption of enzymes which leads to obstruction in the active site of the enzyme. The multilayer adsorption of enzyme also created the repulsive interaction with the already adsorbed enzyme layer which results in enzyme leakage from the support. So further adsorption did not take place with increase of

incubation time and hence no more enhancements in enzyme activity were observed. Similar observation was reported by Zusfahair et al. when *Bacillus thuringiensis* HCB6 amylase was immobilized on chitosan beads (D. Ningsih, et al. 012068).

The effect of initial protein amount on protein loading on to chitosan-metal oxide composites was investigated and the results are depicted in the Figure-5c. The maximum protein loading acquired by CSM composite was 7.2 mg / g support at initial amount of 12.6 mg enzyme. The CSZ and CST composites attained the optimum protein loading of 10.8 and 8.2 mg /g support at 14.2 mg and 12.6 mg, respectively of initial protein. The highest IY% for CSZ composite might be due to its increased surface area compared to others which was obtained by BET surface area analysis. This was also confirmed by TEM images which provided smallest particle size to CSZ composite and hence imparted increased surface area to it.

The change of immobilized enzyme activity with respect to the amount of initial protein is plotted in the Figure-5d. The maximum activity of α-amylase on composites was 10.28 EU for CSM, 13.7 EU for CSZ and 11.28 EU for CST at aninitial protein of 12.6 mg, 14.2 mg and 12.6 mg, respectively. As the enzyme concentration further increases after these saturation points, the accessibility of substrate molecules towards the enzyme active site may be prohibited as a result of the steric hindrance that existed between the enzyme-substrate molecules. The immobilization yield, activity yield and immobilization efficiency were evaluated and the results are given in the Table-2.

3.3. Activity of Enzymes

3.3.1. Effect of pH and Temperature on the Activity of Free and Immobilized α-Amylases

We have studied the effect of pH on the activity of free and immobilized enzymes and are shown in the Figure-6a. The free enzyme exhibited maximum activity at pH 5-5.5, whereas the optimum pH for CSME was at pH 7 and for both CSZE and CSTE, it was at pH 6. Here we noticed that for all immobilized enzymes, the optimum pH shifted to the alkaline region and they have shown a very broad pH profile compared to free enzymes. The increased positive charge on the surface of the support due to the presence of amino groups leads to the decrease of H^+ ions concentration at the microenvironment of the immobilized enzyme and this causes the immobilized enzyme region to be more alkaline than

Table - 2: Immobilization yield, activity yield and immobilization efficiency of α-Amylase loaded on CSM, CSZ and CST Composites. The enzyme was immobilized on different supports at various initial concentrations at optimum experimental conditions

Support	Initial Protein (mg)	Immobilized Protein mg/g support	IY (%)	Initial Activity (EU)	Immobilized Enzyme Activity (EU)	AY (%)	IE (%)
CSM	12.6	7.2	57.14	23.49	10.28	43.76	76.58
CSZ	14.2	10.8	76.05	26.06	13.7	52.57	69.12
CST	12.6	8.2	65.08	20.56	11.28	54.86	84.30

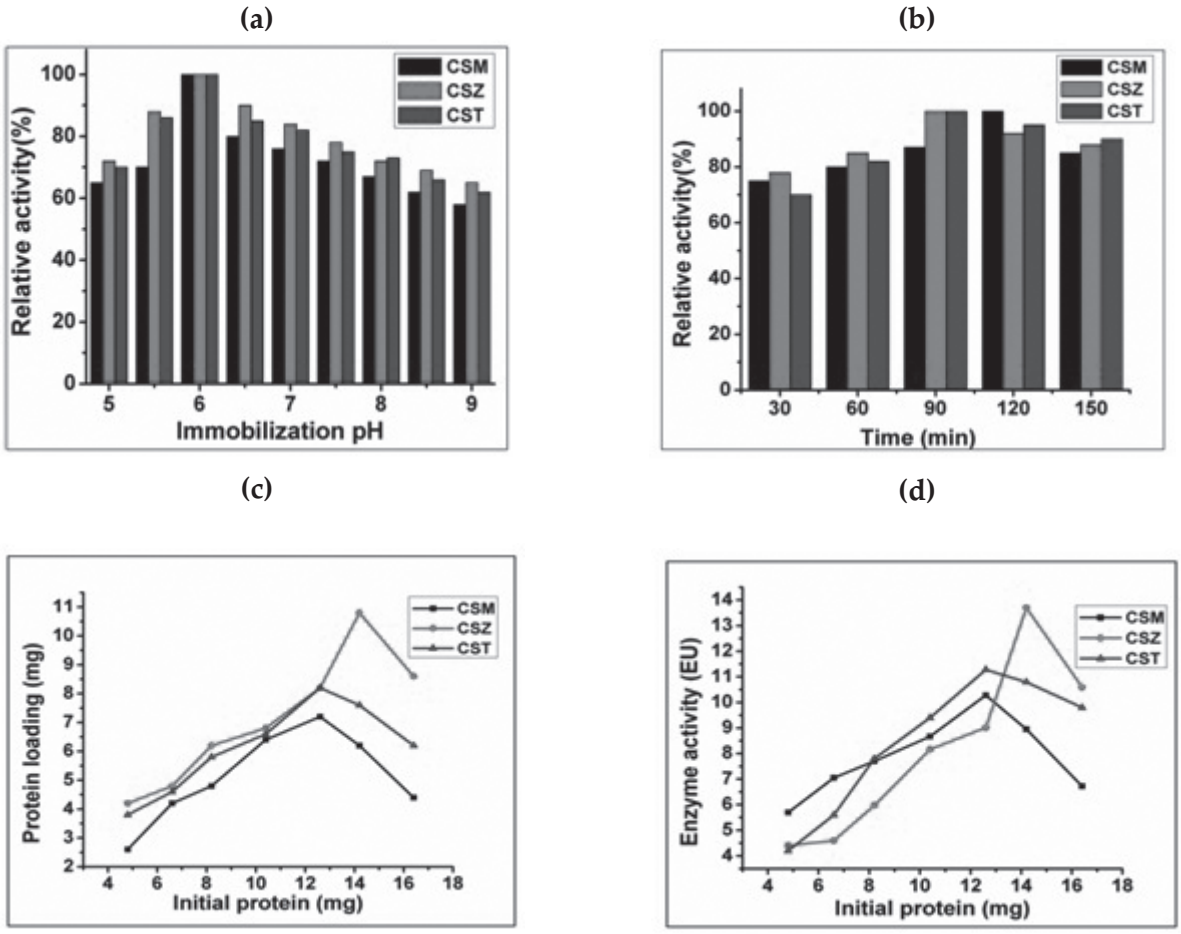

Figure - 5: (a) Effect of pH of immobilization medium on the relative activity of immobilized α-amylases. Buffers used are acetate buffer (5-5.5), Phosphate buffer (6-8) and Glycine Buffer (8.5-9) (b) Effect of contact time on immobilized enzymes activity (c) Effect of initial protein amount on protein loading (d) Effect of initial protein concentration on immobilized enzyme activity

that of external solution. The shift of optimum pH towards the alkaline region was also reported by Egwim, et al., in case of immobilized lipase on chitosan beads (E. Egwim, et al. 2012).

The effect of temperature on the activity of free and immobilized α-amylase was studied by changing the temperature in the range of 30-60°C. The results are depicted in Figure-6b and it was found that the free enzyme has shown maximum activity at 50°C, while for all immobilized enzymes it gets shifted to 35°C. The shift of optimum temperature to the lower region might be due to the conformational changes of enzyme structure as a result of immobilization. This could be due to the fact that the immobilization affected the three dimensional structure of the enzyme, imparted restriction in the movement of enzymes and these led to the changes in substrate affinity towards enzyme active site. The shift of temperature optimum around 10-15°C to the lower region was reported by Ashly et al., for the immobilization of α-amylase on polyanilines (P. Ashly, et al. 1808-13). The immobilization provided increased temperature characteristics to the enzyme structure and reduced the diffusional

limitations of substrate molecules at higher temperatures. This contributed improved activity to the immobilized enzymes at higher temperatures. The increased temperature stability of enzymes was also reported when β-glucosidase immobilized on chitosan beads (Y. Zhou, et al. 6).

The activation energy (Ea) for the enzymatic reaction was evaluated from the slope of Arrhenius plot of log (relative activity percent) vs 1/T (Figure-6c). The Ea of free enzyme was calculated as 11.75 KJmol^{-1} and the values 28.23, 23.77 and 25.46 KJmol^{-1} represented that of CSME, CSZE and CSTE, respectively. Here the immobilized enzymes have attained higher Ea values than that of free enzymes. This might be due to the fact that since the immobilization affected the three dimensional structure of the enzyme, the time required for the contact of enzyme with the substrate molecule has been extended which resulted in reduction in the catalytic activity. Higher Ea values for α-amylase were reported when immobilized on chitin and polyacrylamide (M. A. Abdel Naby, et al. 319-25).

3.4. Thermal Stability

Thermal stability of free and immobilized α-amylases was examined in which they have undergone 1 hr pre-incubation by varying the temperature from 30 to 70°C in the absence of substrate. After that, the enzymatic reaction was carried out at optimum temperature and the activi-

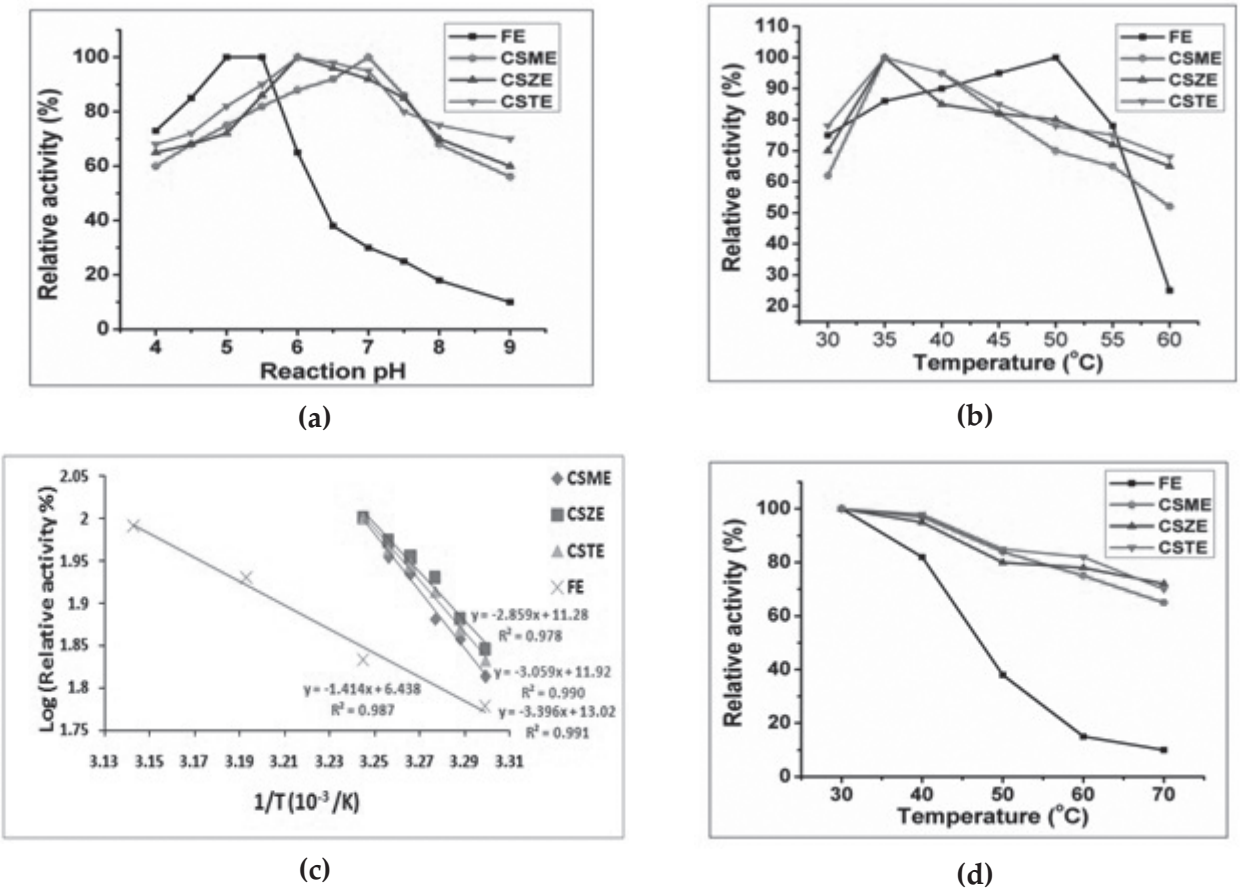

Figure - 6: (a) Effect of reaction pH on the activity of free and immobilized α-amylases. (b) Effect of temperature on activity of free and immobilized enzymes. (c) Arrhenius plot to calculate the activation energy (Ea) of free and immobilized enzymes. (d) Thermal stability of free and immobilized enzymes at different temperatures

ties were determined for the corresponding incubating temperatures. The results are illustrated in the figure 6d and it is observed that all immobilized enzymes have shown enhanced heat resistance compared to free enzymes. After 50°C of pre-incubation, the free enzyme retained only 36% of activity, whereas the immobilized enzymes retained about 80-85% of activity. Even as the temperature increased to higher ranges, the immobilized enzymes underwent slow thermal inactivation. At 70°C, the activity attained by the free enzyme was only 10%, while for immobilized enzymes the activities were in the range of 65%-72%.

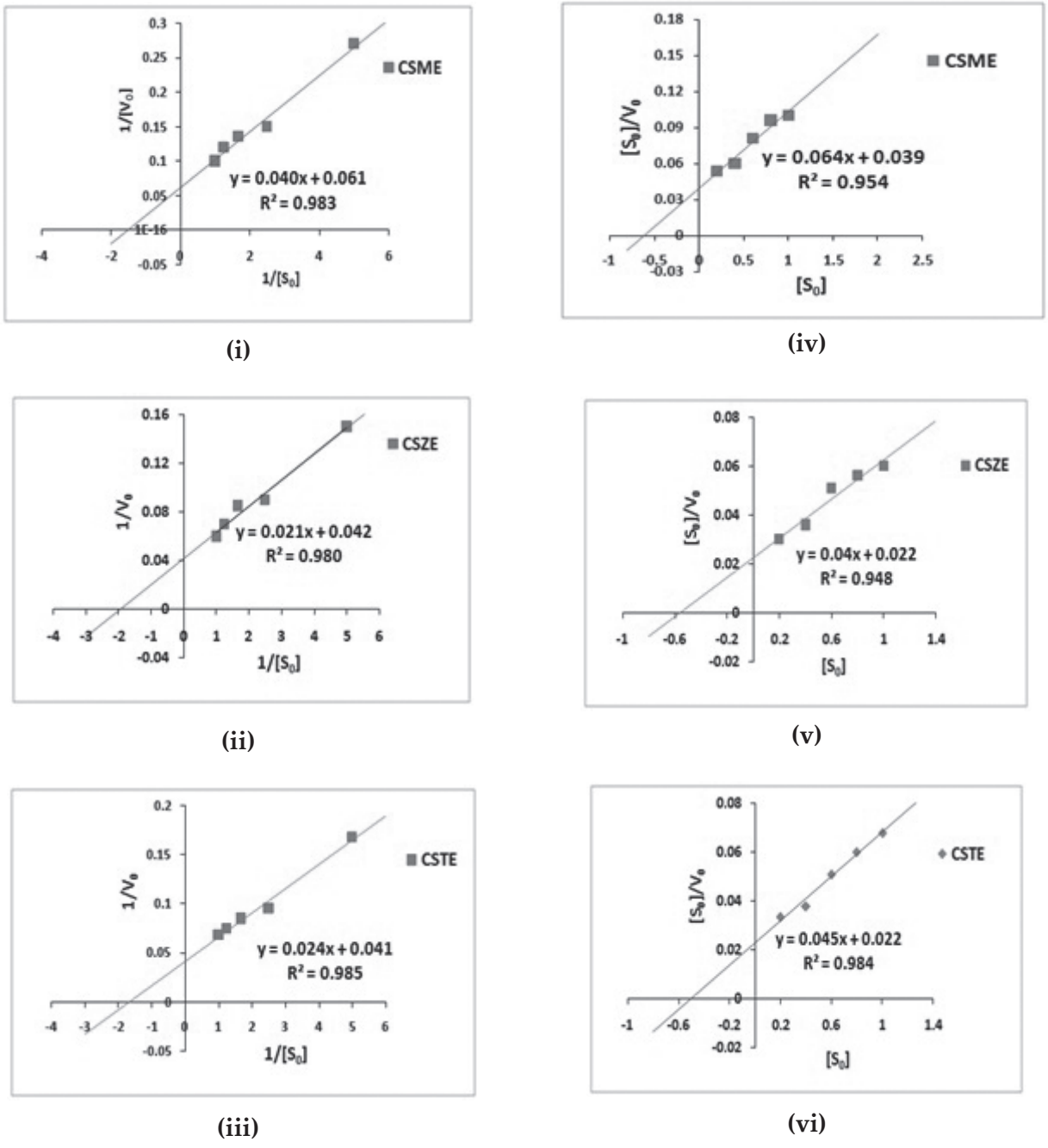

Figure - 7: Lineweaver-Burk Plots for (i) CSME (ii) CSZE (iii) CSTE and Hanes-Woolf Plots for (iv) CSME (v) CSZE (vi) CSTE

3.5 Kinetic Parameters

The effect of immobilization of α-amylase on kinetic parameters was evaluated by determining the starch hydrolysis activities of free and immobilized enzymes at optimum temperature and pH for different concentrations of starch ranging between 0.2-1.0 mg/mL. The kinetic parameters K_m and V_{max} can be calculated from Lineweaver-Burk and Hanes-Woolf plots (Figure - 7). The kinetic parameters (K_m and V_{max}), turnover number (K_{cat}) and catalytic efficiency (K_{cat}/K_m) calculated are given in the Table-3.

The free enzyme exhibited K_m value of 0.45 ± 0.02 mg/mL and that of immobilized enzymes were 0.65 ± 0.04, 0.5 ± 0.04 and 0.58 ± 0.03 mg/mL. For all immobilized enzymes, the K_m values are found to be increased when compared to free enzymes. As the K_m value denoted the affinity of enzyme towards the substrate molecule, the immobilized enzymes with higher values represented their lower affinity. This might be arising from the reduced accessibility of the substrate molecule towards the active site of the enzyme, since the immobilization has caused some conformational changes in the active site. Similar trend was

Table - 3: Kinetic parameters for free and immobilized α-Amylases on chitosan-metal oxide composites

Immobilized Enzyme	K_m (mg/mL)	V_{max} (mmol mg^{-1} min^{-1})	K_{cat} (min^{-1})	K_{cat}/K_m ($mlmg^{-1}min^{-1}$)
Free enzyme	0.45± 0.02	34.48±0.05	1910.19	4244.87
CSME	0.65± 0.04	16.39± 0.01	908.00	1396.92
CSZE	0.5±0.04	23.81± 0.02	1319.07	2638.14
CSTE	0.58± 0.03	24.39± 0.04	1351.21	2329.67

obtained in many literatures (S. A. Ahmed and O. K. Hassan 466-74), (A. Kara, et al. 61-68), and (S. A. Ahmed and O. K. Hassan 466-74), (A. Kara, et al. 61-68, and (A. El-Batal, et al 96-101). The V_{max} explains the capability of enzymes towards catalytic activity and the value for free enzyme was calculated as 34.48 ± 0.05 μmol mg^{-1} min^{-1}. All the immobilized enzymes have attained lower V_{max} values than that of free enzyme and the values were 16.39 ± 0.01, 23.81 ± 0.02 and 24.39 ± 0.04 μmol mg^{-1} min^{-1} for CSME, CSZE and CSTE, respectively. The diffusional limitations of the substrate molecule to the active site of the enzyme due to immobilization provided lower enzyme activity and hence lower V_{max} values to immobilized enzymes. The decrease of V_{max} values for α-amylase was widely reported in many literatures (F. Eslamipour and P. Hejazi 20187-97), (K. Singh and A. M. Kayastha 75-81), and (O. Danis, et al. 205-10).

The free enzyme attained K_{cat} value of 1910.19 min^{-1} and it was found that the immobilized enzymes CSME, CSZE and CSTE showed 52.46%, 30.94% and 29.26% lower values than that of free enzymes. These results indicated that the immobilized enzymes required 66.09, 45.49 and 44.40 milliseconds in order to convert one substrate

molecule into product while that for the free enzyme it was only 31.41 milliseconds. The K_{cat} / K_m values were calculated as 4244.87, 1396.92, 2638.14 and 2329.67 ml mg^{-1} min^{-1} for the free enzymes, CSME, CSZE and CSTE, respectively and this showed the lower catalytic efficiency of immobilized enzymes compared to the free enzyme.

3.6 Reusability and Storage Stability

The repeated use of immobilized enzymes has a significant role in predicting its cost effective applicability in industrial levels. We have investigated the reusability of immobilized enzymes for 10 cycles of repeated uses and the relative activities were determined at optimum conditions. The Figure-8a showed the variation of relative activities of immobilized enzymes on reuses up to 10 cycles in which the relative activity of first cycle was assigned to 100% and the remaining activities were expressed relative to this value.

After 10 cycles of uses the relative activities of immobilized enzymes were calculated as 50%, 60% and 65% for CSME, CSZE and CSTE. The activities of immobilized enzymes were found to be decreased on repeated uses which could be due to desorption of enzymes from the carrier surface. The reuses of immobilized enzymes caused the weakening of enzyme binding with the support and hence this led to the loss in activity. Also the frequent encountering of substrate molecules to the active site of the immobilized enzyme distorted its conformational integrity which caused the reduction in their activities. Mahshid Defaei, et al., noticed the high preserved activity of α-amylase even after ten cycles of repeated uses when immobilized on naringin functionalized magnetic nanoparticles (M. Defaei, et al. 354-60). Similar observations were also found in many reports where α-amylase was immobilized on various supports (M. Jahir Khan, et al. 2012) and (S. Talekar and S. Chavare 2012).

It is very important to investigate how long the enzyme stability existed during the storage period and this determines its applicability in industrial zones. For this study, all immobilized enzymes were kept in desired buffer at 4°C and their activities were analyzed at regular intervals up to six months of storage period (Figure-8b). After six months of storage the immobilized enzymes retained the activities of 50% for CSME, 60% for CSZE and 64.5% for CSTE and this reduction in activity could be as a result of natural loss in enzyme activity during the storage. This tendency was accompanied with the changes in structural conformations of the enzyme active site during the long period of storage. Since the conformational changes of enzyme can be minimized as a result of immobilization, the loss in activity throughout the storage period can be controlled much more in case of immobilized enzyme systems. The enhanced storage stability was observed by Chia-Hung, et al., for immobilized lipase on chitosan coated magnetite nano-particles (C. H. Kuo, et al. 2538-45). Bayramoglu, et al., also reported the improved stability of immobilized α-amylase onto reactive porous membranes in which they achieved about 71% of initial activity during 2 months of storage (G. Bayramoglu, et al. 591-99).

4. Conclusions

Chitosan-metal oxide composites, CSM, CSZ and CST were synthesized, characterized and subjected to α-amylase immobilization. In our study, the enzyme loading ability of CSZ composite was found to be more than that of CSM and CST composites and this is attributed to the higher surface area of CSZ composite. All the immobilized enzymes exhibited good thermal stability compared to the free enzyme. The immobilized enzymes have attained higher Ea values than that of the free enzyme which might be due to the fact that since the immobilization affected the

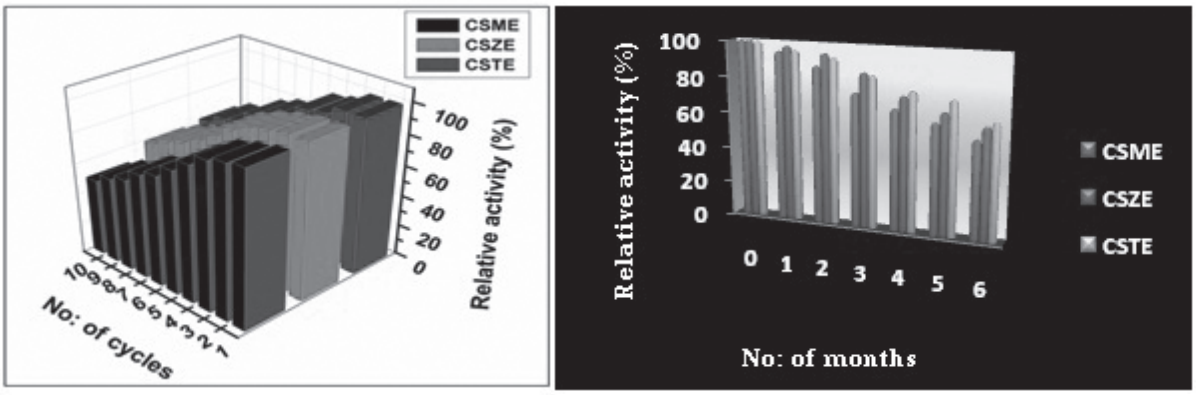

(a) **(b)**

Figure - 8: (a) Reuse of immobilized enzymes, CSME, CSZE and CSTE for several reaction cycles, the enzyme activity was assayed at optimum pH and temperature, the initial activity considered as 100% (b) storage stability of immobilized enzymes for six months, the immobilized enzymes were stored at 4°C

three dimensional structure of the enzyme, the time required for the contact of enzyme with the substrate molecule has been extended, which resulted in reduction in the catalytic activity. The kinetic study showed that the lower substrate affinity of the immobilized enzymes in enzymatic reaction compared to the free enzyme attributed to the conformational change of native enzyme upon immobilization. The studies on pH and temperature, reuse assay and storage stabilities confirmed that the immobilized enzymes are suitable for many industrial applications.

Acknowledgement

The authors are thankful to UGC for the financial support.

References

A. El-Batal, et al. "Stabilization of α-amylase by using Anionic Surfactant during the Immobilization Process." *Radiation Physics and Chemistry,* vol. 74, no. 2, 2005, pp. 96-101.

A. Ghanem and D. "Skonberg. Effect of Preparation Method on the Capture and Release of Biologically Active Molecules in Chitosan Gel Beads." *Journal of Applied Polymer Science,* vol. 84, no. 2, 2002, pp. 405-413.

A. Kara, et al. Immobilization of α-amylase on Cu2+ chelated poly (Ethylene Glycol Dimethacrylate-n-Vinyl Imidazole) Matrix via Adsorption." *Reactive and Functional Polymers,* vol. 62, no. 1, 2005, pp. 61-68.

A. Kaushik, et al. "Iron Oxide Nanoparticles–Chitosan Composite Based Glucose Biosensor." *Biosensors and Bioelectronics,* vol. 24, no. 4, 2008, pp. 676-683.

A. Kaushik, et al. "Nanocomposites Based on Chitosan - Metal/Metal Oxides Hybrids for Biosensors Applications." 2013.

A.L. Cordeiro, et al. Immobilization of Bacillus licheniformis α-amylase onto Reactive Polymer Films, *Journal of Biotechnology,* vol. 154, no. 4, 2011, pp. 216-221.

B. Krajewska. Application of Chitin-and Chitosan-Based Materials for Enzyme Immobilizations: A Review." *Enzyme and Micro-*

bial Technology. vol. 35, no. 2-3, 2004, pp. 126-139.

B. Oktay, et al. "Immobilization of α-amylase onto poly (Glycidyl Methacrylate) grafted Electrospun Fibers by ATRP." *Materials Science and Engineering: C,* vol. 50, 2015, pp. 386-393.

C. Cao, et al. Visible-light Photocatalytic Decolorization of Reactive Brilliant Red X-3B on Cu2O/Crosslinked-Chitosan Nanocomposites prepared via One Step Process." *Applied Surface Science,* vol. 271, 2013, pp. 105-112.

C. Cao, et al. "In situ Preparation of Magnetic Fe3O4/Chitosan Nanoparticles via a Novel Reduction–Precipitation Method and their Application in Adsorption of Reactive Azo Dye." *Powder Technology,* vol. 260, 2014, pp. 90-97.

C.H. Kuo, et al. "Optimum Conditions for Lipase Immobilization on Chitosan-Coated Fe3O4 Nanoparticles." *Carbohydrate Polymers*, vol. 87, no. 4, 2012, pp. 2538-2545.

C.H. Kuo, et al. "Optimum Conditions for Lipase Immobilization on Chitosan-Coated Fe3O4 Nanoparticles." *Carbohydrate Polymers,* vol. 87, no. 4, 2012, pp. 2538-2545.

C.M. Almeida, et al. "Immobilization of Amylase Using Chitosan Beads as Support." *Scientia Plena,* vol. 13, no. 11, 2017.

D. Ningsih, et al. "Bacillus Thuringiensis HCB6 Amylase Immobilization by Chitosan Beads, IOP Conference Series: Materials Science and Engineering." *IOP Publishing*, 2017, p. 012068.

D. Zvezdova. "Synthesis and Characterization of Chitosan from Marine Sources in Black Sea."

E. Cakmakcý, et al. "Immobilization of α-amylase on Aminated Polyimide Membrane: Preparation, Characterization, and Properties." *Starch – Starke,* vol. 66, 2014, pp. 3-4.

E. Egwim, et al. "Optimization of Lipase Immobilized on Chitosan Beads for Biodiesel Production." 2012.

F. Eslamipour and P. Hejazi. "Evaluating Effective Factors on the Activity and Loading of immobilized α-amylase onto Magnetic Nanoparticles using a Response Surface-Desirability Approach." *RSC Advances*, vol. 6, no. 24, 2016, pp. 20187-20197.

F. Wang, et al. "Comparison of Covalent Immobilization of Amylase on Polystyrene Pellets with Pentaethylenehexamine and Pentaethylene Glycol Spacers." *Bioresource Technology,* vol. 102, no. 20, 2011, pp. 9374-9379.

G. Bayramoglu, et al. "Immobilization of a Thermostable α-amylase onto Reactive Membranes: Kinetics Characterization and Application to Continuous Starch Hydrolysis." *Food Chemistry*, vol. 84, no. 4, 2004, pp. 591-599.

G. Spagna, et al. "A Mixture of Purified Glycosidases from Aspergillus Niger for Oenological Application Immobilised by Inclusion in Chitosan Gels." *Enzyme and Microbial Technology.* vol. 30, no. 1, 2002, pp. 80-89.

G. Spagna, et al. "Immobilization of α-L-Arabinofuranosidase on Chitin and Chitosan." *Process Biochemistry,* vol. 33, no. 1, 1998, pp. 57-62.

G.Y. Li, et al. "Kinetics of Adsorption of Saccharomyces Cerevisiae Mandelated Dehydrogenase on Magnetic Fe3O4–Chitosan

Nanoparticles." *Colloids and Surfaces A: Physicochemical and Engineering Aspects*, vol. 320, no. 1. 2008, pp. 11-18.

H. Fang, et al. "Preparation of Magnetic Chitosan Nanoparticles and Immobilization of Laccase." *Journal of Wuhan University of Technology-Mater*, Sci. Ed., vol. 24, no. 1, 2009, pp. 42-47.

H. Gustafsson, "Enzyme Immobilization in Mesoporous Silica." *Chalmers University of Technology,* 2013.

I. Deveci, et al. "Synthesis and Characterization of Chitosan/TiO 2 Composite Beads for improving Stability of Porcine Pancreatic Lipase." *Applied Biochemistry and Biotechnology,* vol. 175, no. 2, 2015, pp. 1052-1068.

I. Deveci, et al. "Synthesis and Characterization of Chitosan/Tio 2 Composite Beads for Improving Stability of Porcine Pancreatic Lipase." *Applied Biochemistry and Biotechnology*, vol. 175, no. 2, 2015, pp. 1052-1068.

J. Jiang et al. "Synthesis of Superparamagnetic Carboxymethyl Chitosan/Sodium Alginate Nanosphere and Its Application for immobilizing α-Amylase." *Carbohydrate Polymers*, vol. 151, 2016, pp. 600-605.

J. Long, et al. "A Novel Method for Pullulanase Immobilized onto Magnetic Chitosan/ Fe3O4 Composite Nanoparticles by In Situ Preparation and Evaluation of the Enzyme Stability." *Journal of Molecular Catalysis B: Enzymatic,* vol. 109, 2014, pp. 53-61.

J. Nilsen-Nygaard, et al. "Chitosan: Gels and Interfacial Properties." *Polymers,* vol. 7, no. 3, 2015, pp. 552-579.

K. Singh and A.M. Kayastha. "Optimal Immobilization of α-amylase from wheat (Triticum Aestivum) onto DEAE-Cellulose using Response Surface Methodology and Its Characterization." *Journal of Molecular Catalysis, B: Enzymatic* vol. 104, 2014, pp. 75-81.

L. Dong, et al. "Immobilization of Glucose Oxidase on a Novel Crosslinked Chitosan Support Grafted with L-Lysine Spacers." *Chemical and Biochemical Engineering Quarterly.* vol. 25, no. 3, 2011, pp. 395-402.

L. Zang, et al. "Preparation of Magnetic Chitosan Nanoparticles as Support for Cellulase Immobilization." *Industrial and Engineering Chemistry Research,* vol. 53, no. 9, 2014, pp. 3448-3454.

L. Zuluaga, et al. "Immobilization of Mannanase on Magnetic Chitosan Microspheres." *Revista Mexicana de Física,* vol. 58, no. 2, 2012, pp. 39-43.

M. Defaei, et al. "Improvement of Stability and Reusability of α-amylase Immobilized on Naringin Functionalized Magnetic Nanoparticles: A Robust Nanobio-catalyst." *International Journal of Biological Macromolecules,* vol. 113, 2018, pp. 354-360.

M. Jahir Khan, et al. "Immobilization of Porcine Pancreatic α-amylase on Magnetic Fe2O3 Nanoparticles: Applications to the Hydrolysis of Starch." 2012.

M. Kamburov and I. Lalov. "Preparation of Chitosan Beads for Trypsin Immobilization." *Biotechnology and Biotechnological Equipment, vol.* 26, sup. 1, 2012, pp. 156-163.

M. Portaccio, et al. "Galactose Competitive Inhbition of β-Galactosidase (A. oryzae) Immobilized on Chitosan andNnylon Supports." 1998.

M. Zhang, et al. "Magnetite/Graphene Composites: Microwave Irradiation Synthesis and Enhanced Cycling and Rate Performances for Lithium Ion Batteries." *Journal of Materials Chemistry,* vol. 20, no. 26, 2010, pp. 5538-5543.

M.A. Abdel-Naby, et al. "Immobilization of Bacillus Subtilis α-amylase and Characterization of Its Enzymatic Properties." *Microbiological Research*, vol. 153, no. 4, 1999, pp. 319-325.

M.M. Abd Elhady. "Preparation and Characterization of Chitosan/Zinc Oxide Nanoparticles for Imparting Antimicrobial and UV Protection to Cotton Fabric. *International Journal of Carbohydrate Chemistry,* 2012, p. 6.

M.N.R. Kumar. "A Review of Chitin and Chitosan Applications." *Reactive and Functional Polymers,* vol. 46, no. 1, 2000, pp. 1-27.

M.Y. Chang and R.S. Juang. "Stability and Reactivity of Acid Phosphatase Immobilized on Composite Beads of Chitosan and Zro2 Powders." 2007.

N. Jaiswal, et al. "α-amylase Immobilization on Gelatin: Optimization of Process Variables." *Journal of Genetic Engineering and Biotechnology,* vol. 10, no. 1, 2012, pp. 161-167.

O. Danis, et al. "α-amylase Immobilization on Epoxy Containing Thiol-Ene Photocurable Materials." *Journal of Microbiology and Biotechnology*, vol. 23, no. 2, 2013, pp. 205-210.

O.H. Lowry, et al. "Protein Measurement with the Folin Phenol Reagent." *Journal of Biological Chemistry,* vol. 193, no. 1, 1951, pp. 265-275.

P. Ashly, et al. "Activity of Diastase α-amylase Immobilized on Polyanilines (PANIs)." F*ood Chemistry*, vol. 127, no. 4, 2011, pp. 1808-1813.

P. Norranattrakul, et al. "Fabrication of Chitosan/Titanium Dioxide Composites Film for the Photocatalytic Degradation of Dye." *Journal of Metals, Materials, and Minerals,* vol. 23, no. 2, 2013.

R. Khan and M. Dhayal. "Electrochemical Studies of Novel Chitosan/Tio_2 Bioactive Electrode for Biosensing Application." 2008.

R. Khan, et al. "Zinc Oxide Nanoparticles-Chitosan Composite Film for Cholesterol Biosensor." *Analytica Chimica Acta,* vol. 616, no. 2, 2008, pp. 207-213.

R.S. Juang, et al. "Solute Adsorption and Enzyme Immobilization on Chitosan Beads Prepared from Shrimp Shell Wastes." *Bioresource Technology,* vol. 80, no. 3, 2001, pp. 187-193.

R. S. Juang, et al. "Use of Chemically Modified Chitosan Beads for Sorption and Enzyme Immobilization." *Advances in Environmental Research,* vol. 6, no. 2, 2002, pp. 171-177.

S. Dhanavel, et al. "Photocatalytic Activity of Chitosan/ZnO Nanocomposites for degrading Methylene Blue."

S. Heon Lee, et al. "Properties of Cellulase Immobilized on Chitosan Beads." 2014.

S. Talam, et al. "Synthesis, Characterization, and Spectroscopic Properties of ZnO Nanoparticles." *ISRN Nanotechnology,* 2012, p. 6.

S. Talekar and S. Chavare. "Optimization of Immobilization of α-amylase in alginate gel and It's Comparative Biochemical Studies with Free α-amylase." 2012.

S. A. Ahmed and O.K. Hassan. "Studies on the Activity and Stability of Immobilized Bacillus Acidocaldarius α-Amylase." *Australian Journal of Basic and Applied Sciences,* vol. 2, no. 3, 2008, pp. 466-474.

S. H. Chiou, et al. "Immobilization of Lipase to Chitosan Beads Using a Natural Cross-Linker." *Preparative Biochemistry and Biotechnology,* vol. 37, no. 3, 2007, pp. 265-275.

T. Theivasanthi and M. Alagar. "Titanium Dioxide (TiO_2) Nanoparticles XRD Analyses: An Insight." *arXiv preprint arXiv: 1307. 1091,* 2013.

T. A. Costa-Silva, et al. "P.S. Marques, C.R.F. Souza, S. Said, W.P. Oliveira, Enzyme Encapsulation in Magnetic Chitosan-Fe3O4 Microparticles." *Journal of microencapsulation,* vol. 32, no. 1, 2015, pp. 16-21.

V. U. Bindu and P.V. Mohanan. "Enhanced Stability of α-amylase via Immobilization onto Chitosan-TiO_2." *Nanocomposite Nanoscience and Nanotechnology,* vol. 4, no. 2, 2017, pp. 1-9.

W. Li, et al. "The Characterization and Thermal Investigation of Chitosan-Fe3O4 Nanoparticles Synthesized via a Novel One-Step Modifying Process." *Journal of Macromolecular Science,* Part A, vol. 48, no. 1, 2010, pp. 57-64.

X. G. Chen, et al. "Preparation and Biocompatibility of Chitosan Microcarriers as Biomaterial." *Biochemical Engineering Journal,* vol. 27, no. 3, 2006, pp. 269-274.

Y. Haldorai and J. J. Shim. "Novel Chitosan-TiO2 Nanohybrid: Preparation, Characterization, Antibacterial, and Photocatalytic Properties." *Polymer Composites,* vol. 35, 2, 2014, pp. 327-333.

Y. Yang and H. A. Chase. "Immobilization of α-amylase on poly (vinyl alcohol)-coated Perfluoropolymer Supports for use in Enzyme Reactors." *Biotechnology and Applied Biochemistry,* vol. 28, no. 2, 1998, pp. 145-154.

Y. Zhou, et al. "Optimal Immobilization of β-glucosidase into Chitosan Beads using Response Surface Methodology." *Electronic Journal of Biotechnology,* vol. 16, no. 6, 2013, pp. 6-6.

Z. Li, et al. "Preparation and Characterization of CdS Quantum Dots Chitosan Biocomposite." *Reactive and Functional Polymers,* vol. 55, no. 1, 2003, pp. 35-43.

Theoretical and Experimental Study on Third Order Nonlinearities and Optical Limiting Properties of Anthracene Picrate

Dr. Anju Linda Varghese
Assistant Professor, Department of Chemistry
Baselius College, Kottayam-686001
Kerala, India
Email: anjulindavarghese@baselius.ac.in

Dr. Maria Linsha P. L.
Assistant Professor, Department of Chemistry
St. Teresa's College (Autonomous)
Ernakulam-682011, Kerala, India
Email: marialinsha@teresas.ac.in

Dr. Ignatious Abraham
Assistant Professor, Department of Chemistry
Sacred Heart College, Thevara
Ernakulam-682013, Kerala, India
E-mail: ignatiousa@shcollege.ac.in

Dr. George Mathai
Associate Professor (Rtd.), Department of Chemistry
Sacred Heart College, Thevara
Ernakulam-682013, Kerala, India
E-mail: georgem_mathai@yahoo.co.in

Abstract

Third-order nonlinearities and optical limiting properties of anthracene picrate have been studied. The third-order nonlinear optical parameters such as nonlinear refractive index (n_2), nonlinear absorption coefficient (β), real, imaginary parts of third-order susceptibility ($\chi^{(3)}$) and second-order hyperpolarizability (γ) of the title compound were measured experimentally by open and closed aperture Z-scan technique. The experimental data are theoretically fitted. The optical limiting study revealed that the transmitted output power decreases with the input power and the transmitted output is clamped at 21.30 J/cm^2. The Z-scan results confirm the reverse saturable absorption behaviour and positive nonlinear refractive property of the anthracene picrate. Second-order hyperpolarizability is computed theoretically by CAM-B3LYP hybrid functionals at DFT level. Both experimental and theoretical values are in good agreement. These attractive third-order nonlinear properties suggest that the title compound can have potential applications in optical limiting devices.

Keywords: *Z-scan, Third-order Susceptibility, Second-order Hyperpolarizability, and Optical Limiting Property.*

Non-Linear Optics (NLO) plays a major role in the field of photonics, including fiber optic communication, optical computing, data storage and optical switching. Nonlinear optical response of the materials depends on their hyperpolarizabilities and a lot of research is focused on hyperpolarizabilities of molecules. Organic molecules with second order hyperpolarizabilities of the order 10^{-31} to 10^{-36} esu show excellent third-order NLO responses (S. Adhikari, et al. 7372-79, 99139-48) and (J. Xu, et al. 2084-89). Third-order NLO processes are having supreme importance as they cover extensive and diverse area in nonlinear optics. The organic materials with aromatic ring are of great interest for third order nonlinear optical applications due to their high optical damage threshold and ultrafast electronic response (M. C. Sreenath, et al. 218-34), (S. Nagaradona and R. B. Dhanakotti 147-57), (M. Khalid, et al. 1-19), and (R. A. Shehzad, et al. 1-10). They offer high degree of synthetic flexibility to tune their optical properties through structural modification (M. Ashfaq, et al. 31211-25).

Picric acid derivatives are interesting candidates for NLO responses (D. Shalini, et al. 129098), (N. Sudharsana, et al. 736-46), (R. M. Jauhar, et al. 57977-85), (G. Anandha Babu, et al. 1957-62), and (A. Chandramohan, et al. 5409-15). Picric acid forms crystalline picrates of various organic molecules through ionic and hydrogen bonding and pi- pi interactions (V. Matulis, et al. 309-14). It is known that picric acid acts not only as an accepter to form various pi stacking complexes with other aromatic molecules but also as an acidic ligand to form salts through specific electrostatic or hydrogen bond interactions (S. El-Medani, et al. 77-87). Research is actively progressing in the field of third order optical non-linearities of aromatic picrate. Anthracene picrate has been least explored for its third order optical nonlinearities. Herein, we report the synthesis, third order nonlinear optical and optical limiting behaviour of anthracene picrate.

2. Experimental Procedures

The experimental methods involve the synthesis, Z-scan studies and DFT investigations on third- order NLO properties of the compound.

2.1. Materials and Methods

The solvents and chemicals used were of A.R. grade purchased from Merck India Ltd. Solvents were purified and dried according to standard procedures.

2.2. Synthesis of Anthracene Picrate

Analytical Reagent grade anthracene and picric acid were obtained from Merck, India. The title compound was synthesized by dissolving anthracene and picric acid in benzene separately, in the ratio of 1:1 and the resulting solution was stirred well. A bright red precipitate of anthracene picrate crystalline substance was obtained. The purity of the synthesized compound was improved by successive recrystallization processes. Purity was checked by TLC and melting point determination. Melting point for the title compound is obtained as 111.3° (Chloroform). The reaction for the synthesis of anthracene picrate is illustrated in Scheme 1.

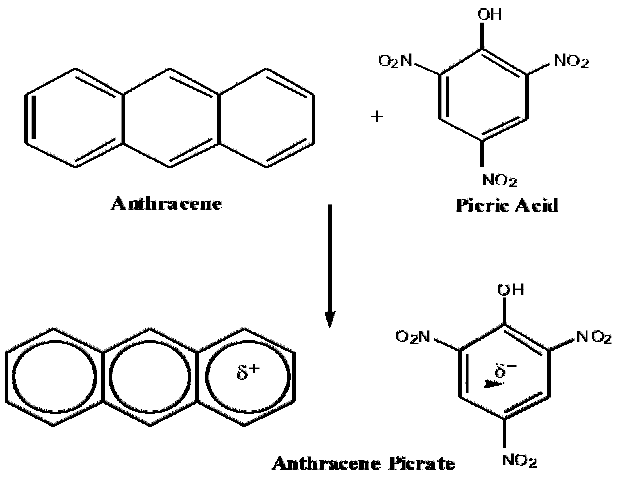

Scheme 1

2.3. Z-scan Studies

Third-order nonlinear optical properties of anthracene picrate were studied using the Z-scan technique. It is an effective and accurate method for measuring nonlinear absorption, nonlinear refraction and third-order nonlinear optical susceptibility of materials. The measurement of third-order nonlinearity is of great importance in the development of optical limiting devices. In this technique the sample is moved along the focal point of the lens. Nonlinear absorption originates from two photon absorption or multiphoton absorption within the compound. Reverse saturable absorption (RSA) is due to two photon absorption whereas, saturable absorption (SA) is by multiphoton absorption. Self-focusing or self-defocusing of the sample is related to nonlinear refraction and from this one can judge the sign of nonlinear refraction of the material. Reverse saturable absorption behaviour and positive nonlinear refractive property are essential for a molecule to show optical limiting property (M. C. Sreenath, et al. 363-377) and (S. Zafar, et al. 164-69).

Z-scan measurement was carried out using Q-switched Nd-YAG laser having 5 ns pulses at a repletion rate of 10 Hz giving second harmonic at 532 nm. The laser beam was focused by a lens of 10 cm focal length. In this technique sample is mounted on the translation stage and translating the sample between +Z and –Z position along Z-direction. The radius of the beam waist ωo was calculated to be 35μm. The Rayleigh length, $z_0 = \pi\omega_0^2/\lambda$ was calculated as 7.42 mm, which is greater than the thickness of the sample cuvette (1mm), an essential requirement for Z-scan experiments.

The third-order nonlinear refractive index n_2, nonlinear absorption coefficient β, third order NLO susceptibility $\chi^{(3)}$ and second hyperpolarizability γ (third order effect) of anthracene picrate in acetone having 0.5 mM concentration and intensity at 1.08 GW/cm^2 were evaluated by closed and open aperture Z-scan techniques.

2.4. Computational Details

Gaussian 09 for windows software package was used for DFT calculation. B3LYP hybrid functional has proven to be reliable for calculating geometrical parameters, electronic and vibrational wave numbers (H. Jochen and G.E. Scuseria 7274-80). The ground state structure was optimized and frequency calculations were performed to ensure that the optimized structure is minimum in the potential energy surface using B3LYP/6-31G (d, p) level. Second hyper-polarizability, γ, for the studied compound was calculated by DFT approach using CAM-B3LYP/6-31G (d, p) which is currently one of the ultimate procedures for obtaining numerically accurate NLO responses (D. Hadji, et al. 110939) and (A. J. Garza, et al. 1202-12). Gauss View 5 for windows software was used for generating the input files and visualization of the results.

3. Results and Discussion

3.1. Third Order Nonlinear Optical Studies

Nonlinear absorption characteristics of anthracene picrate have been obtained from open aperture Z-scan plot. Figure-1 shows the open aperture (OA) Z-scan curve of the compound at 0.5 mM concentration in acetone and 1.08 GW/cm^2 intensity. The curve shows excellent agreement with theoretical fit. The OA curve shows the reverse saturation behaviour, hence the absorption coefficient β is positive (M. C. Sreenath, et al. 363-77) and (S. Zafar, et al. 164-69). A material with reverse saturable absorption property shows enhanced absorption with increase in laser intensity.

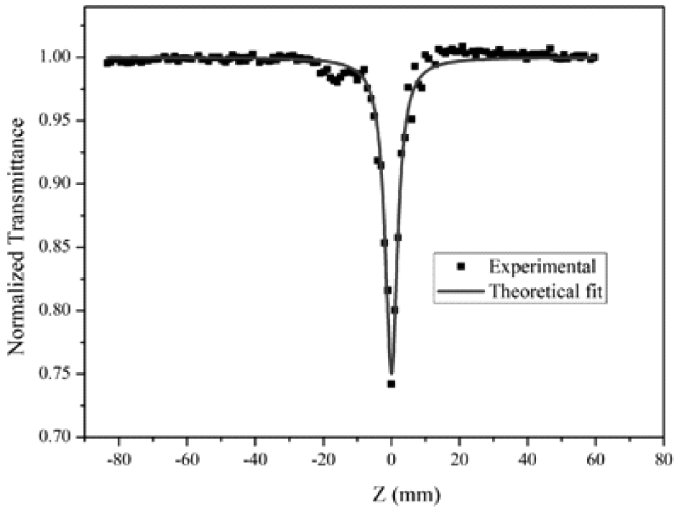

Figure - 1: Open Aperture (OA) Z-Scan plot of Anthracene picrate

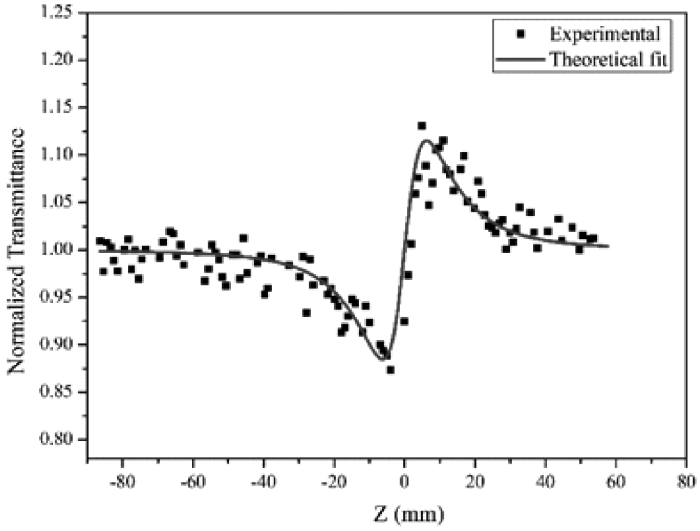

Figure - 2: Closed Aperture Z-Scan plot of Anthracene picrate

The nonlinear refractive index of anthracene picrate has been investigated by recording the closed aperture (CA) Z-scan plot at 0.5 mM concentration and 1.08 GW/cm^2 intensity and is shown in Figure-2.

The valley followed by a peak in the normalized transmittance obtained from the CA curve indicates that the sign of the refractive nonlinearity is positive due to self-focusing (M. Amalanathan, et al. 256) and (A. B. Laczkowska, et al. 819). Pure nonlinear refraction curves have been obtained by division of CA data by OA data. The normalized transmittance T(z) is given by

$$T(z,\Delta\phi_0) = 1 - \frac{4\Delta\phi_0 x}{(x^2+9)(x^2+1)} \quad \text{--------(1)}$$

where, $\Delta\phi_0$ is the one axis nonlinear phase shift and x is z/z_0. The nonlinear refractive index n_2 and real part of third-order nonlinear susceptibility, Re $\chi^{(3)}$ were calculated by the relations.

$$n_2 = \frac{\Delta\phi_0 \lambda}{2\pi I_0 L_{eff}} \quad \text{--------(2)}$$

$$\mathrm{Re}\,\chi^{(3)} = 10^{-4} \frac{\varepsilon_0 n_0^2 c^2}{\pi} n_2 \quad \text{--------(3)}$$

The imaginary part of the third order susceptibility ($Im\chi^{(3)}$) was calculated from β through the relation

$$\mathrm{Im}\,\chi^{(3)} = 10^{-2} \frac{\varepsilon_0 n_0^2 c^2 \lambda}{4\pi^2} \beta \quad \text{--------(4)}$$

where, ϵo is the permittivity of free space, c is the velocity of light in vacuum and n_0 is the linear refractive index.

The third-order nonlinear susceptibility, $\chi^{(3)}$ was calculated from the relation

$$\chi^{(3)} = \left[(\mathrm{Re}\chi^{(3)})^2 + (\mathrm{Im}\,\chi^{(3)})^2\right]^{1/2} \quad \text{--------(5)}$$

The second order hyperpolarizability, γ of the sample is related to the third-order susceptibility through the equation

$$\gamma = \frac{\chi^{(3)}}{\left[\frac{1}{3}\left(n_0^2 + 2\right)\right]^4 N} \quad \text{--------(6)}$$

where, N is the molecular number density in cm^3.

Table – 1: Third Order NLO parameters of Anthracene picrate

β (. 10^{-11}) (m/W)	n_2 (.10^{-19}) (m^2/W)	Re $\chi^{(3)}$ (.10^{-13}) (esu)	Im $\chi^{(3)}$ (.10^{-13}) (esu)	$\chi^{(3)}$ (.10^{-13}) (esu)	γ (.10^{-33}) (esu)
1.0465	6.8519	5.7852	3.7404	6.8890	10.7510

Nonlinear absorption coefficient β, third order nonlinear refractive index n_2, third order NLO susceptibility $\chi^{(3)}$ and second hyperpolarizability γ of anthracene picrate in acetone evaluated using closed and open aperture Z-scan techniques are given in Table-1.

The nonlinear absorption coefficient β (m/w) is of the order of 10^{-11}. The nonlinear refractive index n_2 and $\chi^{(3)}$ are of the order 10^{-19} m^2/W and 10^{-13} esu, respectively. Second order hyperporizability (third order effect), γ is of the order 10^{-33} esu which makes anthracene picrate a promising third order NLO molecule.

3.2. Optical Limiting Property of Anthracene Picrate

One of the important applications of nonlinear optics is optical limiting. The optical limiting materials are used for developing devices for human eye protections and solid state sensors from intense laser beams. The optical limiting behaviour of the compound is due to RSA behaviour. Optical limiting materials show decrease in transmittance as a function of input fluence. In an ideal optical limiter, the transmittance changes abruptly at some critical input intensity or threshold and therefore exhibits an inverse dependence on the intensity; the output is thus clamped at a certain value. Figure-3 shows the optical limiting curves of anthracene picrate where the normalized transmission is plotted as a function of input power for 0.5 mM anthracene picrate solution in acetone. As can be seen from Figure-3, at 21.3 J/cm^2, self-focusing effect occurs, by which intensity of the beam reaching the detector reduces considerably.

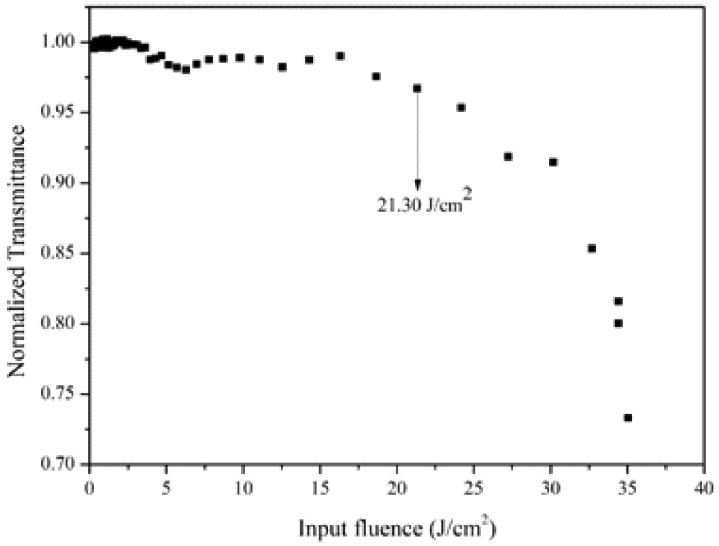

Figure - 3: Optical limiting curve of Anthracene picrate

3.3. DFT Studies on the Structural and Nonlinear Optical Properties of Anthracite Picrate

3.3.a. Geometry Optimization and FMO (Frontier Molecular orbitals) Analysis

Structural optimizations of the title compound were performed at B3LYP/6-31G(d,p) level. The energies of Frontier Molecular orbitals *viz.* HOMO and LUMO are helpful in investigating the electrical and chemical properties of substrates. Figure-4 depicts the optimized geometry, HOMO and LUMO for anthracene picrate obtained using B3LYP functionals and 6-31G(d,p) basis set. Electron population analysis reveals that HOMO extends over anthracene donor moiety, whereas LUMO resides over picric acid part. The orbital energy level analysis for the picrate showed that HOMO value is 7.78 eV while LUMO value is 2.71 eV, and the energy gap value calculated at the DFT level is 2.53 eV. The low HOMO–LUMO energy gap shows the charge transfer interaction taking place within the molecule which is essential for a molecule to have good NLO response.

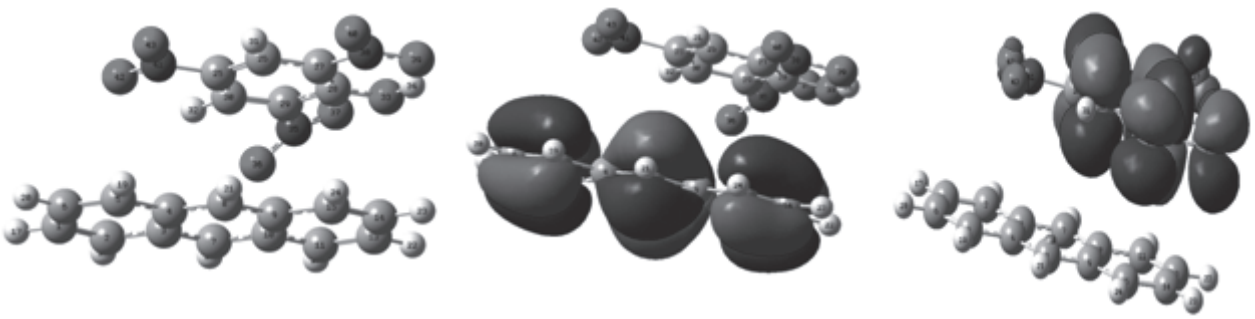

Optimized Geometry **HOMO** **LUMO**

Figure - 4: Optimized geometry and frontier molecular orbitals of anthracene picrate

3.3.b. DFT Studies on the Second Order Hyperpolarizability

The second-order hyperpolarizabilities were studied at CAM-B3LYP at 6-31G (d,p) level and Second order hyperpolarizability is calculated using the equation 7. For the calculations in solution phase, CPCM model (P. B. Jayathilaka, et al. 809-13) was employed which is part of Gaussian 09.

$$\langle\gamma\rangle = \frac{1}{5}\left[\gamma_{xxxx} + \gamma_{yyyy} + \gamma_{zzzz} + 2\left(\gamma_{xxyy} + \gamma_{xxzz} + \gamma_{yyzz}\right)\right] \quad \text{..... (7)}$$

Table - 2: Second Order Hyperpolarizability Components and Resultant Values of γ

γ_{xxxx} **.10^{-33} esu**	γ_{yyyy} **.10^{-33} esu**	γ_{zzzz} **.10^{-33} esu**	γ_{xxyy} **.10^{-33} esu**	γ_{xxzz} **.10^{-33}esu**	γ_{yyzz} **.10^{-33} esu**	<γ> **.10^{-33} esu**
42.46508	15.01223	-6.45286	-3.11035	6.030334	2.65882	11.00099

Second order hyperpolarizability components and resultant values of anthracene picrate in acetone are enlisted in Table-2.

From Table-2, the theoretically calculated γ value is of the order 10^{-33} esu which is in good agreement with the experimental value (10.7510×10^{-33} esu). The high γ value suggests that this molecule might find applications in the development of nonlinear optical gadgets especially in optical limiting devices.

4. Conclusion

Anthracene picrate was synthesized and its third-order nonlinear optical parameters such as nonlinear refractive index (n_2), nonlinear absorption coefficient (β), real, imaginary parts of third-order susceptibility ($\chi^{(3)}$) and second-order hyperpolarizability (γ) were measured experimentally by open and closed aperture Z-scan technique. The experimental data are theoretically fitted. Second-order hyperpolarizability is computed theoretically by CAM-B3LYP hybrid functionals at DFT level. Both theoretical and experimental values are in good agreement. The optical limiting study revealed that the transmitted output power decreases with the input power and the transmitted output is clamped at 21.30 J/cm^2. This optical limiting is due to self- focusing effect which can be attributed to its reverse saturable absorption behaviour and positive nonlinear refractive property. Hence the molecule is having potential applications in photovoltaic device fabrication and optic limiting field.

References

A.B. Laczkowska, et al. *Journal of Computational Chemistry,* vol. 34, 2013, p. 819.

A.J. Garza, et al. *The Journal of Physical Chemistry*, B 119.3, 2015, pp. 1202-1212.

A. Chandramohan, et al. *Journal of Crystal Growth,* 310.24, 2008, pp. 5409-5415.

D. Hadji, et al. *Journal of Molecular Liquids*, vol. 286, 2019, p. 110939.

D.Shalini, et al. *Journal of Molecular Structure*, vol.1225, 2021, p. 129098.

G. Anandha Babu, et al. *Journal of Crystal Growth*, vol. 312.12-13, 2010, pp. 1957-1962.

H. Jochen, and G.E. Scuseria. *Chemical Physics,* vol. 120.16, 2004, pp. 7274-7280.

J. Xu, et al. *Advanced Materials*, vol. 25, 2013, pp. 2084-2089.

M. Amalanathan, et al. *Spectrochimica Acta Part A*, vol. 108, 2013, p. 256.

M. Ashfaq, et al. *ACS Omega*, 6.46, 2021, pp. 31211-31225.

M. C. Sreenath, et al. *Journal of Molecular Structure,* vol.1180, 2019, pp. 363-377.

M. C. Sreenath, et al. *Optics and Laser Technology,* vol. 108, 2018, pp. 218-234.

M. Khalid, et al. *Optical and Quantum Electronics*, vol. 53, 2021, pp.1-19.

N. Sudharsana, et al. *Materials Chemistry and Physics*, vol. 134.2-3, 2012, pp. 736-746.

P. B. Jayathilaka, et al. *Canadian Journal of Chemistry,* vol. 92.9, 2014, pp. 809-813.

R. A. Shehzad, et al. *Journal of Molecular Modeling*, vol. 27.1, 2021, pp. 1-10.

R. M. Jauhar, et al. *RSC Advances*, vol. 6.63, 2016, pp. 57977-57985.

S. Adhikari, et al. *CrystEngComm.*, vol. 15, 2013, pp. 7372-7379.

S. Adhikari, et al. *RSC Advances*, vol. 6, 2016, pp. 99139-99148.

S. El-Medani, et al. *Journal of Molecular Structure,* vol. 644, 2003, pp.77-87.

S. Zafar, et al. *Spectrochimica Acta Part A: Molecular and Biomolecular Spectroscopy,* vol. 114, 2013, pp. 164-169.

S. Nagaradona and R.B. Dhanakotti. *Spectrochim Part A: Molecular and Biomolecular Spectroscopy,* vol. 203, 2018, pp. 147-157.

V. Matulis, et al. *Journal of Molecular Structure,* vol. 649, 2003, pp. 309-314.

In-vitro and *In-silico* Antioxidant Screening of Benzo[b]thiophene Schiff bases: Synthesis, Characterization and their Cytotoxicity Studies

T. M. Dhanya
Research Scholar, Department of Applied Chemistry
Cochin University of Science and Technology
Kalamassery, Cochin-682022
Kerala, India, Email: mdhanyat@gmail.com

G. Anjali Krishna
Research Scholar, Department of Applied Chemistry
Cochin University of Science and Technology
Kalamassery, Cochin-682022
Kerala, India, Email: anjalianju123krishna@gmail.com

Dr. Shanty A. A.
Assistant Professor, Department of Chemistry
St. Teresa's College (Autonomos) Ernakulam
Cochin-11, Ernakulam, Kerala, India
Email: shanty.sheen@gmail.com, shantyaa@teresas.ac.in.

Dr. P. V. Mohanan
Professor, Department of Applied Chemistry
Cochin University of Science and Technology
Kalamassery, Cochin-22, Ernakulam, Kerala, India
Email: mohan@cusat.ac.in

Abstract

Two new Benzothiophene derived Schiff bases named 4-(Benzo[b]thiophene-2-ylvinylideneamino)-1,5-dimethyl-2-phenyl-1,2-dihydro-pyrazol-3-one (BAP) and N-Benzo[b]thiophene-2-ylmethylene-4,5-dimethyl-benzene-1,2-diamine (BTMPD) were synthesized by a simple one pot condensation reaction by reacting benzo[b]thiophene-2-carboxaldeyde with 4-amino antipyrine and 4,5 dimethyl 1,2 phenylenediammine. The prepared compounds were characterized by using UV-Vis., FT-IR, LC-MS, ^{1}H NMR and ^{13}C NMR spectroscopic techniques. Spectral results proved the successful formation of the compounds. The newly prepared compounds were screened for their antioxidant activity by radical scavenging DPPH (2, 2-diphenyl-1-picryl hydrazyl) method. Moreover, the *in-vitro* cytotoxicity studies were conducted using MTT assay against Human hepatocellular carcinoma (HepG-2) cancer and Embryonic BD1X Rat Heart Tissue (H9c2) normal cell lines, as well as their cell viability, was measured. Furthermore, Molecular docking studies were done with an antioxidant enzyme (PDB ID: 1HCK). The *in-vitro* antioxidant activity was measured in terms of their minimum inhibitory concentration denoted by their IC_{50} value. The synthesized compound BAP showed a better IC_{50} value than BTMPD and the experimental values were in good agreement with theoretical values. The results of *in-vitro* cytotoxicity studies proved that the compound BAP possesses moderate cell viability than BTMPD.

Keywords: *Antioxidant, Benzo[b]thiophene, Cytotoxicity, and Molecular Docking*.

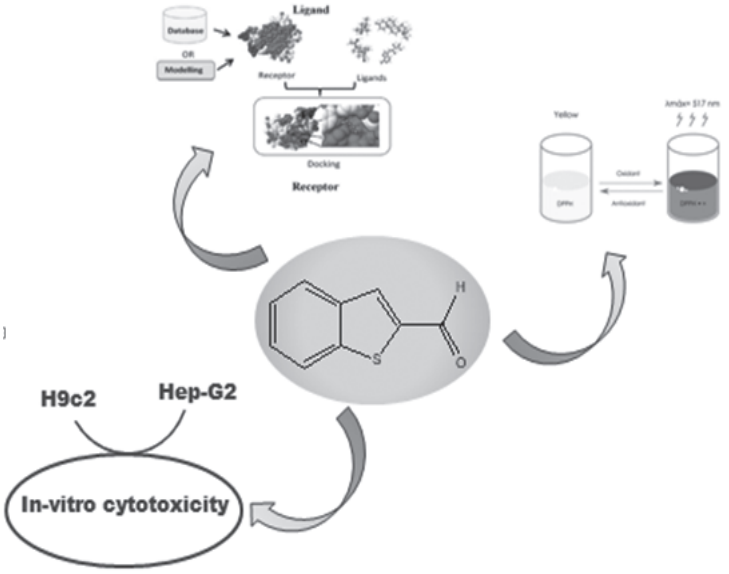

Heterocyclic molecules include many of the biochemical materials essential to life and their biological activity has always attracted the attention of researchers over the years. Many new synthetic approaches to develop functionalized heterocyclic compounds gained much importance in drug discovery. Sulfur-containing heterocyclic compounds are important bioactive compounds because of their wide range of pharmacological applications. Benzo[b]thiophene derivatives display remarkable biological activities such as antioxidant, antiinflammatory, analgesic, antifungal, antidepressant, antiangiogenic, estrogen receptor modulating, antimitotic, anticancer, kinase inhibitors, antituberculosis, anticonvulsant, antimalarial, anthelmintic, antihyperglycemic and pesticide (Jagtap V. A. and Agasimundin Y. S. 10-14), (Berrade L., et al. 3086-90), (Bryant H.U. and Dere W.H. 45-52), (Islam M.S., et al. 2212), and (Naganagowda G., et al. 1043-47). Owing to their remarkable properties, Schiff bases continue to play a significant role in coordination chemistry. In many domains, Schiff bases are the most prevalent and commonly used organic compounds. Many scientists have synthesized and reported various biologically active compounds because of the synthetic flexibility and relative easiness of preparation of Schiff bases. Soumik et al., 2022 discussed the recent advances in the catalytic applications of chiral Schiff base ligands and metal complexes in asymmetric organic transformations, which have attracted manufacturers and researchers in this field. The electrochemistry and indirect electrocatalytic properties of these materials were reported by Ourari, et al., 2022 and Priya, et al., 2022 who described its biomolecular docking interaction and biological application of Schiff base ligand complexes (De S., et al. 2022), (Qurari A., et al. 122441), and (Priya J. and Madheswari D. 2022).

Reactive oxygen species (ROS) such as hydroxyl radicals, superoxide radicals, single oxygen radicals, and hydrogen peroxide radicals cause oxidative stress caused by normal organ functions. Homeostatic balance maintains the production and removal of ROS, which are regulated by various antioxidant enzymatic systems such as superoxide dismutase (SOD), catalase (CAT), glutathione (GSH), and glutathione-s-transferase (GST). Any imbalance in these species has detrimental effects on various biomolecules such as nucleic acid, proteins, lipids, DNA, and carbohydrates (Porter F.D., et al. 56-81) and (Montine T.J., et al. 269-75) and their influence on the biological system is very harmful and may cause

many chronic and neurodegenerative diseases (Berliner J. A. and Heinecke J. W. 707-27) such as cancer, atherosclerosis, aging, hair loss, inflammation, immunosuppression, diabetes, and neurodegenerative disorders (such as Alzheimer's and Parkinson's diseases) (Wu R. P., et al. 7479), (Zhang X., et al. 177-84), (Pradhan A. U., et al. 2022), and (Srivastava S., et al. 113320). Nowadays there is no certainty on whether oxidants trigger these diseases, or are produced as a secondary consequence of the diseases. Here comes the role of an antioxidant and it is very important to design and synthesize new antioxidant drugs. Antioxidants are molecules that slow or prevent other molecules from oxidizing (Kumar B. D. and Rawat D. S. 641-45) and (Laddha P. R. and Biyani K. R. 44-49). The antioxidant prevents the damage caused by ROS by interacting with free radicals. The primary goal of antioxidants was to prevent the free radical formation and to protect active cells (Ak T. and Gulcin I. 27-37), (Gulcin I. 345-91), (Taslimi P. and Gulcin I. 12516), and (Gulcin I. 651-715). The antioxidant acts as a shield to protect the immune system from the harmful effects of ROS (Brewer M. S. 221-47) and (Sies H. 291-95). Antioxidant activity can be evaluated by various methods such as DPPH, ABTS, FRAP, etc. (Tataringa, et al. 2014) The antioxidant studies of benzothiophene [b] Schiff bases have been evaluated using the DPPH method.

Cytotoxicity is an in vitro test that measures a chemical's or mediator cell's ability to destroy cells. The determination of cytotoxicity is primarily dependent on cell viability and cytotoxicity assays that were used for drug screening and chemical cytotoxicity testing. Cell viability is typically measured using an MTT assay, Cell titer Blue, Trypan Blue Exclusion, ATP, Colony Formation method, or Crystal violet method (Soenen S. J., et al. 5767-83). The MTT assay is currently the most widely used method for testing cell growth and toxicity of strains.

The present study focuses on the synthesis of 4-(Benzo[b]thiophen-2-ylvinylideneamino)-1,5-dimethyl-2-phenyl-1,2-dihydro-pyrazol-3-one (BAP) N-Benzo[b]thiophen-2-ylmethylene-4,5-dimethyl-benzene-1,2-diamine (BTMPD) Schiff base ligands produced via the condensation reaction of benzo [b]thiophene-2-carboxaldehyde, 4-amino antipyrine and 4,5 dimethyl 1,2 phenylenediammine. These synthesized compounds were screened against their antioxidant activity using the radical scavenging DPPH method. Molecular docking was carried out to evaluate the receptor-ligand interactions. The cytotoxicity studies were evaluated for all the compounds via MTT assay. The synthetic routes of BAP and BTMPD are presented in Scheme 1 and Scheme 2.

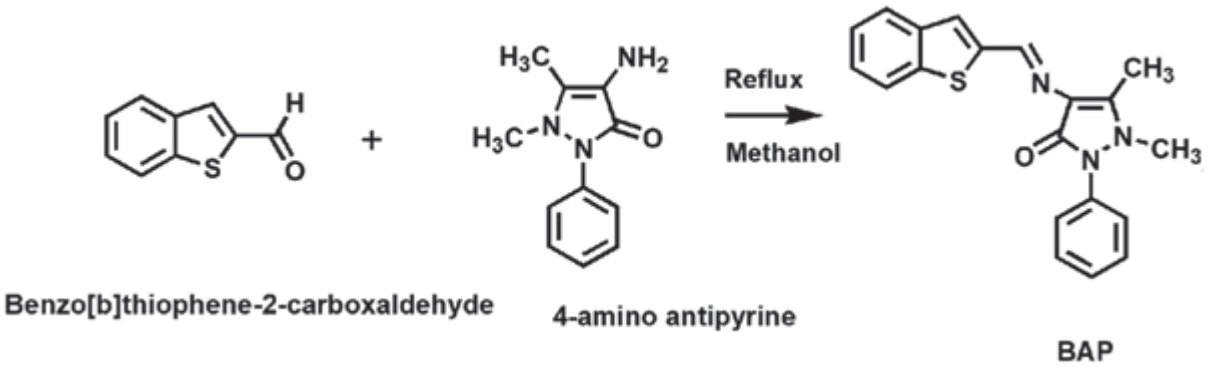

Scheme 1: The Synthesis of BAP

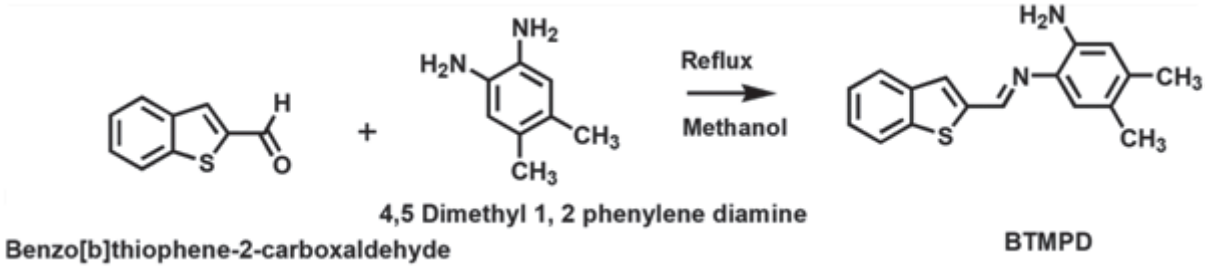

Scheme 2: The Synthesis of BTMPD

2. Experimental

2.1 Materials

Benzo[b] thiophene-2-carboxaldehyde ($C_9H_{60}S$, 97%), 4, 5 dimethyl 1, 2 phenylenediammine ($C_8H_{12}N_2$, 98%), 4-amino antipyrine ($C_{21}H_{17}N_3OS$, 98%), (2, 2-diphenyl-1-picryl hydrazyl) DPPH were purchased from Aldrich.

Solvents; methanol, chloroform, acetone, acetonitrile, and ethyl acetate of analytic grade were purchased from Alpha chemicals. All materials used were of the highest purity available and used without further purification.

2.2. Instrumentation

Absorption spectra were recorded in DMF on a Thermo Scientific Evolution 220 UV-Vis. spectrophotometer in the 200 nm- 900 nm range. FT-IR studies were done using an FT-IR spectrophotometer (JASCO-8000) using KBr pellets. NMR spectra of both (^{13}C &^{1}H) of the synthesized Schiff base were studied in $CDCl_3$ using Bruker AMX 400 FT-NMR Spectrometer with TMS as internal standard. Liquid chromatography-mass spectrometry (LC-MS) was carried out on a Waters 3100 Mass Detector using ESI–MS technique at a Sophisticated Analytical Instrument Facility (SAIF) from Mahatma Gandhi University, Kottayam. The percentage of carbon, hydrogen, nitrogen, and sulfur of the synthesized compound was analyzed using a CHNS analyzer (Vario EL III) at a Sophisticated Test and Instrumentation Center (STIC), Cochin University of Science and Technology, Kochi, India.

2.3. Synthesis of Schiff base ligands of benzo[b]thiophene derivatives

2.3.1 Synthesis of BAP

Equimolar mixtures of benzo[b]thiophene-2-carboxaldehyde (10 mmol) in methanol (10 mL) and 4-amino antipyrine (10 mmol) in methanol (10 mL) were mixed and refluxed at constant stirring for about 6 hours (Parsekar S. U., et al. 2881-96). The dark brown precipitated solution was concentrated by slow evaporation at room temperature. The precipitate obtained was washed several times in various solvents like chloroform, hexane, petroleum ether, etc., and recrystallized with methanol, and dried in a vacuum over anhydrous $CaCl_2$. The purity of the compound was tested using TLC. The synthesis of BAP is shown in Scheme 1. All the spectral details of BAP ligands such as UV (Figure-1a) FT-IR (Figure-2a), mass (ESI-MS), ^{1}H &^{13}C NMR are extensively discussed in the Supporting Information (SI; Figure-S1, S3, S4).

2.3.2 Synthesis of BTMPD

An equimolar mixture of methanolic solution of benzo[b]thiophene-2-carboxaldehyde (10 mmol) is slowly added to aromatic amine such as 4, 5 dimethyl 1, 2 phenylenediammine (10 mmol). The resulting coloured solution was refluxed at constant stirring for about 6 hours. By the si-

multaneous removal of a water molecule from the reaction mixture, the precipitated solution was separated and evaporated slowly at room temperature. The crystalline product was washed several times in various solvents like chloroform, hexane, petroleum ether, etc. It was then recrystallized from methanol and then dried in a vacuum over anhydrous $CaCl_2$. The purity of the compound was tested using TLC. The synthesis of BTMPD is shown in Scheme 2. All the spectral details of BTMPD ligands such as UV (Figure - 1b) FT-IR (Figure-2b), mass (ESI-MS), ^1H & ^{13}C NMR are extensively discussed in the Supporting Information (SI; Figure-S2, S5, S6).

2.4 *In-Vitro* Antioxidant Activity using the DPPH Assay

The DPPH method is the most reliable and widely used method for determining antioxidant activity. We used the DPPH assay with minor modifications to test the antioxidant activity of the synthesized compounds (Afzal H. R., et al. 4470-79). Methanol was used to make stock solutions (1mg/ml) of the samples (BAP, BTMPD) and the standard solution (ascorbic acid). A suitable amount of sample stock solution was added to a definite volume of DPPH (0.01 mmol) in methanol, and the volume was made up to 3 ml using methanol as the solvent and incubated in a dark environment at room temperature for 30 minutes. A system without the compound was taken as control. The absorption of the test samples was measured using a UV spectrophotometer at 517 nm with methanol as the blank and ascorbic acid as the standard. Methanol was used to auto-zero the UV spectrophotometer. The absorbance of test samples was compared to the absorbance of control samples to calculate antioxidant activity. The percentage inhibition was determined by using the following formula percent inhibition = ($A0$ - $A1/A0$) × 100 (A0 = control absorbance, A1 = sample absorbance). Furthermore, IC_{50} values were determined by plotting a graph following free radical scavenging versus compound concentration, which represents the concentration of compounds that scavenge 50% of DPPH radicals (i.e., 50% of absorbance at 517 nm).

2.5 Molecular Docking Studies

Molecular docking is a type of computational modeling that allows for the prediction of the preferred binding orientation of one molecule (e.g., ligand) to another (e.g., receptor) when the two interact to form a stable complex (Limon-Vidal A., et al. 934-43). It has revolutionized research in some areas, particularly interactions where studies between small molecules (ligands) and protein targets (which could be enzymes) can predict enzyme activation or inhibition. Such data could be used as a starting point for rational drug design. Molecular docking was widely used as a tool to predict the studies of receptor-ligand interaction in the inhibition of enzymes related to antioxidant activity. Docking studies aid in the investigation of binding energies, binding affinity, and binding locations (Ghorai P., et al. 153-63).

To investigate the *in-silico* antioxidant activities of the synthesized compounds, the RSC Protein Data Bank was used to download the 1HCK receptor (PDB CODE: 1HCK) Human Cyclin-Dependent Kinase 2 enzyme. Pymol Visualization software was used to clean the enzyme of impure residues. Using Open Babel, the optimized structure was converted to PDB files. The receptor and ligands were created as pdbqt files using autodock tools. The Grid box was placed on the macromolecule, and a conf.txt file was created using the grid parameters. For each set, docking calculations were performed, and the binding free energy of each compound against the target was calculated. To investigate the ability of an antioxidant agent, ligand interactions were evaluated using Discovery Studio, and molecular dock-

ing was first performed with Ascorbic acid used as reference ligand which has a docking score of nearly -3.101 kcal/mol.

2.6 Cytotoxicity Studies

MTT assay was used to assess the *in-vitro* cytotoxicity of the synthesized compounds BAP and BTMPD against normal cell line H9c2 and cancer cell line Hep-G2 cells (Mahmoud N. H., et al. 2022). Both cell lines were seeded at a density of 1×10^5 cells (H9c2) and 2×10^3 cells (Hep-G2 cells) per well in 96 well plates for the assay and grown to 80 percent confluence in DMEM (H9c2) and MEM (Hep-G2 cells) medium containing 10% FBS, penicillin (100U/mL), and streptomycin (100 mg/mL) and cultured in 5% CO_2 at 37°C. For 24 hours, cells were prein-cubated with various sample concentrations (1, 5, 10, and 25 g/mL). After washing the cells, 100 L of MTT (5 mg/ml) in phosphate buffer saline (PBS) was added to all of them. After 4 h incubation at 37°C in a CO_2 incubator, 100 μL DMSO was added to all the wells incubated for 30 min in a shaker, and the absorbance of MTT formazan products solubilized was measured at 570 nm in a microplate reader (Bioteck synergy).

The percentage of cell viability of control cells was kept at 100%. The relative cell toxicity in percent was calculated as:

% Cell toxicity = 100 - Absorbance of treated/Absorbance of control × 100

Table – 1: Elemental Analysis of Schiff base ligand BAP

Compound	Empirical Formula	Formula Weight (g/mol)	Colour (Yield %, mp) °C)	Found (Cal.) %				
				C	H	N	O	S
BAP	$C_{20}H_{17}N_3OS$	347.11	Dark Brown (75,252)	69.14	4.93	12.09	4.61	9.23

Table – 2: Elemental Analysis of Schiff base ligand BTMPD

Compound	Empirical Formula	Formula Weight (g/mol)	Colour (Yield %) %, mp) °C)	Found (Cal.) %			
				C	H	N	S
BTMPD	$C_{17}H_{16}N_2S$	280.39	Yellow (80,248)	72.82	5.75	9.99	11.44

3. Results and Discussions

3.1 Characterization of BAP and BTMPD

Two new Schiff bases were successfully synthesized, characterized, and obtained in high yields. The synthesis route is depicted in Schemes 1 and 2. The Schiff bases are all crystalline, coloured, and non-hygroscopic. The compounds were completely miscible in solvents like chloroform, methanol, DMF, and DMSO but insoluble in wa-

ter. Melting points were in the 220-260°C range. TLC was used to monitor the progress of the reaction as well as the purity of the samples. All of the synthesized compounds' spectral and analytical data agreed well with the proposed structures.

The discovery of a molecular [M + 1] peak as a result of mass spectral measurements confirms the structure of BAP and BTMPD (Figure-S1 and S2). The electronic spectral data of the synthesized compounds were recorded at room temperature in DMF solution and show two bands in the UV region. In the Schiff base ligand BAP (Figure-1a) the first band at 275 nm is assigned to the $\pi \rightarrow \pi^*$ transitions of the aromatic rings (Sreekanth A. and Kurup M R. P. 969-78) and the second at 370 nm corresponds to the $n \rightarrow \pi^*$ transition within the azomethine group (Berhanu A. L., et al. 74-91), over 450 nm the compound is transparent. The absorption spectrum of BTMPD (Figure-1b) shows three peaks at 265 nm, 339 nm, and 358 nm, with the peak at 265 nm corresponding to a $\pi \rightarrow \pi^*$ transition in the aromatic ring and the peaks at 339 and 358 corresponding to $\pi \rightarrow \pi^*$ transitions in the C=N group (Ceyhana G., et al. 184-98), which confirms the product formation. The IR spectrum of BAP (Figure-2a) shows a strong band at 1562 cm^{-1} is assigned to ν (C = N) of the azomethine (Shakir M., et al. 1866-75). The band at 862 cm^{-1} corresponding to the ν (C-S-C) stretching vibration of thiophene moiety. Stretching vibration modes ν C=N, ν NH, and ν C-S seen in BTMPD (Figure-2b) were assigned to the bands appearing at 1568 cm^{-1}, 3579 cm^{-1}, and 724 cm^{-1}, respectively (Mohana K.N., et al. 584-90). The NMR studies of BAP(^{1}H and ^{13}C NMR), the following data obtained from the spectrum ^{1}H NMR (300 MHz,$CDCl_3$, 25°C): δ ppm = 9.92 (1H, s, imine), 7.81-7.46 (4H, m, benzothiophene ring), 7.40 (1H, s, benzothiophene ring), 2.48 (3H, s, methyl protons) 1.64 (3H, s, methyl protons) 7.39-7.28 (5H, m, aromatic ring), ^{13}C-NMR (300 MHz, $CDCl_3$, 25°C): δ ppm = 160.78 (C=N), 152.03 (C=O), 150.98 (heterocyclic C), 145.46 (ArC), 140.60 (benzothio-phene C), 140.03 (benzothiophene C), 134.70 (benzothiophene C), 129.34 (benzothiophene C), 127.46 (benzo-thiophene C), 127.23 (benzothio-phene C), 125.70 (benzothiophene C), 124.70 (ArC), 124.48 (ArC), 122.66 (ArC), 118.29 (heterocyclic C), 35.77 (Methyl C), 10.22 (Methyl C) (Figure -S3 and S4). The following data from the NMR studies (^{1}H and ^{13}C NMR depicted in Figure-S5 and S6) indicate the structural confirmation of BTMPD. The following data obtained from the spectrum ^{1}H NMR (300 MHz, $CDCl_3$, 25°C): δ ppm = 9.42 (1H, s, C=N), 2.69 (2H, s, broad,

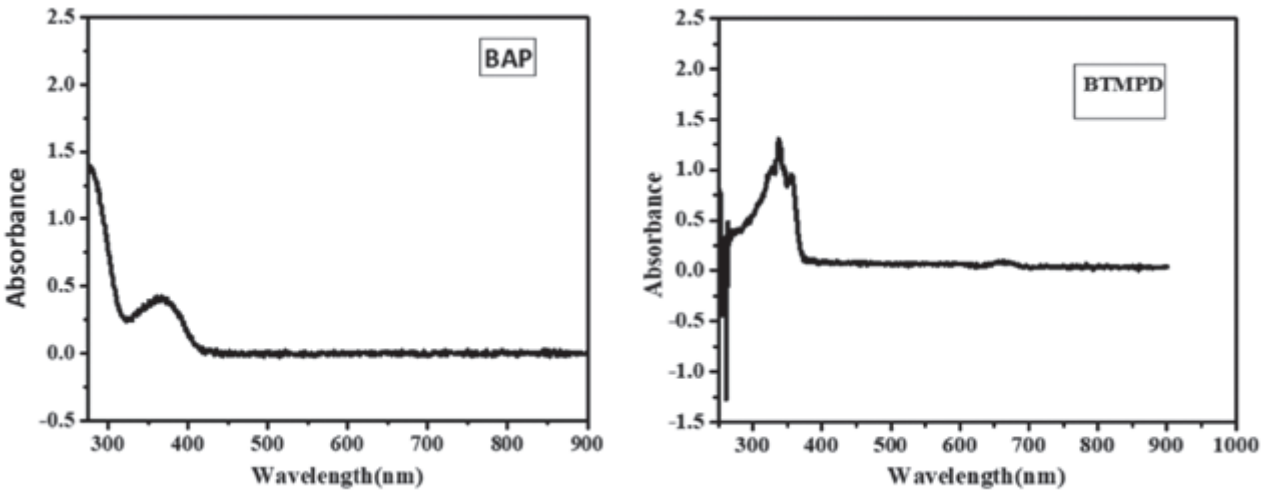

Figure - 1a and 1b: The UV-visible absorption spectra of BAP and BTMPD

NH_2) 8.04 -7.22 (4H, m, benzothiophene ring), 7.53 (1H, s, benzothiophene ring), 6.99 (1H, s, aromatic ring) 6.97 (1H, s, aromatic ring), 2.29, 2.36 (6H, s, methyl protons) (Figure-S5) ^{13}C-NMR (300 MHz, $CDCl_3$, 25°C): δ ppm = 145.69 (C=N), 144.16 (benzothiophene C), 140.35 (benzothiophene C), 139.70 (ArC), 134.59 (ArC), 132.88 (ArC), 128.29 (ArC), 126.38 (benzothiophene C), 125.66 (benzothiophene C), 125.37 (benzothiophene C), 124.88 (benzothiophene C), 124.40 (benzothiophene C), 123.43 (ArC), 123.03 (benzothiophene C), 122.52 (ArC), 20.48 (Methyl C). (Figure-S6).

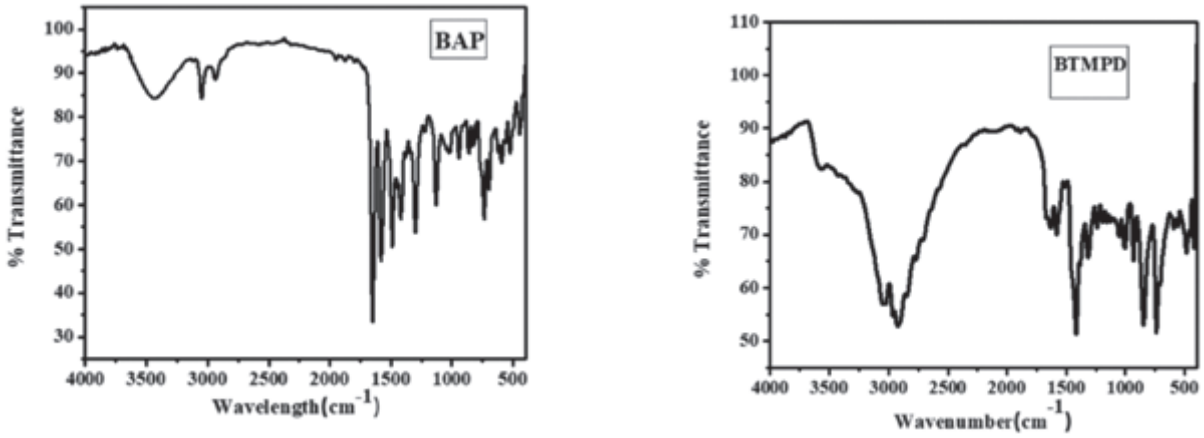

Figure - 2a and 2b: The FT-IR spectra of BAP and BTMPD

3.2 Antioxidant Activity (DPPH Assay)

The *in-vitro* antioxidant activity was studied using the 2, 2-diphenyl-1-picrylhydrazyl (DPPH) method. This spectrophotometric method measures the decrease in absorbance of methanolic DPPH solution in the presence of an antioxidant compound at 517 nm. The absorbance of the control and samples were measured at 517 nm at different concentrations. All synthesized Schiff bases had antioxidant properties comparable to the standard drug ascorbic acid. The percentage of scavenging activity of the compound synthesized and their minimum inhibitory concentration (IC_{50}) with reference to ascorbic acid as standard (Yusuf T. L. 12968-80) are shown in Table-3. All Schiff bases showed low free radical scavenging activity to the standard. The antioxidant

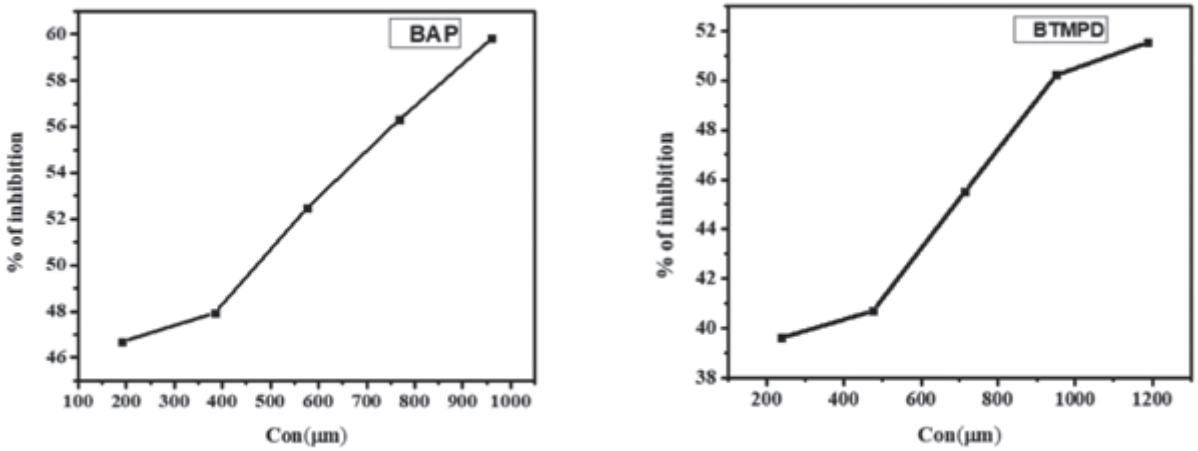

Figure - 3: Concentration vs. % inhibition graph for Schiff bases BAP and BTMPD

activity of compounds BAP and BTMPD were demonstrated by IC_{50} values of 429.20 and 1032.77, respectively. The typical antioxidant activity graph is obtained by plotting concentration against the percentage of inhibition which is shown in Figure-3.

Table – 3: Antioxidant parameters of synthesized compounds BAP, BTMPD

Ligands	IC_{50}(μm)
BAP	429.20
BTMPD	1032.77

3.4 Molecular Docking

Molecular docking is a current research requirement. If performed before the experimental portion of any investigation, it can demonstrate the feasibility of any task. Docking studies were performed in this study to obtain accurate predictions on the optimized conformations for both the new synthesized derivatives and protein targets to form a stable complex and gain a better understanding of the structure-activity relationships (SARs) of the synthesized compounds. We are evaluating the antioxidant activity of all synthesized compounds against an enzyme, 1HCK, in this study.

The PDB file of the 1 HCK receptor was downloaded and visualized through the Pymol software and the view of the prepared receptor is shown in Figure-4. The synthesized compounds were optimized using Avogadro software (Figure-5.) and converted to a PDB file using Open Babel. The binding site was observed using the docking software Discovery studio (Figure-6). The receptor and synthesized compounds were saved as pdbqt files using autodock tools. The Grid box was placed on the macromolecule, and a conf.txt file was created using the grid parameters. For each set, docking calculations were performed. Ligand interactions were evaluated using Discovery Studio. Figure-7 and 8 show the docking interaction results and their respective 2D diagrams of BAP and BTMPD with 1 HCK receptor. The view of 1 HCK receptor protein using Pymol software is shown below:

Pymol view 1HCK **Prepared receptor 1HCK**

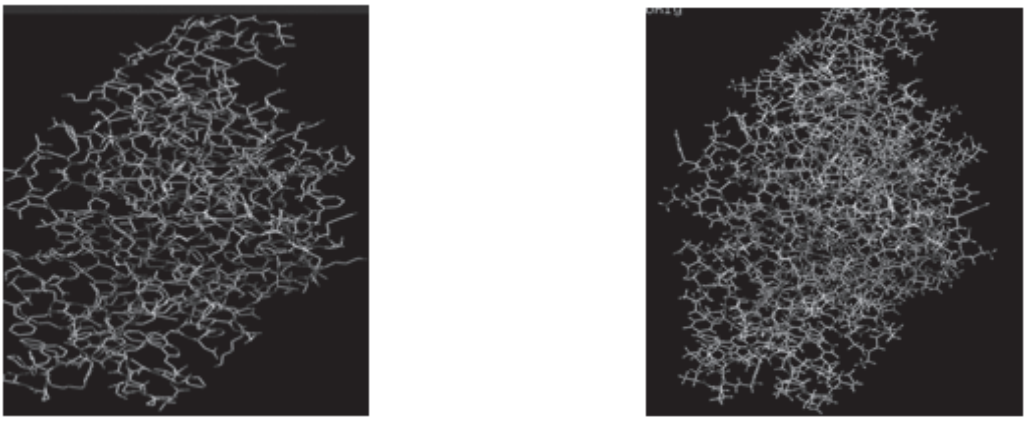

Figure - 4: The 3D-view of 1HCK receptor using pymol software

The optimized structure of synthesized Schiff base ligands BAP and BTMPD using Avogadro software to get a 3D view to execute molecular docking to evaluate the binding affinity of the protein-ligand.

The PDB file of the prepared receptor is opened in Discovery studio to know the binding site and values of the targeted protein. The PDB file is then converted into Pdbqt using autodock tools.

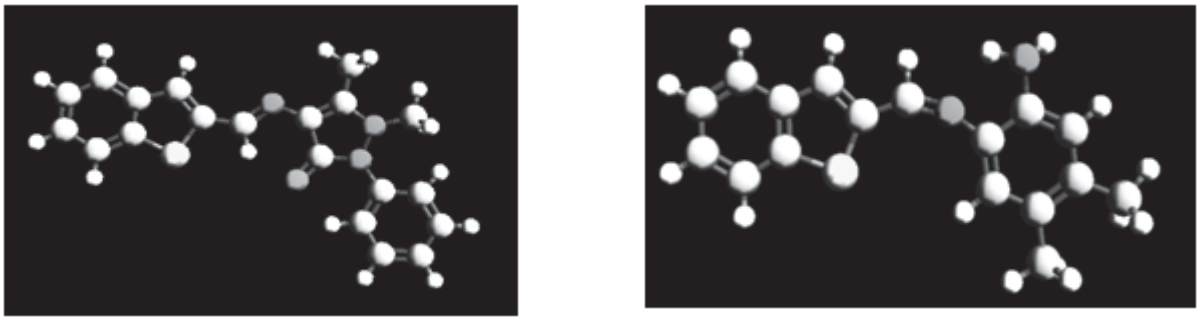

Figure - 5: Optimized geometry of BAP and BTMPD using Avogadro software

PDB 1HCK **PDBQT 1HCK**

Figure - 6: Receptor 1 HCK view in Discovery Studio

In the autodock vina using the grid box on the macromolecule, a conf.txt file was formed using the grid parameters. By executing vina, docking calculations were performed in the Discovery studio and the binding free energy of each compound against the target was calculated and compared with the standard Ascorbic acid.

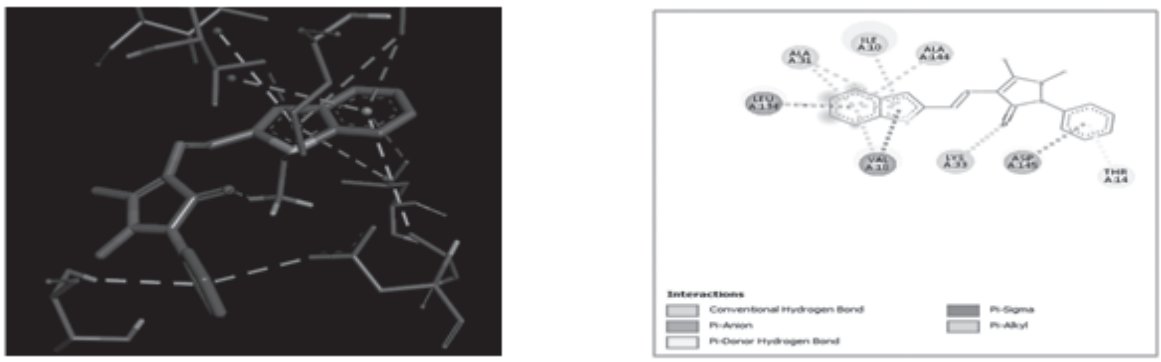

Figure - 7: The docking interaction and 2D diagram of 1 HCK- BAP

Figure - 8: The docking interaction and 2D diagram of 1 HCK- BTMPD

The binding affinity is important in showing the interaction between the ligand and the protein. The ideal conformation for a higher interaction with the protein represents lower binding energy (Sreekanth A. and Kurup M. R. P. 969-78). Table-4 shows the binding energy of the compounds within the active site of the target protein. The docking results suggested that the synthesized compounds had strong binding interactions with the binding site of the antioxidant enzyme.

Table – 4: Binding Energy values of compounds

Ligand	Binding Energy (Kcal/mol)
BAP	-8.8
BTMPD	-8.1
Ascorbic acid (Reference)	-3.101 Kcal/mol

3.5 Cytotoxicity Studies

Cell viability and cytotoxicity assays became important criteria for drug screening and cytotoxicity tests of chemicals. These investigations are essential for the introduction of new compounds into the pharmaceutical industry. The *in-vitro* cytotoxicity effect of BAP and BTMPD Schiff base ligands were evaluated using MTT assay in H9c2 cells and Hep-G2 cells. Cells were prein-cubated with different concentrations of samples (1, 5, 10, and 25 μg/mL) for 24 h and the results were analyzed using cell viability. The percentage of cell viability in normal cell line H9c2, the synthesized Schiff base compound BAP at an increasing concentration (1 μg/ml, 5 μg/ml, 10 μg/ml, 25 μg/ml) exhibited inhibition of (13.30%, 48.54%, 49.31%, 47.93%) whereas in the case of BTMPD the percentage of inhibition was (-7.22%, 42.57%, 37.37%, 39.19%), respectively listed in Table-5. In both cases, as concentration increases the percentage of inhibition was high in normal cell line H9c2. In Hep-G2 cancer line the synthesized compound BAP showed the following result at a concentration of sample (1μg/ml, 5 μg/ml, 10 μg/ml, 25 μg/ml) the inhibition percentage was (12.05%, 9.34%, 28.74%, 27.89%) whereas BTMPD inhibition occurred at (-24.97%, 35.56%, 12.53%, 15.49%) as listed in Table-6.

Table – 5: The Percentage of Cell viability of synthesized compounds against H9c2 cells (24 h Treatment)

Compound	1 μg/ml	5 μg/ml	10 μg/ml	25 μg/ml
BAP	13.30	48.54	49.31	47.93
BTMPD	-7.22	42.57	37.37	39.19

Table – 6: The Percentage of Cell Viability of Synthesized Compounds against Hep-G2 cells (24 h Treatment)

Compound	1 μg/ml	5 μg/ml	10 μg/ml	25 μg/ml
BAP	12.05	9.34	28.74	27.89
BTMPD	-24.97	35.56	12.53	15.49

4. Conclusion

Two benzothiophene Schiff bases have been well synthesized and characterized by using UV-Vis., FT-IR, LC-MS, ^{1}H NMR and ^{13}C NMR spectroscopic techniques. All the synthesized compounds exhibited less DPPH scavenging activity indicating high IC_{50} values. Antioxidant activity determined by DPPH radical scavenging of BAP is better compared to BTMPD. DPPH radical scavenging assay confirmed the low antioxidant activity of these compounds compared to their standard ascorbic acid. The results obtained from the *in-vitro* antioxidant activity were very low compared to their theoretical studies using the tool molecular docking. The binding energy of BAP showed good results than that of BTMPD and can be used in the development of drugs. The cytotoxicity studies of BAP and BTMPD Schiff base ligands were evaluated using MTT assay against normal H9c2 and cancer Hep-G2 cell lines.

Data Supplementary Information

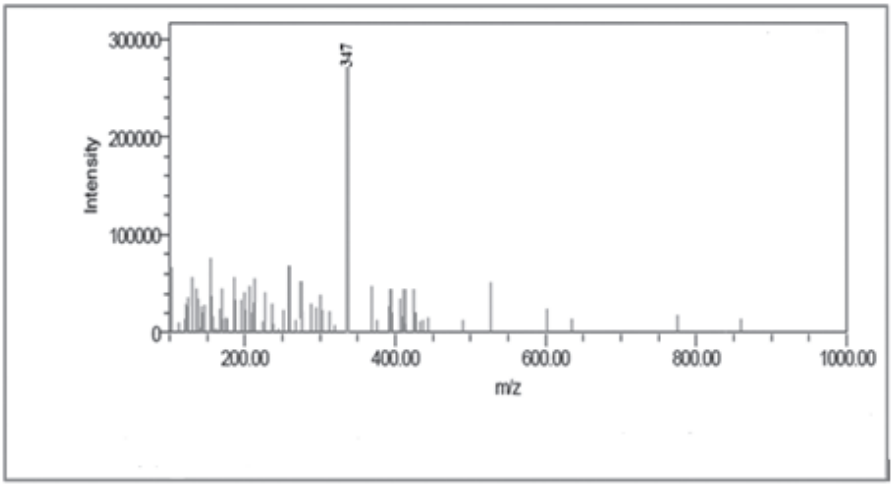

Figure - S1 Mass Spectrum of BAP

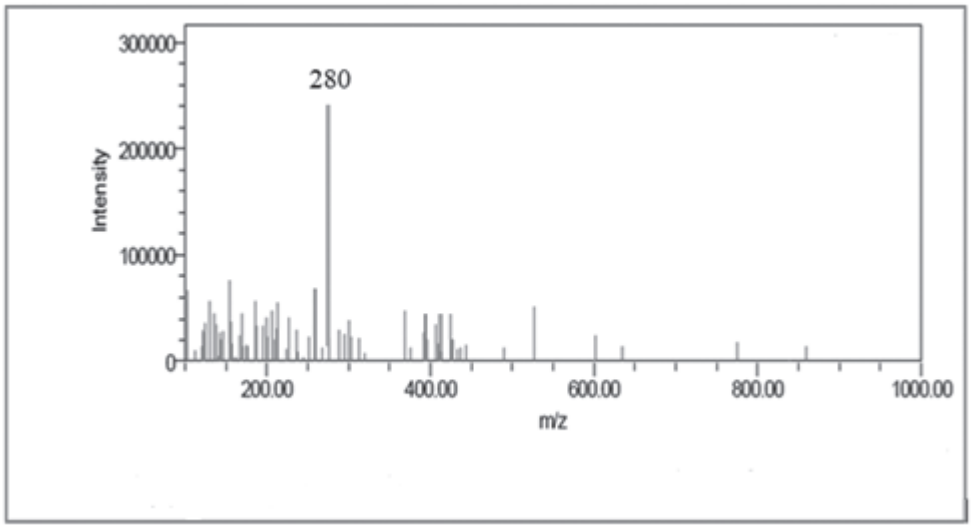

Figure - S2 Mass Spectrum of BTMPD

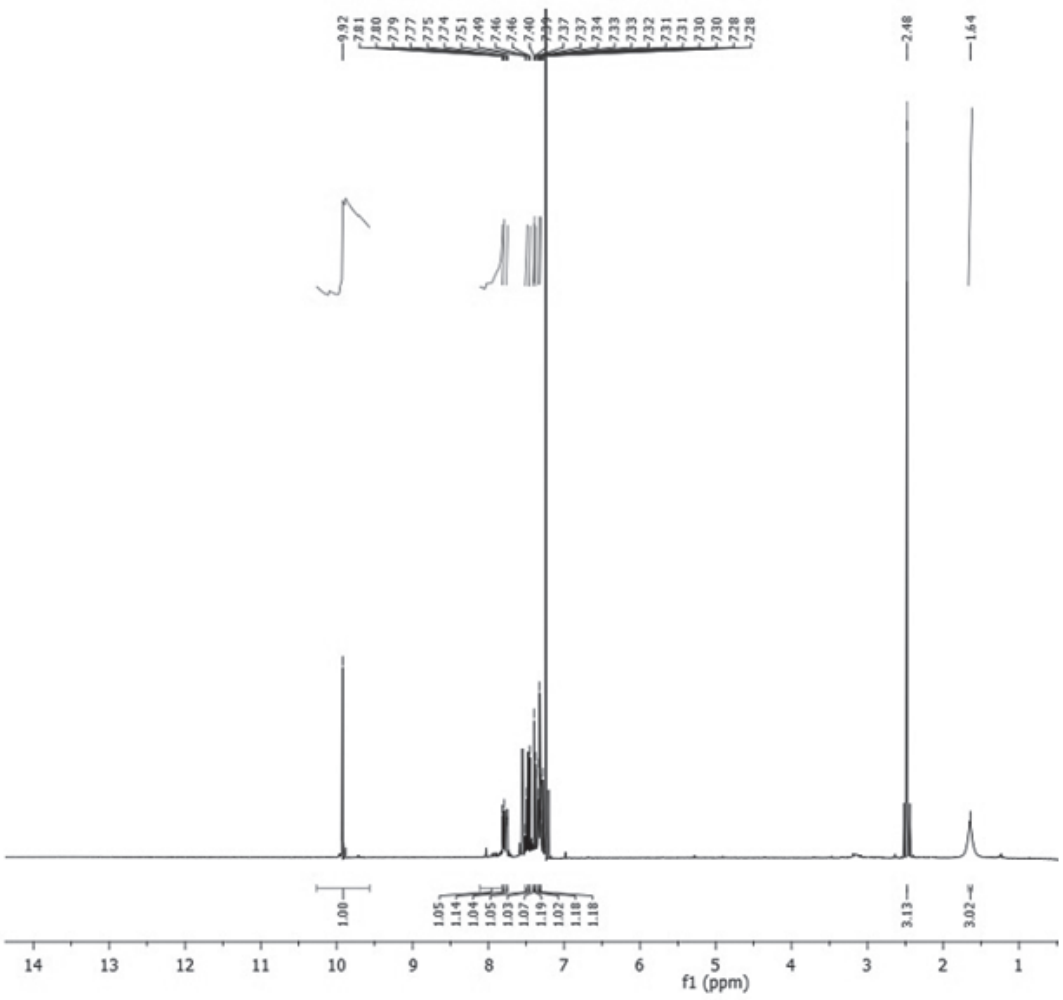

Figure - S3 ^{1}H NMR Spectrum of BAP

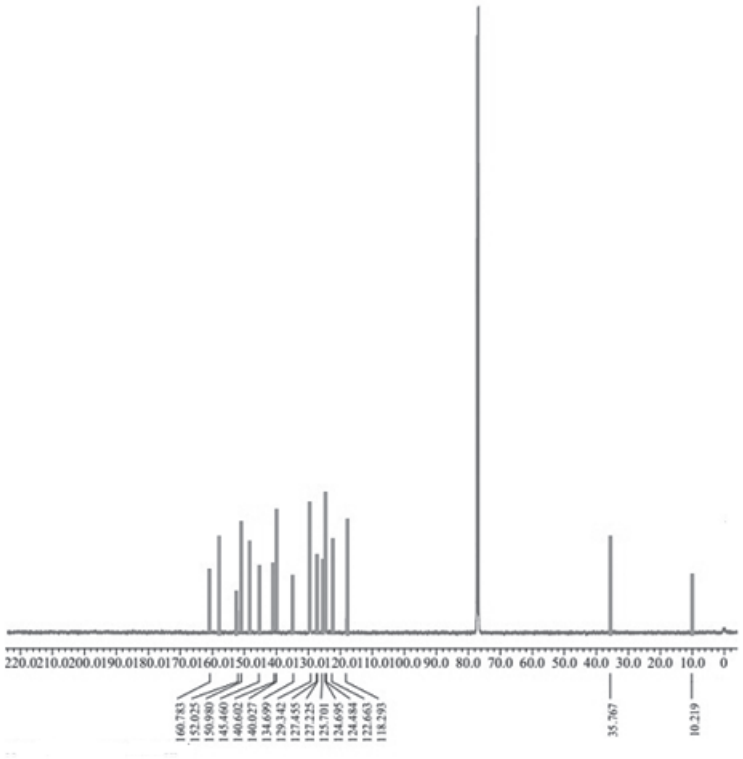

Figure - S4 ^{13}C NMR Spectrum of BAP

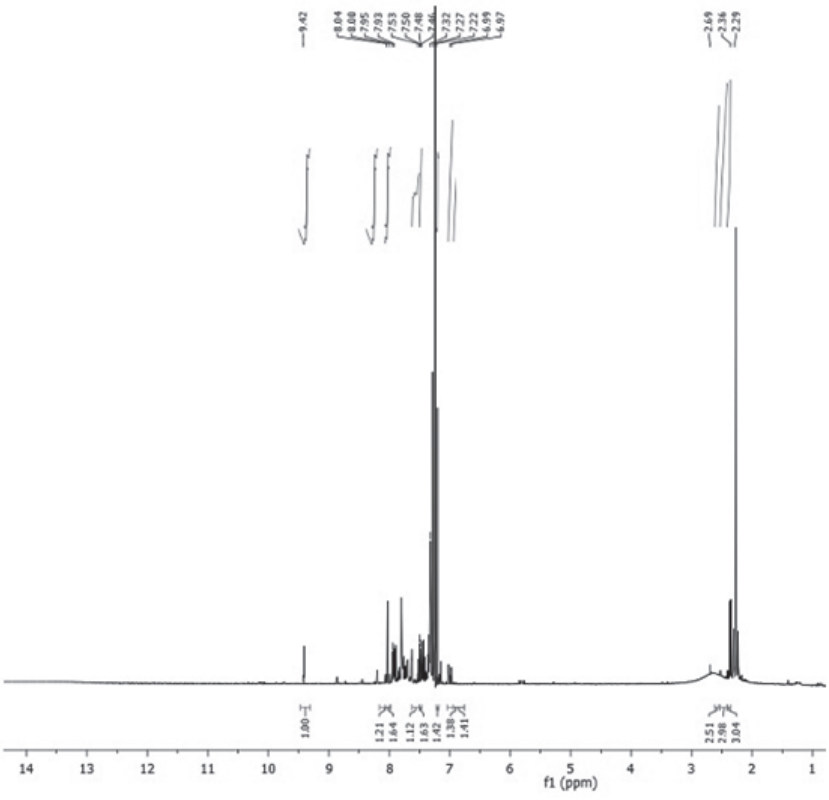

Figure - S5 ^{1}H NMR Spectrum of BTMPD

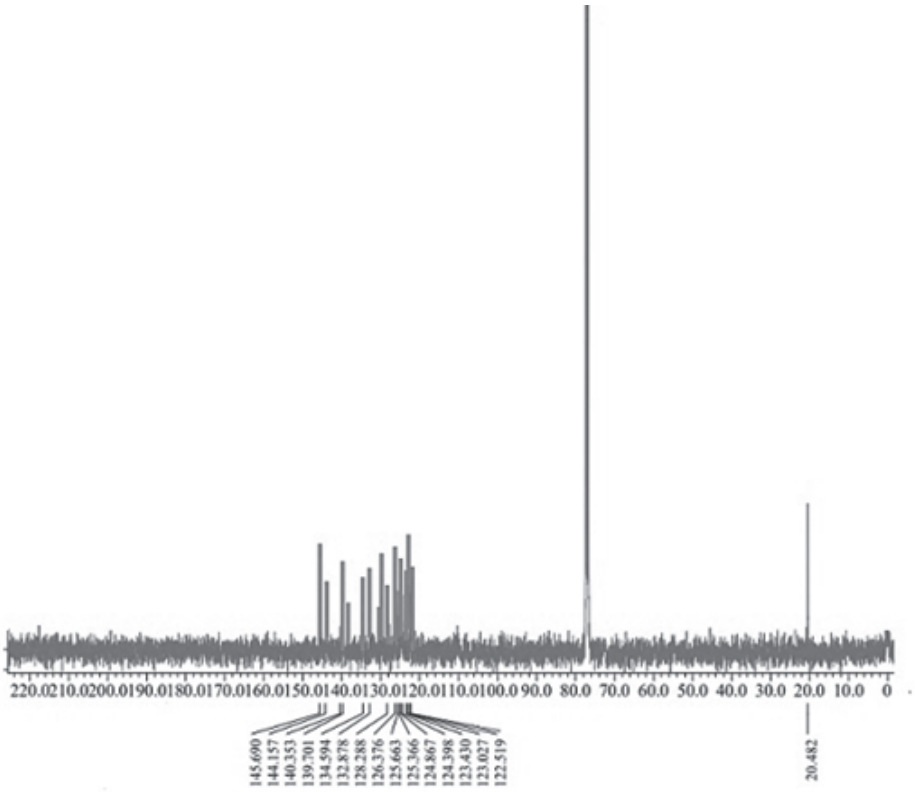

Figure - S6 ^{13}C NMR Spectrum of BTMPD

Acknowledgment

The authors would like to acknowledge STIC CUSAT for CHNS Analysis, SAIF M.G. University, Kottayam for LC-MS Analysis and Government College Trivandrum for NMR analysis, Amala Cancer Center Thrissur and NIIST, Trivandrum for Cytotoxicity studies and Dr. Abi T.G., Sacred Heart College, Thevara for optimization studies.

Appendix A. Supplementary

LC-MS spectra, ^{1}H NMR, ^{13}C NMR of the Schiff bases 1-2 are provided in the supplementary information.

References

Afzal, H.R., et al. "Schiff Bases of Pioglitazone Provide Better Antidiabetic and Potent Antioxidant Effect in a Streptozotocin–Nicotinamide-Induced Diabetic Rodent Model." *ACS Omega,* 2021, vol. 6, pp. 4470–4479.doi.org/10.1021/acsomega.0c06064.

Ak, T. and Gulcin, I. "Antioxidant and Radical Scavenging Properties of Curcumin." *Chemico-Biological Interactions,* 2008, vol. 174, pp. 27-37. doi.org/10.1016/j.cbi.2008.05.003.

Berhanu, A.L., et al. "A Review of the Applications of Schiff Bases as Optical Chemical Sensors." *Trends in Analytical Chemistry*, 2019, vol. 116, pp. 74-91. doi.org/10. 1016/j.trac.2019.04.025.

Berliner, J.A. and Heinecke, J.W. "The Role of Oxidized Lipoproteinsin Atherogenesis." *Free Radical Biology and Medicine*, 1996, vol. 20, pp. 707-727. doi.org/10.1016/0891-5849(95)02173-6.

Berrade, L., et al. "Novel Benzo[*b*]thiophene Derivatives as New Potential Antidepressants with Rapid Onset of Action." *Journal of Medicinal Chemistry*, 2011, vol. 54, pp. 3086-3090. doi.org/10.1021/jm 2000773.

Brewer, M. S. "Natural antioxidants: Sources, Compounds, Mechanisms of Action, and Potential Applications." *Comprehensive Reviews in Food Science and Food Safety*, 2011, vol. 10, pp. 221-247. doi.org/10. 1111/ j.1541-4337.2011.00156.x.

Bryant, H. U. and Dere, W. H. "Selective Estrogen Receptor Modulators: An Alternative to Hormone Replacement Therapy." *EXBMAA.* 1998, vol. 217, pp. 45-52. doi. org/10.3181/00379727-217-44204.

Ceyhana, G., et al. "Antioxidants, Electrochemical, Thermal, Antimicrobial and Alkane Oxidation Properties of Tridentate Schiff Base Ligands and their Metal Complexes." *Spectrochimica Acta Part A: Molecular and Biomolecular Spectroscopy*, 2011, vol. 81, pp. 184-198. doi.org/10. 1016/ j.saa.2011.05.106.

De, S., et al. "Recent Advances in the Catalytic Applications of Chiral Schiff-Base Ligands and Metal Complexes in Asymmetric Organic Transformations." *Chemistry Select*, 2022, vol. 7, e2021043 34. doi.org/10.1002/slct.202104334.

Ghorai, P., et al. "Syntheses of Zn (II) and Cu (II) Schiff Base Complexes using N, O Donor Schiff Base Ligand: Crystal Structure, DNA binding, DNA cleavage, docking, and DFT Study." *Polyhedron*, 2018, vol. 141, pp. 153-163. doi.org/10.1016/j. poly.2017.11.041.

Gulcin, I. "Antioxidant Activity of Food Constituents: An Overview." *Archives of Toxicology*, 2012, vol. 86, pp. 345-391. doi.org/10.1007/ s00204-011-0774-2.

Gulcin, I. "Antioxidants and Antioxidant Methods: An Updated Overview." *Archives of Toxicology*, 2020, vol. 94, pp. 651-715. doi.org/10.1007/s00204-020-02689-3.

Islam, M. S., et al. "Bimetallic Iron–Palladium Catalyst System as a Lewis-Acid for the Synthesis of Novel Pharmacophores Based Indole Scaffold as Anticancer Agents." *Molecules,* 2021, vol. 26, p. 2212. doi.org/10.3390/molecules26082212.

Jagtap, V.A. and Agasimundin, Y.S. "Synthesis and Preliminary Evaluation of Some Amino-n'-[substituted]-4, 5, 6, 7-tetrahydro-1-benzothiophene-3-carbohydrazide as Antimicrobial Agents." *Journal of Pharmacy Research,* 2015, vol. 9, pp. 10-14. www.jprsolutions.info.

Kumar, B.D. and Rawat, D.S. "Synthesis and Antioxidant Activity of Thymol and Carvacrol Based Schiff Bases." *Bioorganic and Medicinal Chemistry Letters*, 2013, vol. 23, pp. 641-645. DOI: 10.1016/j.bmcl.2012. 12.001.

Laddha P.R. and Biyani K.R. "Synthesis and Biological Evaluation of Novel Schiff Bases of Aryloxy Moiety." *Journal of Drug Delivery and Therapeutics,* 2005, vol. 9, pp. 44-49. doi.org/10.22270/jddt.v9i5-s. 3635.

Limon-Vidal, A., et al. "Integration of Molecular Docking Analysis and Molecular Dynamics Simulations for Studying Food Proteins and Bioactive Peptides." *Journal of Agricultural and Food Chemistry*, 2022, vol. 70, pp. 934–943. doi.org/10.1021/ acs.jafc.1c06110.

Mahmoud, N. H., et al. "Spectroscopic studies, DFT Calculations, Cytotoxicity Activity, and Docking Stimulation of Novel Metal Complexes of Schiff base Ligand of Isonicotinohydrazide Derivative." *Applied Organometallic Chemistry*, 2022, vol. 36, e6697. doi.org/10.1002/aoc.6697.

Mohana, K. N., et al. "Synthesis and Antimicrobial Activity of 5-aminoquinoline and 3-aminophenol Derivatives." *International Journal of Drug Discovery and Technology*, 2011, vol. 2, pp. 584-590.

Montine, T.J., et al. "F2-Isoprostanes in Alzheimer and Other Neurodegenerative Diseases." *Antioxid Redox Signal*, 2005, vol. 7, 269-275. doi.org/10.1089/ars.2005.7.269.

Naganagowda, G., et al. "Synthesis and Antimicrobial Activities of Benzothiophene Derivatives." *Journal of the Chilean Chemical Society*, 2012, vol. 57, pp. 1043-1047.

Ourari, A., et al. "Electrochemistry and Study of Indirect Electrocatalytic Properties of a Novel Organometallic Schiffbase nickel (II) Complex." *Journal of Organometallic Chemistry*, 2022, vol. 976, p. 122441. doi.org/10.1016/j.jorganchem.2022.122441.

Parsekar, S. U., et al. "Synthesis, Characterization, Crystal Structure, DNA and HSA Interactions, and Anticancer Activity of a Mononuclear Cu(II) Complex with a Schiff Base Ligand Containing a Thiadiazoline Moiety." *ACS Omega*, 2022, vol. 7, pp. 2881-2896. doi.org/10.1021/acsomega.1c05750.

Porter, F. D. et al. "Cholesterol Oxidation Products are Sensitive and Specific Blood-Based Biomarkers for Niemann-Pick C1 Disease." *Science Translational Medicine*, 2010, vol. 2, pp. 56-81. doi.org/10.1126/scitranslmed.3001417.

Pradhan, A. U., et al. "A Review of Stem Therapy: An Emerging Treatment for Dimentia in Alzheimer's and Parkinson's Disease." *Brain and Behaviour*, 2022, e2740. doi. org/10.1002/brb3.2740.

Priya, J. and Madheswari, D. "Biomolecular Docking Interactions, Cytotoxicity and Antioxidant Property Evaluations with Novel Mn(II), Ni (II), Cd (II) and Pb (II) Schiff Base Ligand Complexes: Synthesis and Characterization." *Journal of Biosciences*, 2022, p. 29. doi.org/10.1007/s12038-022-00262-x.

Shakir, M., et al. "Synthesis, Spectroscopic Studies and Crystal Structure of the Schiff Base Ligand L derived from Condensation of 2-thiophene carboxaldehyde and 3,32-diaminobenzidine and its Complexes with Co(II), Ni(II), Cu(II), Cd(II) and Hg(II): Comparative DNA Binding Studies of L and its Co(II), Ni(II) and Cu(II) Complexes." *Spectrochimica Acta Part A: Molecular and Biomolecular Spectroscopy*, 2011, vol. 79, pp. 1866–1875. doi.org/10.1016/j. saa.2011.05.077.

Sies, H. "Oxidative stress: Oxidants and Antioxidants." *Experimental Physiology*, 1997, vol. 82, pp. 291"295. doi.org/10.1113/expphysiol.1997.sp004024.

Soenen, S. J., et al. "Cytotoxic Effects of Gold Nanoparticles: A Multiparametric Study." *ACS Nano*, 2012, vol. 6, pp. 5767-5783. doi.org/10.1021/nn301714n.

Sreekanth, A. and Kurup, M. R. P. "Synthesis, EPR and Mössbauer Spectral Studies of New iron(III)complexes with 2-benzoylpyridine-N(4), N(4)-(butane-1, 4-diyl) thiosemicarbazone (HBpypTsc): X-ray structure of $[Fe(BpypTsc)_2]FeCl_4.2H_2O$ and free ligand." *Polyhedron*. 2004, vol. 23, pp. 969-978.

Srivastava, S., et al. "Alzheimer's Disease and its Treatment by Different Approaches: A Review." *European Journal of Medicinal Chemistry*, 2021, vol. 216, p. 113320. doi. org/10.1016/j.ejmech.2021.113320

Taslimi, P. and Gulcin, I. "Antioxidant and Anticholinergicproperties of Olivetol." *Journal of Food Biochemistry*, 2018, vol. 42, p. 12516. doi.org/10.1111/jfbc.12516.

Tataringa, G., et al. "Preliminary Screening of Biological Activities of Some New Schiff Bases of Isatins." *Farmacia*, 2014, vol. 62, p. 1.

Wu, R. P., et al. "Nrf2 Responses and the Therapeutic Selectivity of Electrophilic Compounds in Chronic Lymphocytic Leukemia." *Proceedings of the National Academy of Sciences of the United States of America*, 2010, vol. 107, p. 7479. doi. org/10.1073/pnas.1002890107.

Yusuf, T. L., et al. "The Effect of Structural Configuration On the DNA Binding and *in vitro* Antioxidant Properties of New Copper(II) N_2O_2 Schiff Base Complexes." *New Journal of Chemistry*, 2022, vol. 46, pp. 12968-12980. doi.org/10.1039/D2N J014 77G.

Zhang, X., et al. "Epigenetic Modifications and Neurodegenerative Disorders: A Biochemical Perspective."*ACS Chemical Neuroscience*, 2022, vol. 13, pp. 177–184. doi. org/10.1021/acschemneuro.1c00701.

Teresian International Journal of Chemical Sciences (TIJCS)

Aims and Scope

Teresian International Journal of Chemical Sciences is a double blind peer-reviewed quarterly Journal. The Journal's mission is to submit to the readers, fresh fruit of academic studies leading to novel thoughts and current innovative research. The format of the Journal is designed reader-friendly. The academia is provided an easy access to the Journal. The Journal looks for articles conceptually sound, at once methodologically rigorous. The Journal loves to deal knowledge in different fields in Chemical Sciences individually and in unison. Journal caters to the needs of Science students with special reference to Chemistry researchers for articles that demonstrate clear and bold thinking, fresh and useful ideas, accessible and jargon-free expression, and unambiguous authority.

The following may be taken care of while papers are prepared:

What is the central message of the paper you propose to write? Moreover, what is new, useful, or important about your idea? What are the real-world implications of the proposed paper? Can the central message be applied in Chemical Sciences today, and if so, how? Who is the audience for your paper? What kind of research have you conducted to support the argument or logic in your paper? What academic, professional, or personal experience will you draw on to make the argument convincing? In other words, what is the source of your authority?

The manuscript should accompany the following separately: An abstract of about hundred words; **a brief biographical sketch** of author/authors describing designation, affiliation, specialization, number of books and articles published in the refereed journals, membership on editorial boards; **a declaration** to the effect that the work is original and it has not been published earlier; **tables, charts and graphs,** typed in separate sheets and numbered as Table 1, Graph 1 etc.; **references,** listed at the end of the text (follow *MLA Handbook*).

The Editor reserves the right to modify and improve the manuscripts to meet the Journal's standards of presentation and style.

The Editor has full right to accept or reject a paper for publication. Editorial decisions will be communicated within a period of four weeks on receipt of the manuscripts.

Guidelines and Ethical Obligations for Authors

The author shall present an accurate and complete account of research performed with data collected or used and an objective discussion of the relevance of research. The corresponding author shall have obtained the approval of all co-authors of the paper before submission.

Ghost authorship and Gift authorship are not allowed. The material submitted in the form of paper shall be original. Paper based on prior research work shall be honestly attributed. The manuscript shall not contain figures or materials copied from other sources without proper written permission for such use. The author shall find and cite the original publications that have presented similar work. The author shall not make personal reference to an earlier author. The author shall disclose all personal, professional, financial conflicts related to the paper to the Editor along with the submission. The author should have conducted the research leading to the paper, in accordance with the generally accepted ethical standards. The author has the ethical obligation to notify the Editor, should any of the statements to the above list cease to be true.

Guidelines and Ethical Obligations for Peer Reviewers

The peer reviewer should agree to review manuscripts for which they have the subject expertise. The peer reviewer should respect the confidentiality of peer review and should not reveal any details of the manuscript or its review. The peer reviewer should not use the information from the paper for personal gains. The peer reviewer should disclose all potential conflicts of interests (Personal, Professional, and Financial) to the Editor. The peer reviewer should not allow his views to be influenced by the origins of a manuscript; by nationality, religion, political belief, gender, or other characteristics of the author. The peer reviewer shall be objective and constructive in his views and avoid derogatory remarks in reviews. The peer reviewer shall ensure meticulous timeliness in forwarding the review to the Editor. The peer reviewer should keep all manuscripts and review details confidential.

The Journal's Policy towards Piracy and Plagiarism

The journal does not permit misconduct like piracy and plagiarism on the part of author/s. The unauthorized reproduction or use of ideas, data, or methods from others without adequate permission or acknowledgement is piracy and it will not be tolerated.

Plagiarism is a form of piracy that involves the unauthorized use or close imitation of the language (including figures, images, or tables) and thoughts of others. The author is forbidden to use the representation of these as one's own original work without permission or acknowledgement by the original author of the source of these materials. This is serious commission on the part of the author of the paper submitted for publication. Such a paper will be rejected. Plagiarism applies to researchers' duplication of their own previously published reports without acknowledgement.

The journal will take legal or other steps to curb this menace and this anti-academic activity.

Suspect Manuscript Reporting

Teresian International Journal of Chemical Sciences identifies manuscripts as suspect through the following means: Screening for image manipulation, recognizing the text/data from a prior text, Google searching of portions of text, and Screening for plagiarism, using software ***Grammarly*.**

Suspect Manuscript Identifying: *TIJCS* identifies suspect manuscript through the services of Editors, Reviewers, Third-party observers, Editorial Staff, and Anonymous sources.

Action on Discovery of Misconduct:

Teresian International Journal of Chemical Sciences takes action as misconduct is alleged against any paper submitted by an author: The journal suspends peer reviews internally. The journal soon after notifies others also on the issue. The Editor informs the author/authors of the paper on the misconduct involved. The Editor notifies the institution that employs the author/authors on the misconduct involved. The Editor informs the funding agency of the project too, in case there is a funding agency behind the project leading to the publication of the paper.

About Us

Teresian International Journal of Chemical Sciences is a double blind peer-reviewed quarterly journal.

The journal deals with articles on Chemical Sciences authored by academicians or researchers and in unison. The format of research will be reader friendly. The journal looks for articles conceptually sound, at once methodologically rigorous.

International authors/writers: Every issue generally carries papers of reputed authors from both India and abroad.

Quality Assurance: The journal abides by Quality Management system, ISO 9001:2008 Certified.

Legal requirements: The Journal has been registered with The Registrar of Newspapers Society of India as per Reg. No. KERENG/2020/79700 and it has been allotted ISSN: 2583-2565.

Copyright of journals: Copyright of all contents in the journal including articles published therein will be the right of St. Teresa's College (Autonomous), Ernakulam.

Trademarks and patents:

Barcode: Bar code is given.

Journal standing: Archiving by local and international databases, indexing by local and international databases.

International Editorial Board: In order to offer editorial advice for effective publication of the journal, an International Editorial Board has been constituted.

Original vs. cited: The author of a paper shall ensure he/she has written original works. If the author has used work/word of others, it has to be appropriately cited/acknowledged.

Keep Image Integrity

Image shall be properly kept. It is not acceptable to enhance, obscure, move, remove, or introduce a specific feature within an image. Manipulating images for improved clarity is accepted, but manipulation for other purposes could be seen as scientific ethical abuse.

Ph: 91-484-2351870, Fax: 91-484-2381312, Website: <www.teresas.ac.in>

Email: editor.tijcs@teresas.ac.in

Journal Website: www.tijcs.teresas.ac.in

Submit your article to: editor.tijcs@teresas.ac.in

The submission must be in the form of an attachment with a covering letter to be sent as e-mail.

FORM IV

Statement about ownership and other particulars about newspaper (***Teresian International Journal of Chemical Sciences)*** to be published in the month of February.

Place of publication	:	St. Teresa's College (Autonomous) Ernakulam Park Avenue Road, Cochin-682011
Periodicity of its publication	:	Quarterly
Printer's Name	:	Dr. Alphonsa Vijaya Joseph
Nationality	:	Indian
Address	:	St. Teresa's College (Autonomous) Ernakulam Park Avenue Road, Cochin-682011
Publisher's Name	:	Dr. Alphonsa Vijaya Joseph
Nationality	:	Indian
Address	:	St. Teresa's College (Autonomous) Ernakulam Park Avenue Road, Cochin-682011
Editor's Name	:	Dr. Saritha Chandran A.
Nationality	:	Indian
Address	:	St. Teresa's College (Autonomous) Ernakulam Park Avenue Road, Cochin-682011
Owner's Name	:	St. Teresa's College (Autonomous) Ernakulam Park Avenue Road, Cochin-682011

I, Principal, St. Teresa's College (Autonomous) Ernakulam declare that the particulars given above are true to the best of my knowledge and belief.

Saturday, December 31, 2022.

Principal
St.Teresa's College (Autonomous) Ernakulam
Printer and Publisher

Subscription Procedure:

Subscription can be done by visiting www.tijcs.teresas.ac.in choosing a suitable plan and paying online.

Subscription Rates:

1 Year	Rs. 3000/-	($ 150)
2 Years	Rs. 5400/-	($ 270)
Per Issue	Rs. 750/-	($ 40)

Reg. No. KERENG/2020/79700

Printed and Published by Dr. Alphonsa Vijaya Joseph, Principal on behalf of St. Teresa's College (Autonomous), Ernakulam and printed at Green Offset Printing Press, 43/609B, Maria Tower, Powathil Road, Ayyappankavu, Cochin-682018, Kerala and published at St. Teresa's College (Autonomous), Ernakulam, Park Avenue Road, Cochin-11, Kerala. Editor- Dr. Saritha Chandran A.

St. Teresa's College established in 1925, affiliated to Mahatma Gandhi University, now St. Teresa's College (Autonomous), Ernakulam since 2014, has been evaluated and accredited at A++ by NAAC in the fourth cycle in September 2019 and, is one of the best among colleges in India. Turning women into individuals in their own right, individuals who by actualizing their potential, command and earn respect, is the noble task the institution embraces. This vision is an embodiment of the ideals of the Foundress of the college, Mother Teresa of St. Rose of Lima, a far-sighted educationalist who understood the need for educating women. Led by the Congregation of the Carmelite Sisters of St. Teresa (CSST), the College has undertaken this mission with zeal.

Submit your article to: editor.tijcs@teresas.ac.in

Journal website : www.tijcs.teresas.ac.in

THE FEAR OF THE LORD IS THE BEGINNING OF WISDOM

ST. TERESA'S COLLEGE (AUTONOMOUS) ESTD 1925

St. Teresa's College (Autonomous), Ernakulam
Park Avenue Road, Cochin-682011, Kerala, India
Tel: 0484-2351870, Fax: 0484-2381312
Email: principal@teresas.ac.in, Website: www.teresas.ac.in

ISSN 2583-2565